ABSTRACT

HETEROGENEOUS FLOW STRUCTURE AND GAS-SOLID TRANSPORT OF RISER

by
Jun You

This study aims to understand physical mechanisms of gas-solid transport and riser flow, investigate heterogeneous flow structures of gas-solid transport and their formation mechanism of the in riser flows, both in axial and radial directions. It provides sound interpretation for the experimental observation and valuable suggestion to riser reactor design. Chemical reaction is also coupled with flow hydrodynamics to board the industrial applications. This study mainly focuses on mathematical modeling approach based upon physical mechanism, and endeavor to validate model prediction against available experimental data.

First of all, most important physical mechanisms including inter-particle collision force, gas/solid interfacial force and wall boundary effects, which are believed to be most important aspects of the flow hydrodynamics, have been investigated in this part. An energy-based mechanistic model was developed to analyze the partitions of the axial gradient of pressure by solids acceleration, collision-induced energy dissipation and solids holdup in gas-solid riser flows. Thought this part of study, important understanding of the inter-particle collision force (F_C), gas/solid interfacial force (F_D) inside the momentum equations and energy dissipation (Γ), especially in dense and acceleration region, has been reached. Based on these understandings, a mechanistic riser hydrodynamic model was developed on the basis of gas-solid continuity and momentum equations, along with the better formulated drag force correlation and new

formulation for moment dissipation of solids due to solids collisions. The proposed model is capable of yielding the coupled hydrodynamic parameters of solid volume fraction, gas and solid velocity, and pressure distribution along the whole riser. At the same time, special considerations are given to solids back-mixing and resultant cross-section area variation for the upward flow, which is especially prominent for low solids mass flow condition.

With the further understanding of solid collision, gas/solid interfacial and wall boundary effects, in order to soundly interpret the well-known "core-annulus" 2-zone flow structure, newly discovered "core-annulus-wall" 3-zone structure" and provide reasonable explanation for the "choking" phenomena, a comprehensive modeling of continuous gas-solids flow structure both in radial and axial directions has been presented. This model, assuming one-dimensional two-phase flow in each zone along the riser, consists of a set of coupled ordinary-differential equations developed from the conservation laws of mass, momentum, and energy of both gas and solids phases. This part of study not only provides reasonable explanation for the 2-zone and 3-zone structure", but also finds out the potential reasons for the "choking" phenomenon. In order to investigate the different riser inlet configuration's effects on gas-solid mixing in dense region and improve the uniform inlet condition assumption in above models, a systemically study regarding with different inlet conditions have been done based on commercial package. Those simulation results are directly combined with model approach which reached the conclusion that riser flow structure an flow stability are weakly dependent on the type of solids feeding configuration.

This part of study is specifically focused on chemical reaction coupled gas-solid transport flow hydrodynamics. The aim of this work is to develop a generic modeling approach which can fully incorporate multiphase flow hydrodynamics with chemical reaction process. This modeling approach opens up a new dimension for making generic models suitable for the analysis and control studies of chemical reaction units. The chemical reaction model was represented by a relatively simple four-lump based FCC reaction kinetic model, which will not bring us too complicated mathematical derivation without losing its popular acceptance. As a first endeavor to consider the significant mutual coupling between the flow hydrodynamics and cracking reaction, a localized catalyst to oil ratio is introduced. The new developed chemical reaction coupled hydrodynamic model was capable of quickly evaluating the flow parameters including gas and solid phase velocity and concentration, temperature and reaction yield profiles as the function of riser height.

HETEROGENEOUS FLOW STRUCTURE AND GAS-SOLID TRANSPORT OF RISER

by
Jun You

A Dissertation
Submitted to the Faculty of
New Jersey Institute of Technology
in Partial Fulfillment of the Requirements for the Degree of
Doctor of Philosophy in Mechanical Engineering

Department of Mechanical Engineering

May 2009

APPROVAL PAGE

HETEROGENEOUS FLOW STRUCTURE AND GAS-SOLID TRANSPORT OF RISER

Jun You

4/28/09

Dr. Chao ~~Zhu~~, Dissertation Advisor — Date
Professor of Mechanical Engineering, NJIT

04/16/09

Dr. Ernest Geskin, Committee Member — Date
Professor of Mechanical Engineering, NJIT

04/16/09

Dr. Teh C. Ho, Committee Member — Date
Corporate Strategic Research Laboratories
ExxonMobil Research and Engineering Corporation, Annandale, NJ

4/15/09

Dr. Anthony D. Rosato, Committee Member — Date
Professor of Mechanical Engineering, NJIT

4/15/09

Dr. Pushpendra Singh, Committee Member — Date
Professor of Mechanical Engineering, NJIT

BIOGRAPHICAL SKETCH

Author: Jun You

Degree: Doctor of Philosophy

Date: May 2009

Date of Birth:

Place of Birth:

Undergraduate and Graduate Education:

- Doctor of Philosophy in Mechanical Engineering,
  New Jersey Institute of Technology, Newark, NJ, 2009

- Master of Science in Thermal Engineering,
  Huazhong University of Science and Technology, Hubei, P. R. China, 2002

- Bachelor of Science in Thermal Engineering,
  North China Electric Power University, Hebei, P. R. China, 1999

Major: Mechanical Engineering

Presentations and Publications:

You J., Patel R., Wang D.W., Zhu C., Role of Inter-particle Collision on Solids Acceleration in Riser, *Journal of Particuology*, In press, 2009.

Wang D.W., You J., Zhu C., General Hydrodynamic Modeling Approach of Upward Riser Flows, *Powder Technology*, In press, 2009.

You J., Wang D.W., Zhu C., Entrance Effects on Gas-Solid Riser Flow Structure, *Industrial & Engineering Chemistry Research*, 48, 310-319, 2009.

You J., Zhu C., Bing Du, L.S.Fan, Heterogeneous Structure in Gas-Solid Riser Flows, *AIChE Journal*, Vol. 54, No. 6, 1459-1469, 2008.

Zhu C., You J., An Energy-Based Model of Gas-Solids Transport in a Riser, *Powder Technology*, 175, 33-42, 2007.

You J., Zhu C., Hydrodynamic Modeling of Fluid Catalytic Cracking (FCC) Riser Reactor, *AIChE Annual Meeting*, November 17-21, 2008, Philadelphia, PA, USA.

You J., Patel R., Wang D.W., Zhu C., Hydrodynamic Modeling of Gas-solids Riser Flows, *AIChE Annual Meeting*, November 17-21, 2008, Philadelphia, PA, USA.

Wang D.W., You J., Zhu C., Heterogeneous Flow Structure in Gas-Solid Riser: Continuous Model, *AIChE Annual Meeting,* November 17-21, 2008, Philadelphia, PA, USA.

You J., Wang D.W., Zhu C., L.S.Fan, Modeling on Heterogeneous Structure in Acceleration Regime of Gas-Solid Riser Flows, *The 12th International Conference on Fluidization*, May 13-17, 2007, Vancouver, Canada.

Zhu C., You J., Hydrodynamic Model of the Acceleration Zone in a CFB Riser, *Fifth World Congress on Particle Technology*, April, 2006, Orlando, FL, USA.

Zhu C., You J., A One-Dimensional Model of Gas-solids Flows In the acceleration Zone of a CFB riser, *AICHE Annual Meeting*, Oct. 30th -Nov. 4th, 2005, Cincinnati, OH, USA.

This dissertation is dedicated to my beloved parents, my wife and my family.

（献给我深爱的父母，妻子和家人）

三十功名尘与土，
八千里路云和月。
莫等闲，白了少年头，
空悲切。

摘自岳飞《满江红》

ACKNOWLEDGMENT

I would like to express my deepest appreciation to Dr. Chao Zhu, for his remarkable guidance, constant supervision, sincere friendship and moral support throughout this research. Without his guidance, it would have been impossible for me to finish this program so smoothly. I would also like to acknowledge Dr. Teh C. Ho in providing great help and precious support for a portion of this study. Special thanks are given to Dr. Ernest Geskin, Dr. Pushpendra Singh, and Dr. Anthony D. Rosato for their actively participating in my dissertation committee. I am also thankful to Dr. L-S. Fan and Dr. Bing Du at Ohio State University for their valuable suggestions and experimental support in this study.

I would like to acknowledge the Teaching Assistantships from the Department of Mechanical Engineering of New Jersey Institute of Technology, the ExxonMobil Research and Development Corporation and the Petroleum Research Fund for the research fund in the summer. I appreciate the friendship and cooperation of Dr. Qun Yu, Dr. Muhammad M. R. Qureshi, Dr. Tong Lee, Mr. Dawei Wang, Mr. Rajesh Patel and Ms. Zheng Shen in the Particulate Multiphase Flow Laboratory.

I would like to express my endless gratitude to my beloved parents, who have always supported my academic pursuits and helped me in every possible way. Last, I want to thank my wife for her support and encouragement throughout these years.

TABLE OF CONTENTS

TABLE OF CONTENTS
(Continued)

TABLE OF CONTENTS
(Continued)

Chapter **Page**

LIST OF TABLES

LIST OF FIGURES

LIST OF FIGURES
(Continued)

Figure **Page**

LIST OF FIGURES
(Continued)

Figure **Page**

LIST OF FIGURES
(Continued)

Figure **Page**

LIST OF SYMBOLS

A	Cross-sectional area of riser
Ar	Archimedes number
d_p	Particle diameter
C_{ppi}	Transport coefficient
C_i	Molar concentration of component i
$(c/o)_{overall}$	Catalyst to oil ratio
$(c/o)_L$	Localized catalyst to oil ratio
d_s	Average size of solid particles
D	Diameter of riser
f	Moment transport coefficient
F_C	Collision force
F_D	Drag force
G	Acceleration of gravity
G_p	Solid mass flux
G	Gas mass flux
ΔH_r	Heat of reaction
M_i	Molecular weight of component i
M	Mass of a particle
$\dot{m}_s$	Solids transfer across interface
N	Solid number in unit volume
K	Coefficient of polynomial function of Γ

LIST OF SYMBOLS
(Continued)

k_i	Reaction constant of ith pseudo-component
k_{i0}	Initial rate constant
K_A	Coefficient
K_B	Coefficient
P	Pressure
Re_{mt}	Particle Reynolds number
r_i	Disappearance rate of ith pseudo-component
R	Ideal gas constant
R	Riser radius
R_w	Wall region radius
T	Temperature
U	Gas velocity
wt_{coke}	Concentration of coke on catalyst surface
U_p	Particle velocity
U_{pt}	Particle terminal velocity
U_{mt}	Particle minimum transport velocity
W_i	Molecule weight of ith pseudo-component
Z	Axial position in riser

Greeks

α_p	Solid volume fraction
$\alpha_{p,app}$	Apparent solid concentration

LIST OF SYMBOLS
(Continued)

α_{pf}	Solid volume fraction at dilute phase
α_{pmt}	Solid volume fraction at dense phase
α	Gas volume fraction
β	Energy partition for the solid lift up
χ	Energy partition for solid acceleration
δ	Energy dissipation partition
Λ	Chemical reaction rate
Γ	Momentum dissipation
Γ	Energy dissipation rate
$\overline{\rho}_g$	Average density of gas phase
ρ_p	Particle density
P	Gas density
M	Gas kinematics viscosity
$\tau_{p,app}$	Particle residence time of ASC
T	Particle residence time
τ_w	Wall shear stress of gas phase
τ_{wp}	Wall shear stress of particles
ζ_1	Wake effect coefficient
Φ_s	Catalyst activity coefficient

LIST OF SYMBOLS
(Continued)

Subscripts

0	Riser inlet (at x=0)
A	Annulus region
C	Core region
G	Gas phase
S	Solid phase
W	Wall region
i	i^{th} component

CHAPTER 1

INTRODUCTION AND LITERATURE SURVEY

1.1 Background

Multiphase interactions are central to many common processes in the chemical and petroleum industries. Gas-solid interactions occur in vertical columns of co-flowing gas and solids; such reactors are known as "riser". Riser is the reactor system of choice in certain specialized but important applications. Foremost among these is the fluidized catalytic cracking of hydrocarbons into higher-order petroleum products (the so-called "FCC" process) and pulverized coal combustion. A typical riser flow loop, omitting reaction-specific components, is shown schematically in Figure 1.1.

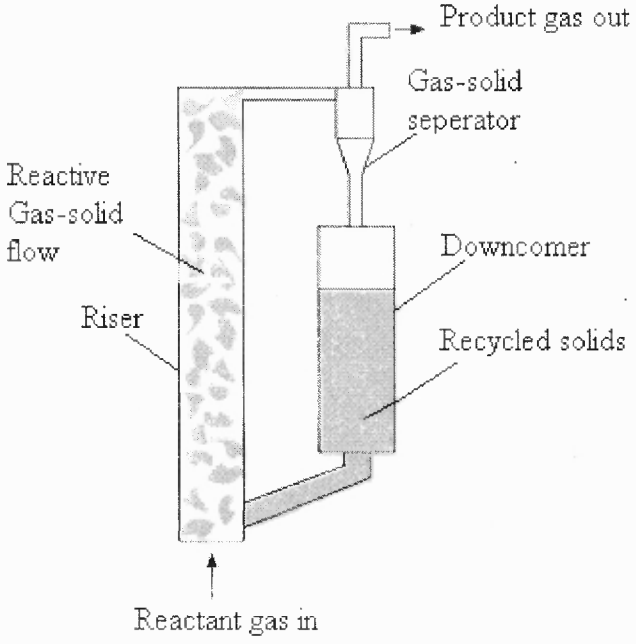

Figure 1.1 Schematic diagram of generic riser configuration.

Particles are fed from storage and/or return leg, known as a "down-comer", into the riser itself, and are mixed with the transport gases and travel upward through the riser column. At the top of the riser, the particles and gas are separated, through multiple stages of cyclone separators. The gas continues to flow to its next destination, and the particles are returned to the down-comer, where they are recycled through the flow. The gas flow in the riser is thus a single-pass in nature, while the particle flow is multiple-pass. As a result, the riser reactor is known as "circulating fluidized beds" (CFBs).

Despite of their acceptance in industrial applications, riser reactors are relatively problem-prone. A Rand Corporation study (Merrow, 1986) found that, solids processing facilities in the petrochemical industries are suffering from an average 37% performance shortfall relative to their design efficiencies. The average shortfall for non-solids plants is only 16% and thus, the industry goal is 5-10% shortfall. The reduced performance in the solids-processing plants is linked very strongly to physical and mechanical solids-flow difficulties and weekly to problems with the intended process chemistry. It should be noted that Merrow's study was not limited to CFB units but examined a wide range of solids-intensive operations; however, "hard" CFB unit reliability data are scarce, and the complications introduced to any generic process step by the addition of solids to the process stream are relatively common across process.

The immense scale of the economy in which such reactors operate must also be borne in mind when considering industrial-scale reaction facilities. It is easy to estimate from the reactor data that, a sustained fractional-percentage increase in

hydrocarbon-processing riser reactor efficiency would result in increase of millions of barrels of annual product yield for economic benefit and the ecological benefit through reduced waste stream. Thus, even small but consistent process improvements are eagerly sought.

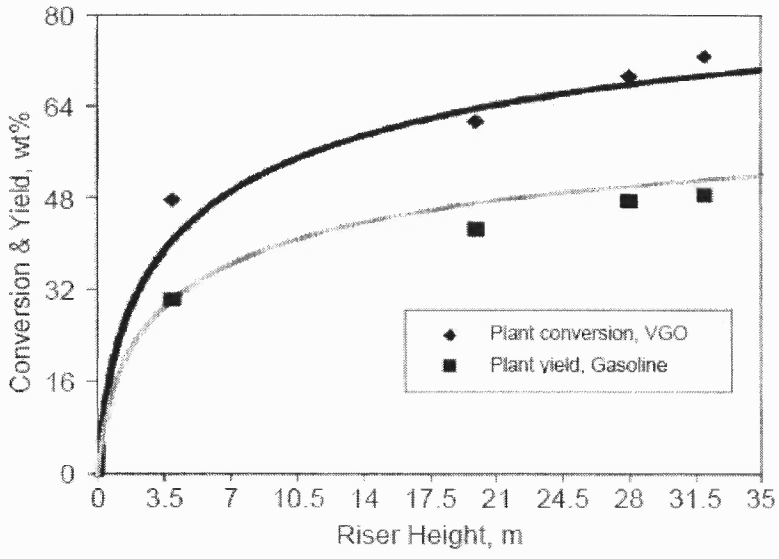

Figure 1.2 Typical conversion & yield pattern of FCC riser.

Efforts are continuously made to improve the process in order to increase the productivity of the refinery industry and also to reduce pollutant emissions to the environment. Over the course of process improvement, cracking reaction time in the FCC unit has become much shorter and hence, flow hydrodynamic effects on cracking processes have a greater impact on product yields. In the riser dense regime (lower than 3 meters), because of the high concentration of reactants and catalyst, plus higher temperature, the cracking reaction is much stronger and faster than the rest of the riser. However, as shown in Figure 1.2, only about 50% of the total reaction takes place in this regime, and cracking

reaction occurring in the rest of the riser is still very critical to the total production yield.

The riser design work involves an interaction between chemists and chemical engineers, with the former designing the reaction and the later developing the ability to carry out profitably at a large scale. The major source of the difficulty in riser design is the inability to predict the accurately hydrodynamics of riser operation. Even when operated with no particles, the gas flow in the riser is turbulent and is thus difficult to predict in any spatial or temporal detail other than by computational means. However, the addition of solid particles to the flow at volumetric concentrations as high as 40% renders the equations of motion even more complex and intractable.

1.2 Literature Survey

1.2.1 Flow Characteristics of Gas-solid Riser Flow

Gas-solids transport in riser flows can be found in many industrial applications such as fluidized catalytic cracking in petrochemical industry, coal combustion in utility industry, and pneumatic conveying of drug powders in pharmaceutical industry. It is well known that the phase transport properties such as solids holdup and solids velocity are non-uniformly distributed along a riser, typically with a dense-phase transport in the lower part of the riser and lean-phase transport in the upper part of the riser [Li and Kwauk, 1980]. The non-uniformity in axial phase distributions depends strongly on the operation conditions including the overall transport mass flux of solids and superficial gas velocity.

From the point of view of energy balance, the solids acceleration and energy dissipations consume some portion of the pressure drop in the riser flow. Hence, strictly speaking, the traditional approach of equating the local solids holdup to the pressure drop in a riser will lead to an overestimation of local solids holdup. This overestimation can be quite large in the acceleration and dense phase transport regions where the effect of solids acceleration and the effect of energy dissipations due to interfacial friction between gas and solids phases and inter-particle collisions are expected to be significant. The following is a brief review of related modeling efforts and remaining challenges, which provides the background and modeling objectives of this paper.

The actual flow structure of gas and solids in a riser flow is very complex, with multidimensional variations in axial, radial and even azimuthal directions (such as near a bend or asymmetric gas-solids feeder inlet); multidirectional flows in core, annulus and wall regions; multi-scaled phase interactions (such as interactions among dispersed solids, clusters, turbulent eddies and pipe wall surfaces in different flow regimes); and other complications from solids cohesion and electrostatic charges. A simple mechanistic model of such a complicated system inevitably requires many assumptions for simplification. In order to evaluate the effects of solids acceleration and energy dissipations on the pressure drop in a riser flow, the simplest and most convenient analysis approach is based on cross-section averaged axial flow models.

Cross-sectional averaged solids holdup in a riser flow can be roughly estimated from pressure drop measurements by equating the gravitational force from local solids

holdup to the local axial gradient of pressure with or without modifications of gas-solid flow frictions on pipe walls [Geldart and Rhodes, 1986; Bader et al. 1988; Rautiainen et al. 1999]. Due to the neglect of effects of solids acceleration and phase friction, the converted volumetric solids holdup is conceptually different from the actual solids holdup and hence termed as apparent solids fraction or apparent solids concentration [Sun et al. 1999; Schlichthaerle and Werther, 1999].

While the above method of solids holdup estimation works reasonably well for gas-solid flows in the dilute transport regime, many studies suggest that the effect of solids acceleration should not be omitted in the estimation of solids holdup from the pressure drop measurements in the solids acceleration region [Weinstein and Li, 1989; Pugsley and Berruti, 1996; Sabbaghan et al. 2004]. In most of these models, the modeling of solids acceleration is based on the drag forces on individual particles or clusters in fluids with semi-empirical correlations of the effective drag coefficients. The Richardson-Zaki equation is used as a basis for the drag force modification in gas-solids fluidization. It is noted, however, that the Richardson-Zaki equation may not be adequate to describe the hydrodynamic forces on particle with net transport mass flux in the riser flows because the solids holdup is expected to be a function of both the gas and solids velocities rather than the gas velocity alone [He and Rudolph, 1996].

In the dense phase transport region, the experimental measurements based on γ-ray absorption or electric capacitance tomography shows that, while the detailed solids holdup distribution is very complex with a core-annulus-wall structure, the cross-sectional

averaged solids volume concentration only varies slightly or virtually remains the same along the riser [Schlichthaerle and Werther, 1999; Du et al. 2004]. The pressure drop measurements in the dense phase transport region however yield apparent solids concentrations much higher than the actual solids concentrations. These measurements strongly show that the solids acceleration is very much damped and significant energy dissipations occur in the dense phase transport region, possibly due to the strong particle collisions and inter-phase frictions.

Modeling efforts to interpret the effect of inter-particle collisions on the solids flow distributions are mostly based on the kinetic theory of granular flows and two-fluid model with apparent viscosity in solids phase [Louge et al. 1991; Miller and Gidaspow, 1992; Büssing and Reh, 2001]. The application of the kinetic theory modeling approach to the gas-solid riser flows, however, has many inherent limitations due to its basic assumptions of center-to-center particle collisions in vacuum. The energy dissipation module in the kinetic theory modeling only depends on the restitution coefficient, a non-material property whose prediction in an arbitrary center-to-center collision of a pair of solid particles is still a mystery. In a fluidization, the dominant module of inter-particle collisions is off-center or oblique collision where the energy dissipation not only depends on the loss from normal-component of collision (restitution coefficient) but also depends on the loss due to sliding and micro-slip friction in tangential and rolling contacts [Fan and Zhu, 1998]. This inadequate description of collision-induced energy dissipation in kinetic theory modeling can also be reflected in the poor predictions of pressure drops in the dense

phase transport region and the large uncertainties in the selections of restitution coefficients for the modeling of gas-solids fluidization.

Above literature survey and mechanistic analysis shows that the effect of solids acceleration and energy dissipations in the acceleration and dense phase transport regions may have significant impact on the pressure drop distribution, which in turn affects the estimation of solids concentration from pressure drop measurements. Currently available models have various inherent flaws in the modeling mechanisms, in addition to the use of questionable empirical correlations. This part of study aims to develop an energy-based mechanistic model to analyze the partitions of the axial gradient of pressure by solids acceleration, collision-induced energy dissipation and solids holdup in gas-solid riser flows. Based on this model, the correct estimation of axial distributions of solids holdup and solid velocity can be obtained.

1.2.2 Heterogeneous Structure of Riser Flow

In a gas-solids riser flow, the hydrodynamic flow characteristics of both gas and solids phases are strongly heterogeneous, represented by the non-uniform distributions of solids concentration and phase velocities in both the axial and radial directions. The axial non-uniformity is due to the phase acceleration whereas the radial uniformity is mainly caused by the wall boundary effect.

The heterogeneous flow structure has been poorly understood, mainly due to the lack of appropriate measurement techniques applicable to gas-solids riser flows at

moderate or high solids loadings, especially in the riser bottom where the dense and acceleration regimes are located. The cross-section averaged distribution of solids holdup along the riser is commonly estimated from the pressure drop measurements by assuming the solids in a fully-developed suspension state without acceleration, which is probably true for gas-solids flows in the dilute transport regime in the upper part of riser, yet away from the riser exit. The local solids holdup can be estimated either from the intrusive probe measurements (e.g., optical fiber probe (Nakajima et al. 1991); capacitance probe (Brereton et al. 1993, Yates and Simons 1994) or from the non-intrusive measurements (e.g., X-ray imaging (Rowe, 1971); gamma-ray imaging (Schlichthaerle and Werther, 1999); laser-sheet imaging (Horio and Kuroki, 1994); tomography [Halow et al. 1993, Warsito and Fan, 2001).

Most of these techniques fail to yield accurate and instantaneous measurements for a precise description of the flow structure in a gas-solids riser flow, especially near the wall region or in the riser bottom. The recently developed electrical capacitance tomography (ECT) appears to be the most promising tomography technique for the flow structure diagnosis of gas-solid riser flows, with a much improved spatial and temporal imaging resolution (Warsito and Fan, 2001). Despite the lack of accurate measurements, it has become a common understanding that the heterogeneous flow structure in a cross section of riser can be, in general, described by a core-annular structure, in which the upwards moving solids are in the core whereas a dense layer of solids, mostly likely downwards moving, is in the wall (or annular) region. The solids concentration decreases

monotonically towards the center of the cross-section, whereas the solids velocity increases monotonically towards the center. The solids concentration monotonically decreases along the riser, typically in an S-shape, where the transition from dense phase to dilute phase is due to the solids acceleration. This core-annular cross-section structure with an S-shaped axial distribution, however, does not give a clear explanation of the flow structure in the bottom of riser where the downwards moving solids from the wall is conceptually mixed with the upwards moving solids from the riser entrance. None of the core-annular structure model explain the choking --a critical transition of flow structure (and solids transport) that occurs typically in relatively small-sized risers at low transport velocities with moderate solids loadings.

Our recent measurements using ECT reveal that, under certain operating conditions, there exist a radial symmetry of the time-averaged solids holdup distribution, and a double ring structure in solids concentration in a circulating fluidized bed riser (Du et al. 2004). In the dense and acceleration regimes, the solids concentration is much denser in the wall regime than that in the annulus. This core-annulus-wall heterogeneous structure is significantly different from the commonly-known "core-annulus (wall)" two-zone structure in riser flows, which becomes unstable with the increase in solids loading, and eventually leads to the occurrence of choking (Du et al. 2004). In the dilute transport regime, the solids concentrations however follow very much the "core-annulus (wall)" two-zone structure. Such findings are very interesting which indicate that the radial profile

for some dense phase riser flows could be of a core-annulus-wall three-region structure rather than the widely-accepted core-annulus (wall) two-region structure.

Most models of heterogeneous flow structure are based on the core-annulus (wall) flows (Bolton and Davidson, 1988; Rhodes and Geldart, 1987; Horio et al. 1988; Senior and Brereton, 1992; Rhodes et al. 1998), which typically consider a dilute uniform core flow, and a dense wall flow along the riser. These models fail to provide the detailed mechanisms in the bottom region of riser where the flows can be very dense and complex. A primitive model was lately proposed to interpret the reported core-annulus-wall structure (Zhu et al. 2005); using a simplified kinetic theory model to account for the solids acceleration in collision dominated dense flow regimes near the bottom of riser. It is apparent, however, that the most traditional momentum-based models with the assistance of a kinetic theory modeling approach may be insufficient to describe some basic physics of collision-induced energy dissipation in fluidization, such as energy dissipations from tangential slip and rotational slip. This deficiency may be represented by the inability to correctly predict the pressure distribution in the dense flow regime near the bottom of a CFB riser. The importance of correct account of energy transport and dissipation in the momentum equation may be analogous to that of k-ε model in the turbulent momentum transport equations in turbulence flows. Hence an additional term due to energy dissipation should be introduced into the solid momentum transport equation in the collision and acceleration dominated regime [Zhu and You, 2007].

This part of study aims to present a complete study on the formation of mechanisms of the heterogeneous structure (especially the core-annulus-wall structure) in gas-solids risers using both experimental and theoretical approaches.

1.2.3 Chemical Kinetics and Its Coupling with Flow Structure

Fluid catalytic cracking (FCC), developed by American engineers Warren K. Lewis and Edwin R. Gilliland, is a process in which the heavy hydrocarbon molecules are converted into lighter molecules. The first FCC commercialized over half a century ago, is still evolving. Improvements in technology as well as changing feed stocks and product requirements continue to drive this evolution. The hydrocarbon feed enters a transport bed tubular reactor (riser) through feed atomizing nozzles and comes in contact with the hot catalyst coming from the regenerator. The feed gets vaporized and cracks down to the lighter molecules as it travels upwards along with the catalyst. As a result of cracking, the velocity of the vapors increases along the riser height.

The key part of the FCC process is the relatively small riser where a gas/solid suspension rises from bottom to top. In order to keep a sufficiently dense suspension in the riser, particles are continuously recycled to its base. The processes in a CFB can be divided in two main groups:

- Catalytic gas/gas reactions where the solids serve as catalyst and heat transfer medium. The products are gaseous and mostly organic chemicals, as final or intermediate products.
- Gas/solid reactions such as alumina calcinations, iron ore reduction and combustion of coal where both phases react to yield products and/or energy.

The different nature of the reactions requires different working conditions. For catalytic gas-phase reactions, high gas velocities are desirable as gas back-mixing should be avoided and hence plug flow promoted. Furthermore, high gas velocities result in short contact times demanded by the high reaction rates. As the catalyst is quickly deactivated and hence it requires frequent regeneration, high solids circulation rates are also needed. As a result, the solids concentration will be high, thus promoting the reaction rate and permitting frequent catalyst reactivation.

For gas–solid processes on the other hand, the usually reaction rate is low, so it does not require either high gas velocity or high solids circulation rate. Low gas velocity operation is permitted because the solids are usually the key reactant/product so, the extent of gas and/or solids back-mixing may not always be critical. Some gas/solid reactions require operating conditions of gas catalytic reactions since the by-product (char) acts as cracking catalyst for the main product (bio-oil), thus considerably reducing its production yield at high residence times. The conversion of gas and/or particles depends on the reaction rate and the residence time in the riser. Whereas the reaction rate (and its constant) is determined mostly by the chemistry and thermodynamics of the system under scrutiny, the residence time is a function only of the hydrodynamics of the gas/solid flow in the riser.

Detailed modeling of the riser reactor is a challenging task for theoretical investigators not only due to complex hydrodynamics and thousands of unknown hydrocarbons in the FCC feed but also due to the involvement of different types of reactions taking place simultaneously. Such detailed chemistry of catalytic cracking

coupled with a large number of unknown compounds present in the feedstock is very difficult to be used in the mathematical modeling of an industrial scale FCC riser reactor because of the analytical and computational limitations.

The traditional and global approach of modeling of cracking kinetics is based on lumping of compounds. Mathematical models dealing with riser kinetics can be categorized into two main types. In the first category, the lumps are made on the basis of boiling range of feed stocks and corresponding products in the reaction system. This kind of model has an increasing trend in the number of lumps of the cracked components. The other approach in which, the lumps are made on the basis of molecular structure, characteristics of hydrocarbon group composition in reaction system. This category of models emphasizes on more detailed description of the feedstock. These both categories of models do not include chemical data such as type of reaction and reaction stoichiometry. The number of kinetic constants in these models increases very rapidly with the number of lumps. All these models assume that FCC feed and products are made of a certain number of lumps, and the kinetic parameters for these lumps are estimated empirically considering the conversion of one lump into the other. In both of these categories, however, reaction kinetics being considered is that of "conversion" of one lump to another and not the "cracking" of an individual lump.

Numerous articles are found on catalytic cracking reaction in the published literature. Most of them are based on representation of oil in few lumps (like 4-lump, 10 -lump, 14-lump and so on). Weekman and Nace (1970) were the first to develop a

three-lump cracking model to study the gasoline production of a FCC unit. The three lumps considered were gas oil, gasoline and light gases plus coke lumps. The subsequent study conducted by Farag (1993) showed the need to consider light gases and coke as separate lumps, therefore considering a four lump model. Jacob et al. (1976) developed a more detailed ten-lump kinetic model taking into account different feed properties in addition to boiling point range. All these models considered isothermal plug flow in the riser reactor. Pitault et al. (1994) proposed kinetic model based on a molecular approach and the kinetic model was built from experiments with a small fixed bed reactor (the micro activity test).

In the present work, we have considered two of the most widely used cracking models namely the four-lump model of Farag et al. (1994) and the ten-lump model of Jacob et al. (1976). Liguras and Allen (1989a) proposed a lumped kinetic model so as to utilize the pure components cracking data for the catalytic cracking of oil mixtures. The authors in their subsequent work (Liguras and Allen, 1989b) divided the petroleum feedstock into a number of pseudo-components. Gas–solid flow through vertical riser with high solids flux (400 kg/m2 s) used in practice is a subject of intense investigation over the last few decades. When a gas vertical riser transports the particle, experimental studies have shown that they are distributed non-uniformly all over the cross-section of the riser (Horio and Kuroki (1994)). In the last decade, with the advancement in computational capabilities, the computational fluid dynamics (CFD) is being used increasingly to simulate gas–solid flows in vertical risers. Most of the research groups used Eulerian–Eulerian approach

where the dispersed solid particles are treated as interpenetrating continuum (Das et al. 2004; Theologos and Markatos, 1993). The kinetic theory of the granular flow is used to simulate gas–solid flow in riser for different particle size and /or particle density (Mathesian et al. 2000; Van Wachem et al. 2001; Neri and Gidaspow, 2000). However, the detailed comparison of predicted model results with experimental data at high solids flux (Ranade, 2002) revealed severe inadequacies of these models to simulate complex gas–solid flows.

In Eulerian–Lagrangian approach, each particle is treated by solving Lagrangian equation of motion for all the particles of the system with a prescribed set of initial conditions. It offers more natural way to simulate complex particle level processes like evaporation and cracking reactions. Heat and mass transfer and chemical reactions occurring at the individual particle scale can be conveniently accounted. The approach also provides the particle history starting from injection into flow field. The approach however requires significantly more computational resources and therefore rarely used for dense gas–solid risers. Momentum transfer, heat transfer, catalytic cracking reaction are interrelated and occur simultaneously in commercial FCC riser reactor. To predict the behavior the riser reactor accurately, all these processes must be modeled. Theologos et al. (1999) extended their CFD model to account for feed atomization effects on overall reactor performance. They assumed feed spray vaporization occurs in single-phase and they used only modified the heat transfer coefficient of gas-phase.

Gao et al. (2001) showed the synergetic effects of the hydrodynamics, heat transfer

and droplet size on the overall conversion of the FCC riser reactor. They assumed simplified d2 law for droplet vaporization without considering the influence of solid particles on heat transfer. Gupta and Subba Rao (2003) have used an empirical correlation to account for influence of solids on droplet evaporation rates in their model. However; their model is not applicable to oil, which boils over a range of temperatures rather than a specific value of boiling point. Berry et al. (2004) developed a two-dimensional adiabatic model for FCC riser. Their model combines a predictive riser hydrodynamic model with a four lump kinetic model. However, the model uses empirical correlation (Buchanan, 1994) for estimating the heat transfer coefficient for droplet vaporization which does not include influence of key parameters like solid heat capacity, particle diameter and so on. The model also considered a single value for the heat of reaction and a specific boiling point for the gas oil, which limits the applicability of their model. The model predictions were matched with the plant data by adjusting the value of activation energy. This brief review of published information on different aspects of FCC riser reactor clearly indicates the need for further work.

The fluid dynamics of this gas solid two-phase flow are very complex and strongly dominated by particle-particle interactions. Furthermore, the numerous homogeneous and heterogeneous catalytic gas-phase reactions interacting with complicated flow dynamic are not completely known. Therefore, it is necessary to develop simplified modeling approaches, which can describe both. The portion of this study aims to develop, a steady-state mechanistic riser model which takes into account of flow hydrodynamics and

catalytic cracking reactions. The emphasis is not on developing accurate flow model but to develop a framework to simulate simultaneously, the multi-phase flow and cracking reactions in riser reactor.

1.3 Dissertation Structure, Objectives and Approaches

The series of this study aims to understand the strong couplings between gas-solid transport flow hydrodynamics and chemical reaction kinetics in a riser reactor. The overall study is divided into two major parts. In the first part, the study is focused on the gas-solid riser flow hydrodynamics without reaction. In this part, we fully investigated gas-solid transport and formulation of mechanisms of heterogeneous structures in riser flows w/o chemical reaction, both in axial and radial directions, providing sound interpretation for the experimental observation and valuable suggestion to riser reactor design. With the better understandings of gas-solid transport flow mechanism, in the second part, FCC cracking reaction is coupled with flow hydrodynamics to widen the model's application in variety of industrial processes. To achieve this goal, the whole research study is composed of following three stages of work shown in Figure 1.3.

The first stage of work focus on better understand important physical mechanisms including inter-particle collision force, gas/solid interfacial force and wall boundary effects, which are believed to be most important aspects of the flow hydrodynamics. Based on these understandings, a mechanistic riser hydrodynamic model is developed on the basis of gas-solid continuity and momentum equations, along with the modified drag

force correlation and new formulation for momentum dissipation of solids due to solids collisions. At the same time, special considerations are given to solids back-mixing and resultant cross-section area variation for the upward flow, which is especially prominent for low solids mass flow condition.

In the second stage of work, with the further understanding of solid collision and acceleration, in order to soundly interpret the well-known "core-annulus" 2-zone flow structure and newly discovered "core-annulus-wall" 3-zone structure", a comprehensive modeling of continuous gas-solids flow structure both in radial and axial directions has been presented. This part of study not only provides reasonable explanation for the 2-zone and 3-zone structure", but also finds out the potential reasons for the "choking" phenomenon. In order to investigate the effects of riser inlet configuration's on gas-solid mixing in dense region and to improve the uniform inlet condition assumption in above models, a systemically study regarding with different inlet conditions have been done based on commercial package- Fluent. Upon further understanding in the inlet condition's effect, outputs of FLUENT simulation are directly combined with model approach in order to yield better results.

This second part of study is specifically focused on chemical reaction coupled with gas-solid transport flow hydrodynamics. The study is specifically focused on the inter-coupling between chemical reaction and gas-solid transport flow hydrodynamics. A complete mechanistic model has been developed to simulate simultaneously the multiphase flow hydrodynamics, cracking reaction and their coupling characteristics in

riser reactor model. The new developed chemical reaction is capable of quickly evaluating the flow parameters including gas and solid phase velocity and concentration, temperature and reaction yield profiles as the function of riser height. Instead of using the averaged catalyst to oil ratio, our model approach adopted a localized catalyst to oil ratio to consider the local flow hydrodynamics effects on FCC cracking reaction.

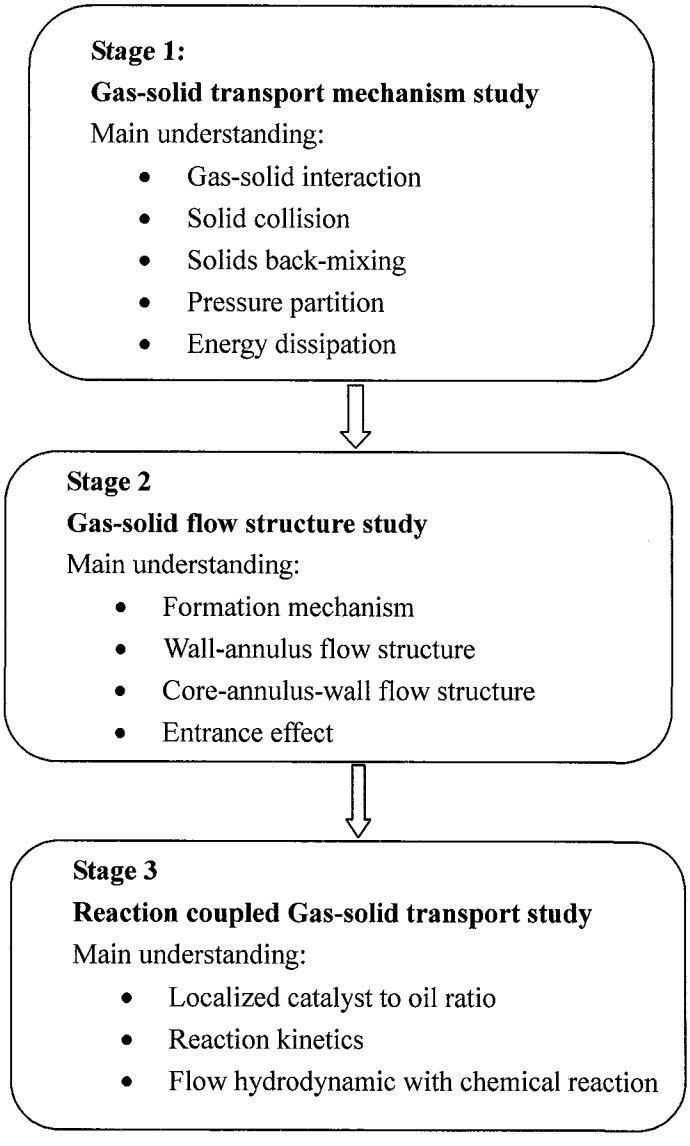

Figure 1.3 Three stages of overall thesis structure.

CHAPTER 2

MECHANISMS OF GAS-SOLID TRANSPORT

This part of study is divided into three parts. In the first part of study, an energy-based mechanistic model was developed to analyze the partitions of the axial gradient of pressure by solids acceleration, collision-induced energy dissipation and solids holdup in gas-solid riser flows. In the second part, a mechanistic riser hydrodynamic model was developed on the basis of gas-solid continuity and momentum equations, along with the modified drag force correlation and new formulation for moment dissipation of solids due to solids collisions. At the third part, special considerations are given to solids back-mixing and resultant cross-section area variation for the upward flow, which is especially prominent for low solids mass flow condition.

2.1 New Understanding of Collision Force and Energy Dissipation

The traditional approach of equating the local solids holdup to the pressure drop in a riser overlooks the effects of solids acceleration and energy dissipation in the acceleration and dense phase transport regions. The energy dissipation in these regions is mainly due to the interfacial friction between interstitial gas and suspended solids, inter-solids collisions, as well as solids-wall fraction. Most momentum-based models fail to account for the energy dissipation of inter-solids collisions, and the models using the simple granular kinetic theory fail to account for the energy dissipation in micro-sliding or rolling from off-center inter-solids collisions. This

paper presents an energy-based mechanistic model to analyze the partitions of the axial gradient of pressure by solids acceleration, collision-induced energy dissipation and solids holdup in gas-solid riser flows. Based on this model, more reasonable estimation of axial distributions of solid holdup and resulted solid velocity can be obtained. Our analysis shows that the effect of solids acceleration on the pressure drop can be significant in a range of moderate solids holdup (typically from 3.5% to 12% by solids volume fraction) whereas the effect of energy dissipation becomes important in the dense phase transport region (typically when the solids volume fraction above 5%). The exemplified results indicate that the traditional approach of equating the local solids holdup to the pressure drop overestimates the solids holdup by an error up to 50% in the acceleration and dense phase transport regions in typical gas-solid riser flow applications.

2.1.1 Governing Equations of Energy Based Model

Consider a steady gas-solid riser flow without end effect (i.e., ignoring the deceleration of solids near the top of riser), as shown in Figure 2.1.1 The mass continuity equations of cross-sectional averaged phase parameters of gas and solids can be expressed, respectively, by

$$G = (1-\alpha_p)\rho U \qquad\qquad G_p = \alpha_p \rho_p U_p \qquad (2.1)$$

Where G and G_p are the cross-sectional averaged mass fluxes of gas and solids, which are constant. α_p is the cross-sectional averaged volume fraction of solids. In Equation (2.2), the cross-sectional averaged velocities of gas and solids, **U** and $\mathbf{U}_p$, are

defined by

$$\mathbf{U} = \frac{\int_A \alpha\rho\mathbf{u}dA}{\int_A \alpha\rho dA} = \frac{\int_A \alpha\rho\mathbf{u}dA}{(1-\alpha_p)\rho A} \qquad \mathbf{U}_p = \frac{\int_A \sum_i m_{pi}\mathbf{u}_{pi}dA}{\int_A \sum_i m_{pi}dA} = \frac{\int_A \sum_i m_{pi}\mathbf{u}_{pi}dA}{\alpha_p\rho_p A} \quad (2.2)$$

Where **u** represents the local gas velocity with voidage α in a cross-section; $\mathbf{u}_{pi}$ is the velocity of ith particle of mass m_{pi} within the area element dA in a cross-section. It is noted that, while the local gas and velocities of individual particles in fluidization are three-dimensional and unsteady (i.e., $\mathbf{u}=\mathbf{u}(\mathbf{r}, t)$ and $\mathbf{u}_{pi}=\mathbf{u}_{pi}(\mathbf{r}, t)$), the cross-sectional averaged velocities of gas and solids are in the axial direction and are functions of axial coordinate only, i.e., $\mathbf{U}=\mathbf{U}(z)$ and $\mathbf{U}_p=\mathbf{U}_p(z)$, which is shown in Figure 2.1.

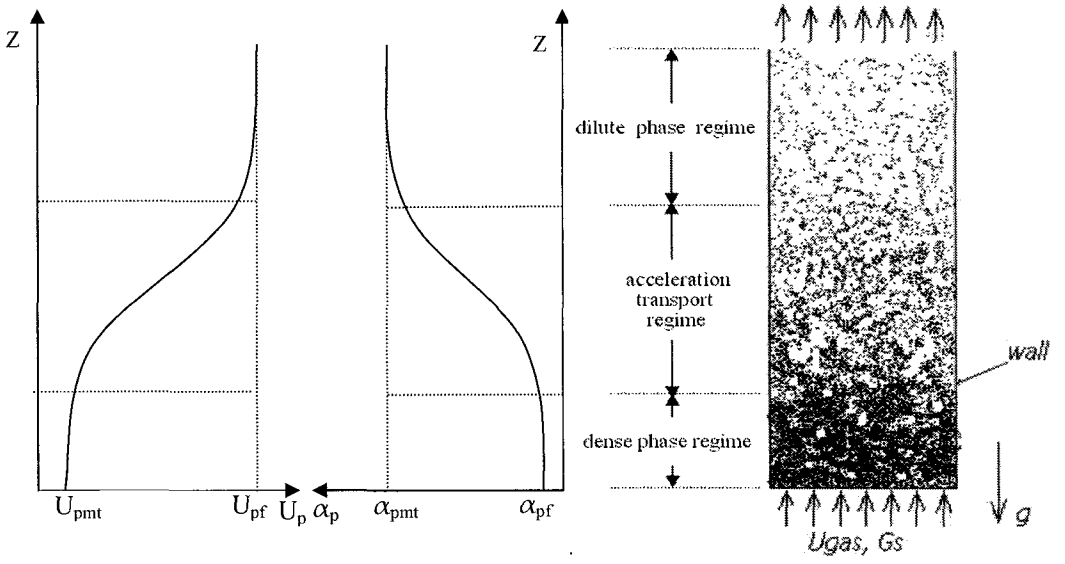

(a) Velocity (b) Concentration (c) Flow Regimes

Figure 2.1 Schematic distribution of solids in a riser.

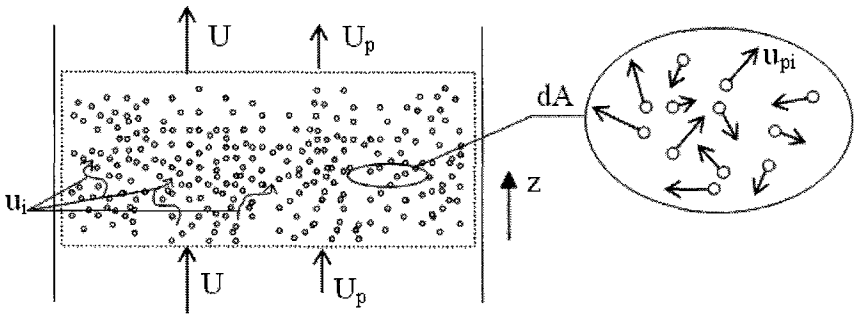

Figure 2.2 Concept of cross-sectional averaged velocities.

The cross-sectional averaged momentum equation of gas can be expressed by

$$-\frac{dp}{dz}=\frac{\tau_w l_w}{A}+(1-\alpha_p)\rho g+G\frac{dU}{dz}+F_D \tag{2.3}$$

where the first term on the right hand side of the equation stands for the wall friction; the second term is the gravitational force; and the third term represent the gas acceleration. The last term is the cross-sectional averaged drag force between the gas and solids, which is defined by

$$\mathbf{F}_D=\frac{1}{A}\int_A\sum_i f_{gi}(\mathbf{u}-\mathbf{u}_{pi})\,dA \tag{2.4}$$

Where f_{gi} is the momentum transfer coefficient between the local gas and the ith particle within the area element dA in the cross-section. It should be pointed out that, in a turbulent fluidized bed, the momentum transfer coefficient represents all kinds of particle-fluid interactions including drag forces, carried mass force, historic integral force (Basset force), velocity gradient force (such as Saffman force), rotation-related forces (such as Magus force), as well as the neighboring particle compacting effects on these particle-fluid interactions and on the turbulence modulations.

The equation of motion of an individual particle (ith particle) is given by

$$m_{pi}\frac{d\mathbf{u}_{pi}}{dt} = f_{gi}(\mathbf{u}-\mathbf{u}_{pi}) + \sum_{j\neq i} f_{pij}(\mathbf{u}_{pj}-\mathbf{u}_{pi}) + m_{pi}\mathbf{g} \tag{2.5}$$

Where f_{pij} is the momentum transfer coefficient due to the collision between the ith particle and the jth particle. Applying regional-averaged theorem [Delhaye, 1981] to Equation (2.5) yields the cross-sectional averaged momentum equation of solids as

$$G_p\frac{dU_p}{dz} = F_D - \frac{\tau_{wp}l_{wp}}{A} - \alpha_p\rho_p g - F_C \tag{2.6}$$

where the term on the left hand side of the equation denotes for the solids acceleration; the first term on the right hand side of the equation is the particle-fluid interfacial force; the second term stands for the particle-wall friction; the third term is for the gravitational force; and the last term is the cross-sectional averaged collision force, which is defined by

$$\mathbf{F}_C = \frac{1}{A}\int_A \left[\sum_i\sum_{j\neq i} f_{pij}(\mathbf{u}_{pj}-\mathbf{u}_{pi})\right] dA \tag{2.7}$$

Combining Equation (2.3) and Equation (2.7) yields the cross-sectional averaged momentum equation of gas-solids flow in the riser as

$$-\frac{dp}{dz} = \frac{\tau_w l_w}{A} + \frac{\tau_{wp}l_{wp}}{A} + (1-\alpha_p)\rho g + \alpha_p\rho_p g + G\frac{dU}{dz} + G_p\frac{dU_p}{dz} + F_C \tag{2.8}$$

It is noted that, in the acceleration and dense phase transport regions, F_C represents the axial stress force of solids or compression stress of solids, which are not zero. In order to solve Equation (2.8), a mechanistic model of F_C has to be developed. Unfortunately, due to the complicated off-center collisions that dominate the collisional momentum transfer in fluidization, the development of detailed

mechanistic models that include all collision modules of normal compression and rebounding, sliding, micro-slip, and rolling in fluidization appears to be a formidable task at the current stage.

The cross-sectional averaged energy equation of gas-solid flow in a riser can be expressed by

$$-\frac{dp}{dz}U = G_p U_p \frac{dU_p}{dz} + GU\frac{dU}{dz} + \Gamma + Gg + G_p g \tag{2.9}$$

Where Γ represents the energy dissipations that include (1) the frictional loss between gas and solids; (2) the frictional loss between gas and wall and between solids and wall; and (3) the collisional energy dissipation from inelastic normal compression and rebounding, sliding, non-sliding micro-slip and rolling. Equation (2.9) clearly indicates that the total energy input (characterized by the product of gas velocity and axial pressure gradient) is converted to the increase of kinetic energy of gas and solids via the phase acceleration, to the increase of potential energy of gas and solids via the vertical transport of gas and solids against gravity, and to the energy dissipations in the transport process via phase frictional loss and collision loss.

Based on Equation (2.1) and given G and G_p, U and U_p are clearly not independent to each other. Therefore the terms involving U in Equation (2.9) can be represented by terms involving U_p, as shown in Equation (2.9a).

$$-\frac{dp}{dz}U = \left(1 - \frac{\rho}{\rho_p}\left(\frac{U}{U_P}\right)^3\right) G_p U_p \frac{dU_p}{dz} + \Gamma + Gg + G_p g \tag{2.9a}$$

It is noted that, given the energy dissipation function $\Gamma=\Gamma(\alpha_p, G, G_p)$ and from the measurements of axial gradient of pressure distribution $dp/dz=f(z)$, the axial

distribution of U_p (and hence solids holdup α_p) can be directly solved from Equation (2.9a).

2.1.2 Energy Equations in Different Flow Regions

It is interesting to take a closer look of the importance of each term in Equation (2.9a), via the order of magnitude comparison, in different regions of gas-solids flows in a riser.

(A) Dilute phase transport region

In the dilute phase transport region where both gas and solid flows can be regarded as fully developed, we have

$$\frac{dU_p}{dz} \approx 0 \qquad \frac{\rho_p}{\rho} \approx O(10^3)$$
$$\frac{\alpha_p}{\alpha} \approx O(10^{-2}) \qquad \Gamma = U_{pt}\frac{dp}{dz} \tag{2.10}$$

Thus Equation (2.9a) reduces to

$$-\frac{dp}{dz} \approx \alpha_p \rho_p g \tag{2.11}$$

Which is the common equation for estimating solid holdups in riser flows.

(B) Solids acceleration region

In the solids acceleration region, we have

$$\frac{U}{U_p} \approx O(10^0) \qquad \frac{\rho_p}{\rho} \approx O(10^3) \qquad \frac{\alpha_p}{\alpha} \approx O(10^0) \tag{2.12}$$

Therefore, Equation (2.9a) is simplified to

$$-\frac{G}{(1-\alpha_p)\rho}\frac{dp}{dz} \approx G_p U_p \frac{dU_p}{dz} + \Gamma + G_p g \tag{2.13}$$

Moreover, if we only consider the friction loss of gas relative motion in Γ, i.e.,

$\Gamma \approx -(U-U_p)\frac{dp}{dz}$, Equation (2.9a) becomes the equation proposed in Louge and Chang's paper (Equation (2.10) in Louge and Chang, 1990).

(C) Dense phase transport region

In the dense phase transport region, we have

$$\begin{aligned} &\frac{dU_p}{dz} \approx 0 && \frac{\rho_p}{\rho} \approx O(10^3) \\ &\frac{\alpha_p}{\alpha} \approx O(10^0) && \alpha_p \approx \text{const} \end{aligned} \tag{2.14}$$

Thus, Equation (2.9a) gives

$$-U\left(\frac{dp}{dz}\right)_{dense} \approx \Gamma + G_p g \tag{2.15}$$

Which clearly shows the inequality between the axial gradient of pressure and solids holdup, as observed in many experimental measurements in this region. It is interesting to apply Equation (2.15) to dense phase fluidized beds where G_p vanishes. In these cases, $U_{mf} < U < U_{mt}$ and the axial gradient of pressure equals the solids weigh in the fluidized bed. Equation (2.15) leads to

$$\Gamma \approx U\alpha_p \rho_p g \qquad \text{at } U_{mf} < U < U_{mt} \tag{2.16}$$

Which shows that all energy input is now dissipated via gas-particle friction and particle collisions in the fluidized bed.

2.1.3 Determination of Energy Dissipation Function

It may be reasonable to assume that the energy dissipation function, $\Gamma=\Gamma(\alpha_p, G, G_p)$, is a strong function of α_p but a weak function of G and G_p, i.e.,

$$\left|\frac{\partial \Gamma}{\partial \alpha_p}\right| \gg \left|\frac{\partial \Gamma}{\partial G_p}\right|, \left|\frac{\partial \Gamma}{\partial G}\right| \tag{2.17}$$

The functional dependence of energy dissipation on solid volume fraction can be checked at two limiting cases, i.e., at the fully-developed dilute transport regime and at the minimum transport condition (the limit of batch operation of fluidized beds). At the limit of dilute transport, all energy dissipation is due to the frictional loss of relative motion of gas passing through the suspended solids, whose formulation is given by Equation (2.19a). At the limit of minimum transport, the energy dissipation can be expressed by the product of superficial velocity and solids weight, as shown in Equation (2.19c). Both expressions of Γ at the limiting cases yield the sole dependence on the solid volume fraction. Consequently, in our modeling, G and G_p are regarded as parameters in the energy dissipation function whereas α_p is the only function variable. Γ may be further expressed as a polynomial function of α_p so that

$$\Gamma = \sum_{i=0}^{N} k_i \alpha_p^i \tag{2.18}$$

where N is the highest power index of the polynomial function.

For a given gas-solids riser flow, the cross-sectional averaged velocity slip between the gas and solids in the dilute transport region can be assumed to be the particle terminal velocity U_{pt}. Since the gas-solid flow is fully developed and the effect of energy dissipation on axial gradient of pressure is negligibly small (assuming the solids concentration is extremely dilute), we have

$$\Gamma = -U_{pt}\frac{dp}{dz} \approx -U_{pt}\alpha_{pf}\rho_p g \qquad \text{at } \alpha_{pf} = \frac{G_p}{\left(\frac{G}{\rho} - U_{pt}\right)\rho_p} \tag{2.19a}$$

and

$$\frac{d\Gamma}{d\alpha_p} = 0 \qquad \text{at } \alpha_{pf} = \frac{G_p}{\left(\frac{G}{\rho} - U_{pt}\right)\rho_p} \tag{2.19b}$$

Now let us consider another extreme case in the dense phase transport region, with the gas phase velocity slightly above the minimum transport velocity. Under this condition, the axial gradient of pressure basically balances the solids weight and $G_p \approx 0$ so that, from Equation (2.15), we obtain

$$\Gamma = U_{mt}\alpha_{pmt}\rho_p g \qquad \text{at } \alpha_{pmt} = 1 - \frac{G}{\rho U_{mt}} \tag{2.19c}$$

and

$$\frac{d\Gamma}{d\alpha_p} = 0 \qquad \text{at } \alpha_{pmt} = 1 - \frac{G}{\rho U_{mt}} \tag{2.19d}$$

Where the minimum transport velocity U_{mt} may be determined by [Bi and Fan, 1992]

$$Re_{mt} = 2.28Ar^{0.419} \tag{2.20}$$

Where Re_{mt} is the Reynolds number defined at U_{mt} and Ar is the Archimedes number.

Equations (2.19a) to (2.19d) enable us to determine a third-order polynomial function for the estimation of energy dissipation. The coefficients for the energy dissipation function are thus obtained as:

$$k_0 = U_{pt}\alpha_{pf}\rho_p g + \frac{\alpha_{pf}^3\rho_p g(U_{mt}\alpha_{pmt} - U_{pt}\alpha_{pf})}{(\alpha_{pf} - \alpha_{pmt})^3} \quad k_1 = \frac{6\alpha_{pf}\alpha_{pmt}\rho_p g(U_{mt}\alpha_{pmt} - U_{pt}\alpha_{pf})}{(\alpha_{pf} - \alpha_{pmt})^3}$$

$$k_2 = \frac{-3(\alpha_{pf} + \alpha_{pmt})\rho_p g(U_{mt}\alpha_{pmt} - U_{pt}\alpha_{pt})}{(\alpha_{pf} - \alpha_{pmt})^3} \quad k_3 = \frac{2\rho_p g(U_{mt}\alpha_{pmt} - U_{pt}\alpha_{pt})}{(\alpha_{pf} - \alpha_{pmt})^3} \tag{2.21}$$

2.1.4 Partition Functions of Axial Gradient of Pressure

In order to demonstrate the significance of effects of solids acceleration and energy dissipation to the axial gradient of pressure in a gas-solid riser flow, it may be convenient to define the partition functions of axial gradient of pressure. Based on Equation (2.13), the following partition functions of axial gradient of pressure can be defined as

$$\beta = \frac{\frac{G_p g}{U}}{(-\frac{dp}{dz})} \qquad \chi = \frac{\frac{G_p U_p}{U}\frac{dU_p}{dz}}{(-\frac{dp}{dz})} \qquad \delta = \frac{\frac{\Gamma}{U}}{(-\frac{dp}{dz})} \tag{2.22}$$

so that

$$\beta + \chi + \delta = 1 \tag{2.23}$$

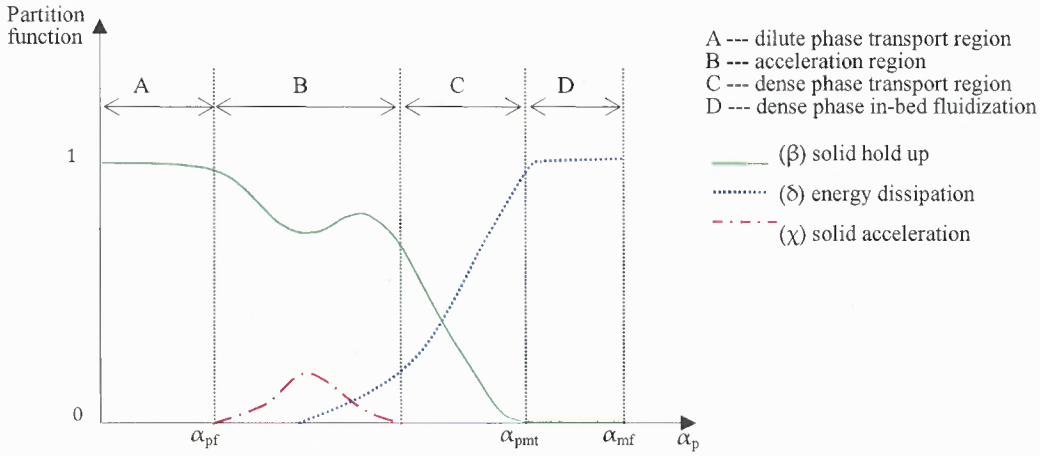

Figure 2.3 General patter of input power partition by β, δ, χ in a riser flow.

Here, β, χ, and δ represent the energy partition for the solid lift up, energy partition for solid acceleration, and energy dissipation partition during the transport, respectively. It is clearly that, in the dilute phase transport region, β = 1 with χ ≅0

and $\delta \cong 0$. In the dense phase transport region, however, $\chi \cong 0$ with $\beta + \delta = 1$. The intrinsic relationships among them can be illustrated by Figure 2.3. In all transport regions in a riser flow, the solids holdup (and the solids velocity) can be solved from above equations, provided that the axial distribution of pressure gradient is given.

The iterative procedure of solving the model equations is outlined in the flowchart of Figure 2.4. The main input includes the operation conditions such as G and G_p, the distribution of axial gradient of pressure, and material properties. For comparison, the apparent solid concentration obtained without the consideration of solids acceleration and energy dissipation is also included in the program.

2.1.5 Model Validation and Discussion

2.1.5.1 Axial Distributions of Solid Velocity and Concentration. Due to the lack of knowledge in the determination of momentum transport coefficients in the solids acceleration and collision-dominated dense phase transport regimes, we bypass the momentum equation in our modeling approach. As a trade-off, we have to use the axial distribution of pressure as an input rather than an output of the model in order to solve for the axial distributions of solid velocity and solid concentration. The following are exemplified modeling results that are solved based on the experimental input of axial distributions of pressure from Pugsley and Berruti (1996), Sun et al. (1999), and Schlichthaerle and Werther (1999).

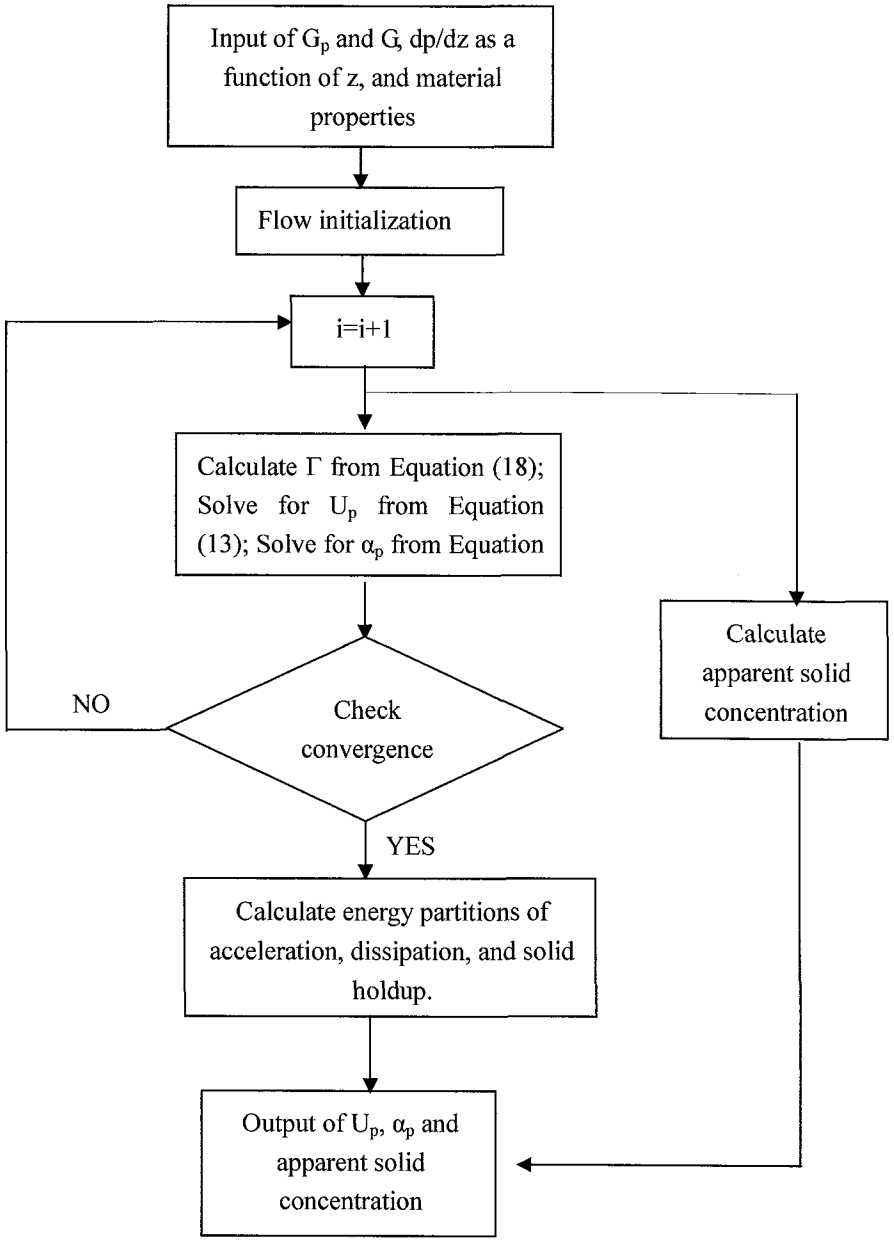

Figure 2.4 Flowchart of model solving procedures.

Table 2.1 Major Experimental Parameters

CASE	MASS FLUX		PARTICLE		RISER		REFERENCE
	G_p kg/m^2.s	G kg/m^2.s	ρ_p kg/m^3	d_p μm	Z m	D m	
1	113	5.1	1460	58	14	0.20	Sun et al. (1999)
2	125	6.4	1460	58	14	0.20	Sun et al. (1999)
3	156	5.1	1460	58	14	0.20	Sun et al. (1999)
4	240	10	2580	208	5	0.05	Pugsley & Berruti (1996)
5	400	10	2580	208	5	0.05	Pugsley & Berruti (1996)
6	700	10	2580	208	5	0.05	Pugsley & Berruti (1996)
7	23	4.8	1500	200	15	0.40	Schlichthaerle & Werther (1999)

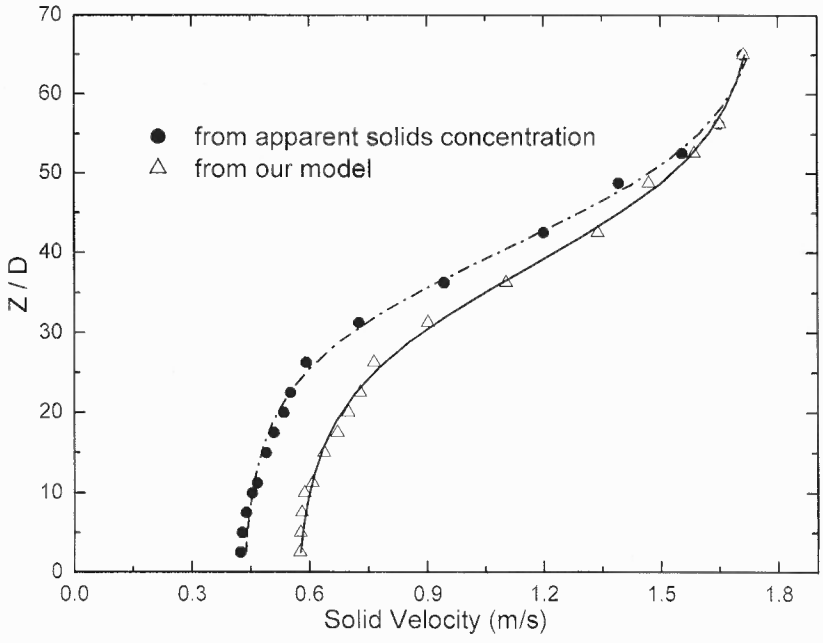

(a) Case 3

Figure 2.5 Axial solid velocity distribution.

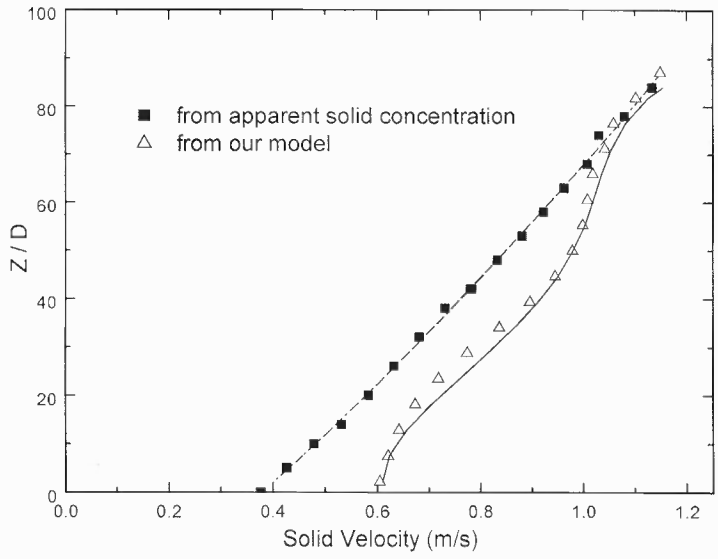

(b) Case 6

Figure 2.5 Axial solid velocity distribution (Continued).

Given distributions of axial gradient of pressure and operation conditions and material properties, based on the energy balance Equation (2.13), we can calculate the axial distributions of solid velocity, as illustrated in Figure 2.5 with two different cases. The corresponding axial distributions of solid volume fraction are obtained from the mass balance Equation (2.1), as shown in Figure 2.5. It is noted that the apparent solid concentration is based on a direct and total conversion from the pressure gradient without any consideration of the effects of solids acceleration and energy dissipation, which represents the traditional method of estimation of solid concentration in riser flows. Figure 2.6 clearly suggests that, without the consideration of solid acceleration and energy dissipation, the solid concentration can be largely overestimated, for example, by more than 30% in the acceleration and dense phase transport regimes. Accordingly, as shown in Figure 2.5, the solid velocity is significantly underestimated.

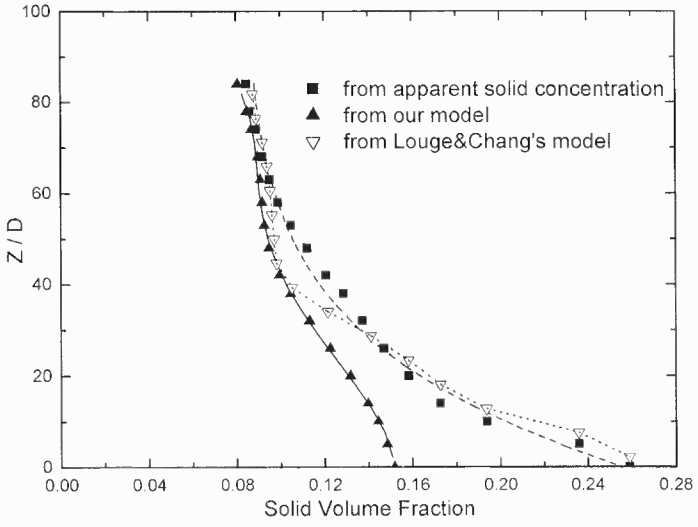

Case 6

Figure 2.6 Axial solid volume fraction distribution.

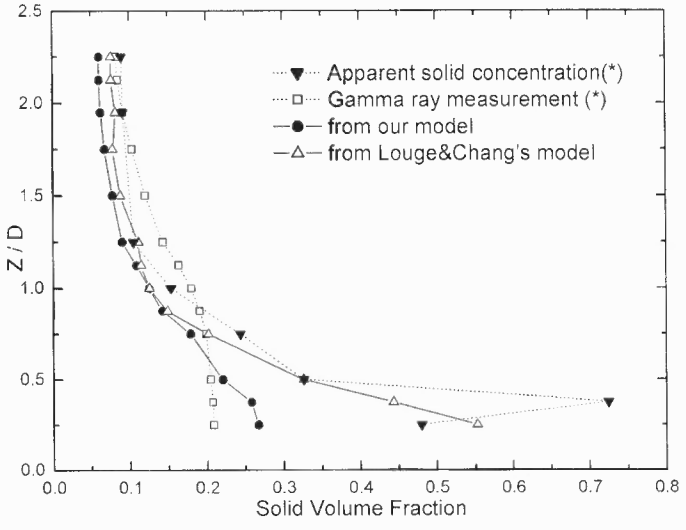

Figure 2.7 Axial solid volume fraction distribution.

(* data are from Schlichthaerle and Werther, 1999)

The underestimation of solid velocity from apparent solid concentration further leads to an overestimation of the solid residence time in the riser flow. Table 2.2 gives the examples of estimated solid residence time from both methods, showing the overestimation of solid residence time in a range of 7 to 20% for the six cases in

this study.

To validate our modeling approach, direct measurements of solid concentration and axial distributions of pressure in the acceleration and dense phase transport regime are very much desired. However, the reported experimental data are very scarce, mainly due to the difficulties and uncertainties in the direct measurement of solid concentration in these regimes. Figure 2.7 shows a reasonably good comparison between the calculated solid volume fraction from our model and experimental results of gamma-ray measurements from Schlichthaerle and Werther (1999), especially in the dense phase regime. The experimental conditions are given in Table 2.1 (case 7). Moreover, the comparison between our model and the model of Louge and Chang (1990) indicates the significance of effect of solid collision.

Table 2.2 Comparison of Calculated Solid Residence Time

Case	$\tau_{p,app}$ (s)	τ (s)	$(\tau_{p,app} - \tau)/\tau$ (%)
1	64	60	6.7
2	50	44.5	12.4
3	112	93	20.4
4	22	20.5	7.3
5	17	15.7	8.3
6	49	42.5	15.3

2.1.5.2 Distributions of Partition Functions. It is important to evaluate the significance of effects of solid acceleration and energy dissipation on the axial gradient of pressure in various transport regimes in a riser flow. The quantitative evaluation can be done by either plotting the axial distributions of partition functions, defined by Equation (2.22), against the riser height (as shown in Figure 2.8(a)) or the distributions of partition functions against the solid volume fraction (as shown in

Figure 2.8(b)). The exemplified calculation shows that, in thedense phase region, the dominant factors leading to total pressure drop are solid lift-up (δ) and energy dissipation (β). In this region, there is little energy consumption on solid acceleration. The energy consumption for solid lift-up is approximately 77%, whereas the energy dissipation by collision and friction reach its maximum value, approximately 23%. In the acceleration region, the energy partition on solid acceleration becomes important, with a maximum value of 20%, whereas the energy dissipation by collisions and frictions may also play an important role. Energy partitions on solid acceleration and energy dissipation are negligibly small in the dilute transport region where the total amount of energy is consumed on solid lift-up.

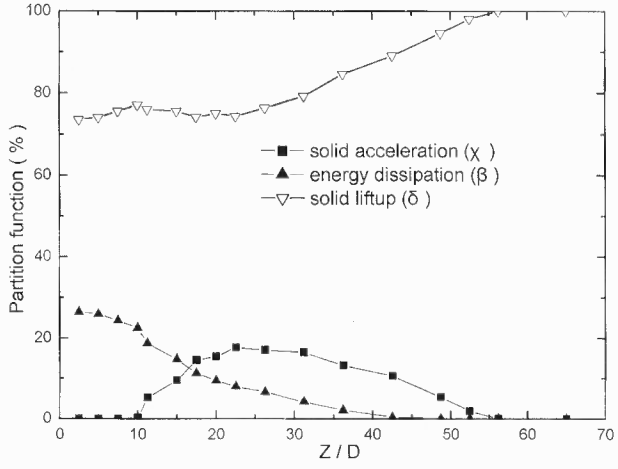

(a) Partition functions versus riser height.

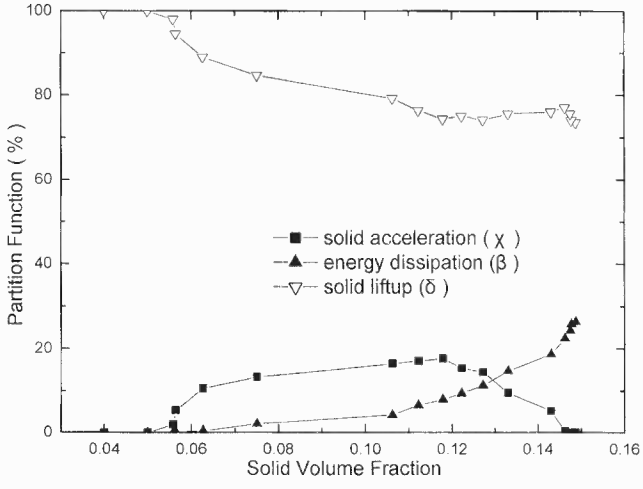

(b) Partition functions versus solid volume fraction.

Figure 2.8 Typical distributions of partition functions (case 3).

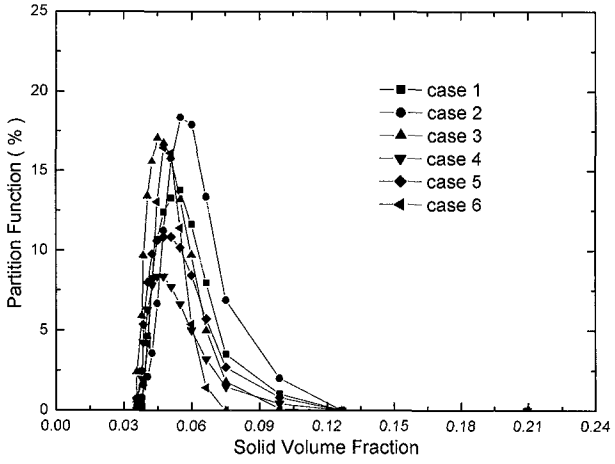

Figure 2.9 Partition function of solid acceleration.

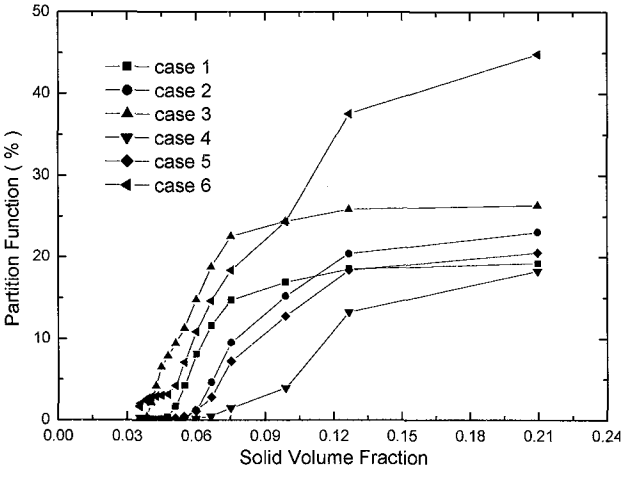

Figure 2.10 Partition function of solid energy dissipation.

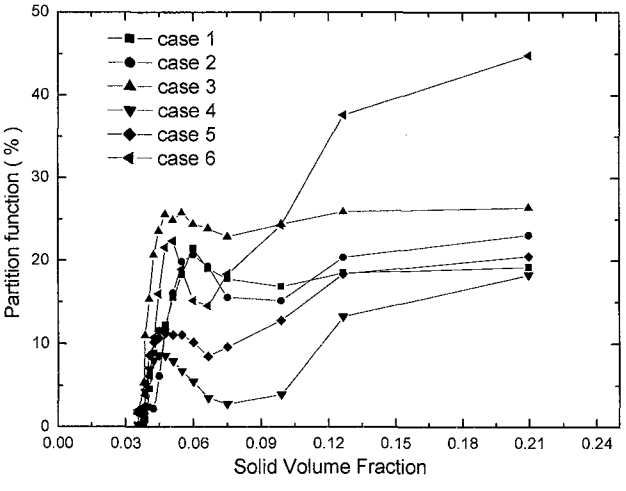

Figure 2.11 Combined partition function of solid acceleration and energy dissipation.

Figure 2.9 shows the partition functions of solid acceleration versus the solid volume fraction under various riser flow conditions. Our calculations show that the energy consumption on the solids acceleration is typically within a range of solid volume fraction from 3.5% to 12%. The partition functions of energy dissipation at various operation conditions are illustrated in Figure 2.10, which shows that the energy dissipation become important when the solid volume fraction is over 5% and, in the dense phase transport regime, it can even consume about 50% of the total energy. Figure 2.11 shows the combined partition functions of solid acceleration and energy dissipation, which are not monotonically increased as the solid volume fraction increases.

In this study, we have developed an energy-based model that considers the effects of solid acceleration and energy dissipation in the estimation of solid velocity and solid concentration in the riser flows. Our model shows that the transport energy is typically partitioned by three basic modes, namely, kinetic energy for solids acceleration, energy dissipation by collisions and frictions, and potential energy for solid lift-up. The combined energy partition of solid acceleration and energy dissipation in the solid acceleration and dense phase transport regimes is typically about 20% and can be as high as 50%. The traditional method of estimation of solid volume fraction from a direct conversion of axial gradient of pressure leads to significant overestimations of solids volume fraction, underestimations of solid velocity, and overestimation of solid residence time in the solid acceleration and dense phase transport regimes. Our calculation further shows that the effect of solid

acceleration is important when the solid volume fraction is in a range from 3.5% to 12% whereas the effect of energy dissipation is important when the solid volume fraction is beyond 5%.

2.2 Hydrodynamic Modeling of Gas-Solid Riser Flows

The actual gas and solids flow in a riser is a multi-dimensional, especially at the bottom of the riser where gas and solids are injected. However, for the concern of phase transport along the riser, a most common modeling approach is to assume that the phase properties vary as function of axial coordinate only, namely, one-dimensional flow (Louge and Chang, 1990). Each phase forms a continuum and the flow is considered to be steady [Adewumi and Arastoopour, 1986].

Consider a gas-solids riser flow as shown in Figure 2.12. The flow is assumed to be steady and isothermal without any chemical reactions, and the solids are spherical, non-porous, and mono dispersed with a uniform material density. The riser flow is characterized by a dense region at the bottom of the riser, a dilute region at the top of riser and acceleration region in between. In the dense phase region, the solids concentration is very high, and the relative motion between the particles is very small. The particle-particle interaction can be very strong compare to particle-fluid interaction in dense phase region. In the acceleration region, the solids particles are accelerated asymptotically towards a state with constant velocity. In the dilute phase region, both the gas and solid lows are fully developed, and the particles are nearly uniformly distributed in the axial direction. In this region, the flow characteristics are invariant with the riser height. Here, we ignore the exit effect at the end of the riser.

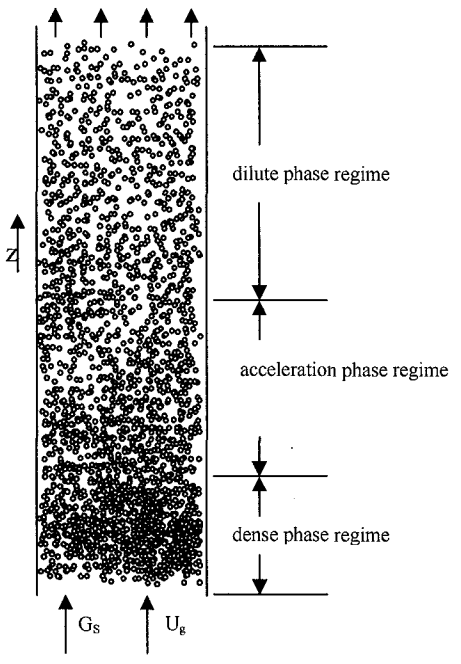

Figure 2.12 Flow regimes in a riser.

2.2.1 Theoretical Model and Closure

2.2.1.1 General Modeling. For a cross-section averaged riser flow, the generalized equations of mass continuity and momentum conservation for both gas and solids phases can be expressed, respectively, as following:

$$\frac{d}{dz}\int \alpha_g \rho_g u_g dA = 0 \tag{2.24}$$

$$\frac{d}{dz}\int \alpha_s \rho_s u_s dA = 0 \tag{2.25}$$

$$-\frac{d}{dz}\int \alpha_g \rho_g u_g^2 dA = \tau_w l_w + \int \alpha_g \rho_g g dA + \int F_D dA + \frac{d}{dz}\int P dA \tag{2.26}$$

$$\frac{d}{dz}\int \alpha_s \rho_s u_s^2 dA = \tau_{sw} l_w - \int \alpha_s \rho_s g dA - \int \gamma dA + \int F_D dA \tag{2.27}$$

where τw is wall shear stress of gas phase, FD is drag force on solids by gas; τsw is wall shear stress of particle; γ is the solid axial compact momentum due to inter particle collisions, which is the normal stress component in solids collisions tensor.

In order to solve the above equations, we should know about the radial profile

of phases, wall boundary conditions, inlet boundary conditions, drag force(F_D) on solid particles, and momentum transfer for the solid axial compact due to inter particle collisions (γ).

2.2.1.2 Modeling with Uniform Radial Profiles. Due to the lack of knowledge of radial distributions of the flow parameters and the mechanisms governing the radial mass and momentum transports of both the gas and solids phases, it is impossible to directly solve the problem with above model. The approximation with uniform radial profiles would make the model the simplest and most convenient to closure the problem. In addition, the wall friction may be neglected (He and Rudolph, 1996).

Assuming the gas can be treated as ideal gas and under isothermal condition, the density of gas at any riser height can be related to the local static pressure, which is expressed by:

$$\rho_g = \frac{P}{P_{atm}} \rho_{atm} \tag{2.28}$$

The mass continuity equations of gas and solids can thus be expressed by:

$$\alpha_g \rho_g U_g = G_{g0} \qquad \alpha_s \rho_s U_s = G_{s0} \tag{2.29}$$

The momentum equation of gas phase can be simplified from (2.26);

$$-\frac{dP}{dz} = \alpha_g \rho_g g + \alpha_g \rho_g u_g \frac{dU_g}{dz} + F_D \tag{2.30}$$

This shows that, the pressure gradient is balanced against gas weight, gas acceleration and drag force.

The momentum equation of solids phase can be expressed based on (2.27);

$$F_D = \alpha_s \rho_s g + G_s \frac{dU_s}{dZ} + \gamma \tag{2.31}$$

Equation (2.31) shows that, the particle-fluid interfacial force balances for the solids weight, solids acceleration, and a compact momentum from solids collisions that constrain the solids acceleration. To solve the above equations, we must know intrinsic correlations for γ and F_D.

2.2.1.3 Constitutive Equations. In a dense-phase fluidized bed the statistical average solid velocity is null. Wake effects are very much damped in this flow region. The particle-fluid interfacial force is typically expressed by Richard-Zaki equation, which is constituted purely based on the modifications of the drag force on a single particle in the flow.

$$F_{D0} = \frac{18\mu}{d_s^2} \cdot \frac{\alpha_s}{(1-\alpha_s)^n} \cdot (U_g - U_s) \tag{2.32}$$

where n - Richard-Zaki index (with an experimental value around 4 ~ 5).

In the solids acceleration regime, the stabilized wake effect becomes important (Zhu et al. 1994; Joseph, 1993), which leads to a reduction in drag force of trailing particles of collision pair. Hence, the modified drag force may be expressed by:

$$F_D = k_1 F_{D0} \tag{2.33}$$

K_1 is the coefficient of wake effect of the neighboring particles on the particle-fluid interfacial force (Zhu et al. 1994), which is represented as,

$$k_1 = 0.3 \cdot \left(1 - (1-A) \exp\left[B \cdot \left(\sqrt[3]{\frac{\pi}{6\alpha_s}} - 1 \right) \right] \right) \tag{2.34}$$

In a dense phase region, particles collide with each other and the loss of kinetic energy due to inter-particle collision cannot be neglected. This may be reflected by adding an overlooked term in the momentum transfer of solids that

actually controls the non-free solids acceleration in this region. As a matter of fact, this non-free solids acceleration in the dense phase regime has been well known from experimental observations and measurements of solids volume fraction, i.e., the lower portion of the S-shaped voidage distribution along the riser. However few efforts of mechanistic modeling on this non-free acceleration have been reportedly attempted. The main factors which govern this new term of axial momentum of compacting solids with an acceleration tendency include:

i) Constraint to local solids acceleration, which is enhanced with both solids concentration and slip velocity.

ii) Effect of compacting that increases the local solids concentration and dissipates kinetic energy via compacting collisions.

iii) Physical properties of the particle and fluid, which not only affect the flow ability but also cause the formation of phase heterogeneity in forms of cluster or agglomerates.

Based on the above information, a simple model for axial compact momentum of solids phase (γ) is proposed as:

$$\gamma = \frac{\rho_s g}{U_{pt}}(1-k_2)\frac{k_1 k_3 \alpha_s}{(1-\alpha_s)^4}(U_g - U_s) \tag{2.35}$$

where k_2 & k_3 represent, respectively, the cascading effect of particles distribution structure and acceleration factor which are dominated by the solids volume fraction, as give below:

$$K_2 = \left[1-\exp\left(-\left(\frac{\alpha_s+0.2}{\alpha_{sc}}\right)^2\right)\right] \tag{2.36}$$

$$K_3 = \frac{1}{\pi}\tan^{-1}\left[\frac{24-100\cdot\alpha_s}{0.9}\right]+0.5 \tag{2.37}$$

It is noted that K2 represents an S-shaped axial profile for cross-section averaged voidage in riser (Li and Kwauk, 1980).

With the sub-models of the intrinsic mechanisms of the particle-fluid interfacial force and collisional momentum term, the coupled equations (2.29) to (2.31) now can be solved to find four coupled variables, namely pressure (P), solids volume fraction (α_s), gas velocity (U_g) and solids velocity (U_s), which are the essential parameters to understand a gas-solids riser flow. The input boundary conditions to simulate our model results are corresponding to the experimental conditions.

2.2.2 Results and Discussion

In this section the proposed model is first validated by directly comparing the model predictions with available experimental data. Then the model is used to investigate the parametric effect of different operation conditions, including solid mass flux and gas velocity, on axial gradient of pressure, solid volume fraction and phase velocities.

2.2.2.1 Model Validation. In order to validate the proposed model, the model predictions of solid volume fraction and axial distribution of pressure are directly compared with the experimental data of different research groups (Arena et al. 1985, Knowlton, 1995; and Pugsley and Berruti, 1996). In order to examine the model robustness and rationality of working conditions, the relevant parameters of experiments were purposely chosen in a wide range for particle type (including glass beads, FCC particles, sand), gas velocity (from 4 to 11 m/s) and solid mass flux (from 199 to 700 kg/m2.s). The detailed operating conditions of the experiments used for the comparison of the proposed model predictions are shown in Table 2.3.

As a part of the model validation, the model predictions of axial distribution of solids volume fraction are first compared with two set of experimental data of (Arena et al. 1985) in which solid mass flux changes from 199 to 600 kg/m2s. Besides, all following figures are in dimensionless format to make the comparison more representative.

Table 2.3 Experimental Parameters for Model Validation

References	Particle Type	d_p (μm)	G_s (kg/m^2.s)	U_g (m/s)	ρ_s (kg/m^3)	Z (m)	D (m)
Arena et al. 1985	Glass Beads	88	600	7	2600	6.4	0.041
Arena et al. 1985	Glass Beads	88	199	7	2600	6.4	0.041
Pugsley and Berruti, 1996	Sand	208	400	8.5	2580	5.0	0.05
Pugsley and Berruti, 1996	Sand	208	700	8.5	2580	5.0	0.05

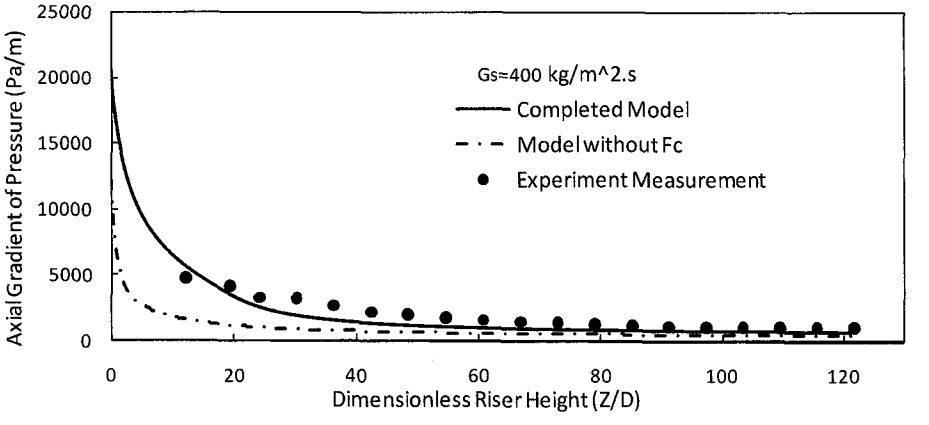

(a) Case 1

Figure 2.13 Model validation of axial profile of solid volume fraction (Arena et al. 1985).

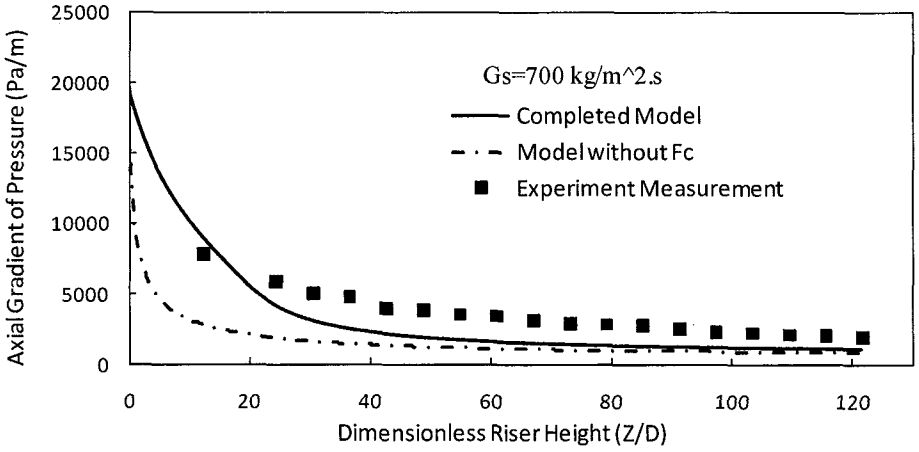

(b) case 2

Figure 2.13 Comparison of model predictions and experimental results of axial profile of solid volume fraction (Arena et al. 1985) (Continued).

As shown as both of cases in Figure 2.13, the model predictions for solid volume fraction fit the experimental data (Arena et al. 1985) satisfactorily along the riser height. Basically the distribution of solid volume fraction along riser height presents typical S-shape. It means that in the lower part of the riser, the flow is in the dense phase regime because of the low initial solids velocity. Then the solids are gradually accelerated under the interaction with gas phase, and finally reach the relatively steady and dilute regime at the upper part of riser. It is shown in Figure 2.13 that, in the dilute phase transport regime, solid volume fraction remains constant in the rest of the riser height for both of the cases. The model predictions demonstrated the same trend for the solid volume fraction as experimental measurement and quantitatively matched with their values along the whole riser with reasonable accuracy. However, for very low solids mass flux, solids back-mixing will have significant influence on the overall flow structure, which can not be neglected. Special attention should be given to the amount of solids back-mixing and variation of wall

thickness. This part of study will be further covered in our next step study.

In Figure 2.13 we also compared the model prediction of solid volume fraction with/without the consideration of collision force. When the model did not consider the collision force, the solids phase picked up the velocity very fast and quickly reach the steady dilute phase. From the comparison, the function of the collision force can be described as placing certain limitation on the acceleration of the solid phase in a swamp of fluidized particles, especially in the dense and acceleration regions of the riser. In the dilute phase, due to the relatively large distance among particles, the collision force becomes very weak and its influence on the flow structure could be reasonably neglected.

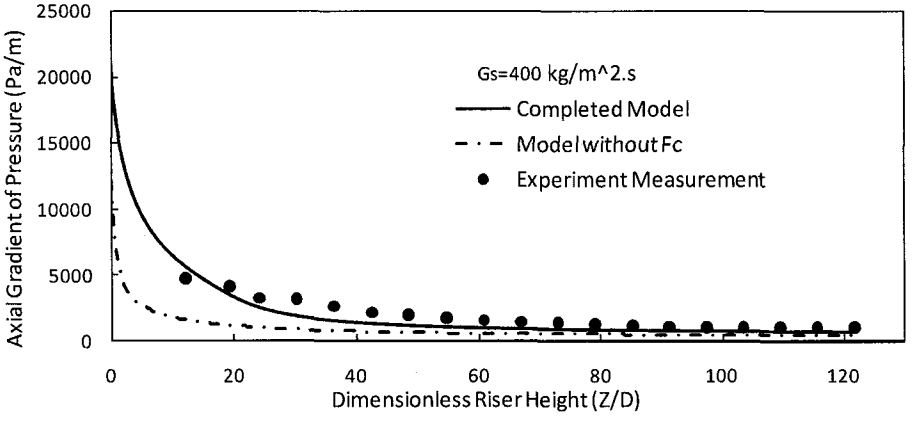

(a) case 3

Figure 2.14 Model validation of axial pressure gradient profile (Pugsley and Berruti, 1996).

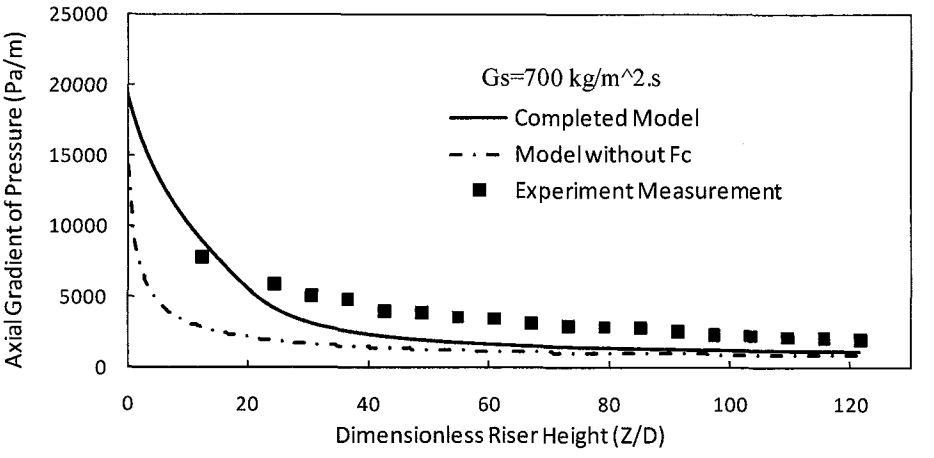

(b) Case 4

Figure 2.14 Model validation of axial pressure gradient profile (Pugsley and Berruti, 1996) (Continued).

Similarly, the comparison of model prediction of axial pressure gradient w/o consideration of collision force is also shown in Figure 2.14. It was shown that when the collision force was not included in the model, the pressure drop gradient is much larger than the case when collision force was considered. From energy conservation point of view, some portion of the total mechanical energy will be consumed by the inter-particle collision in the form of energy dissipation, as shown in the result of completed model prediction.

2.2.2.2 Parametric Study. In order to extend the model applications beyond experimental conditions, a parametric study is carried out to study the effect of gas velocity and solids mass flux on axial gradient of pressure, solid volume fraction, and phase velocity. We tested the proposed model in conditions that the gas velocity changes from 6 to 20 m/s and solid mass flux changes up to 1000 kg/m^{2}s.

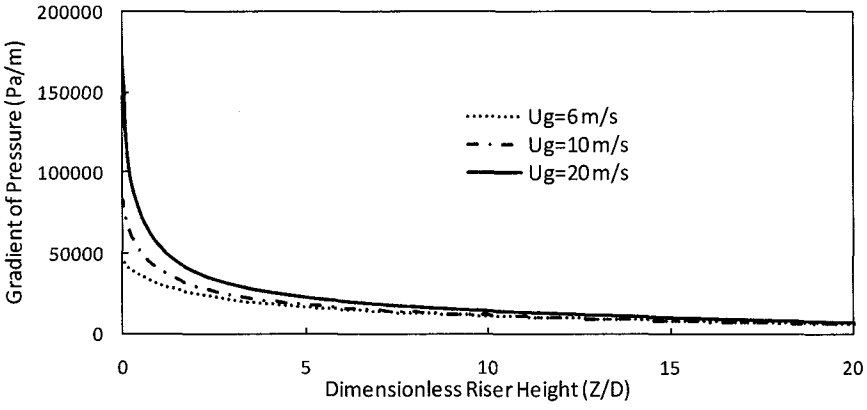

(a) Axial gradient of pressure

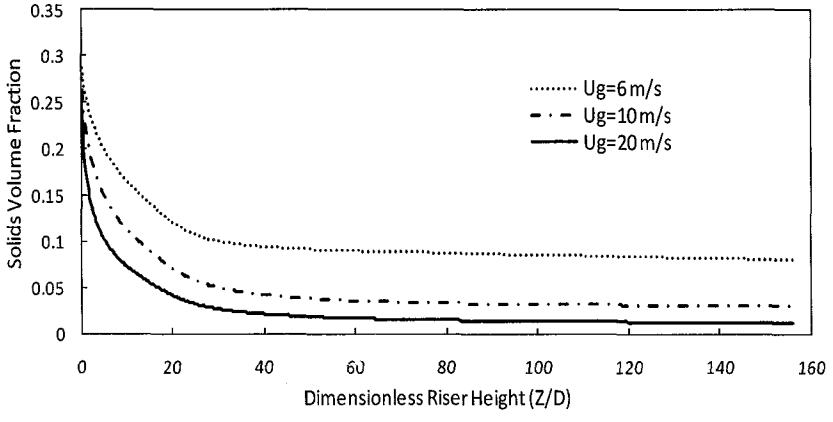

(b) Solid volume fraction

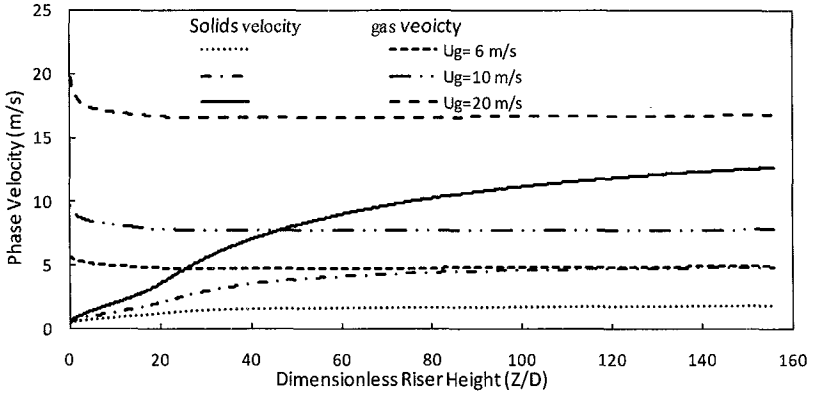

(c) Solid and Gas Velocity

Figure 2.15 Effect of gas velocity on flow pattern (G_s= 382 kg/m^2.s).

Figure 2.15(a), (b) and (c) shows, the effect of gas velocity on axial gradient of pressure, solid volume fraction and solid velocity, when initial gas velocity changes

from 6m/s to 20 m/s with constant solid mass flux at 382 kg/m^{2}s.

It is seen from Figure 2.15(a) that, for given constant mass flux rate as the gas velocity is decreased, the total pressure drop also decreases along the whole riser, especially in the lower part of the riser. This is because more intensive energy dissipation due to inter-particle collision when the gas velocity is relatively high. However in the upper part of the riser, the pressure drop gradient is almost constant, because the major contribution to the pressure drop in this regime is due to friction loss and solid gravity, which don't change significantly with the change of gas velocity.

Figure 2.15(b) shows the effect of gas velocity on axial profile of solid volume fraction at constant solid mass flux. In the dense phase regime as the gas velocity increases the momentum gained by the solid phase leads to the decrease in solid volume fraction in this zone. While the flow is in the dilute transport regime, the solid volume fraction is almost remains constant, which indicates the fully developed solid-gas flow. However, for different initial gas velocity, the solid volume fraction in the dilute phase is quite different because the solid momentum gained from gas phase is different, so the final solid velocities are also different. With decrease in gas velocity, the solid volume fraction increases and pressure drop is almost remaining constant in fully developed transport region.

Figure 2.15(c) shows the axial solid and gas velocity profiles along the riser. It is interesting to notice that the solids velocity in dense phase region is almost constant, because the particles are packed and have no space for acceleration in dense phase

region. However in acceleration phase region, as the solid volume fraction decreases, the particles are unlocked above the minimum fluidization velocity and are free to accelerate so, the solids particle velocity increases in this region with increase of gas velocity. The solids velocity profiles follow the typical S-shape curve. As for the gas velocity profile, it is the combined effect of change of solid volume fraction and pressure drop, which present a little bit different patterns for different initial gas velocity.

Till now, Figure 2.15(a), 2.15(b) and 2.15(c) have presented how the flow pattern, including axial pressure gradient profile, axial solid volume fraction, gas and solids velocity, will be influenced by the variation of initial gas velocity. In the next part, we will discuss the effect of variation of the solids mass flux on overall flow patterns.

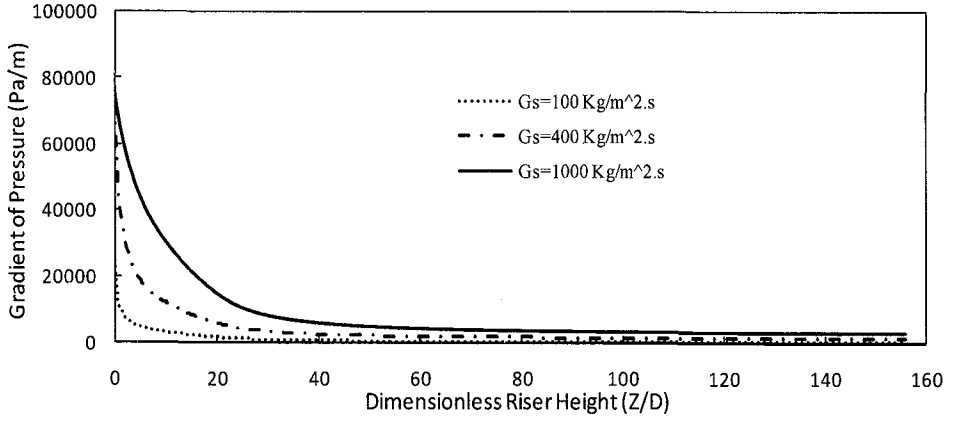

(a) Axial gradient of pressure

Figure 2.16 Effect of solid mass flux variation on flow pattern (U_g = 7 m/s).

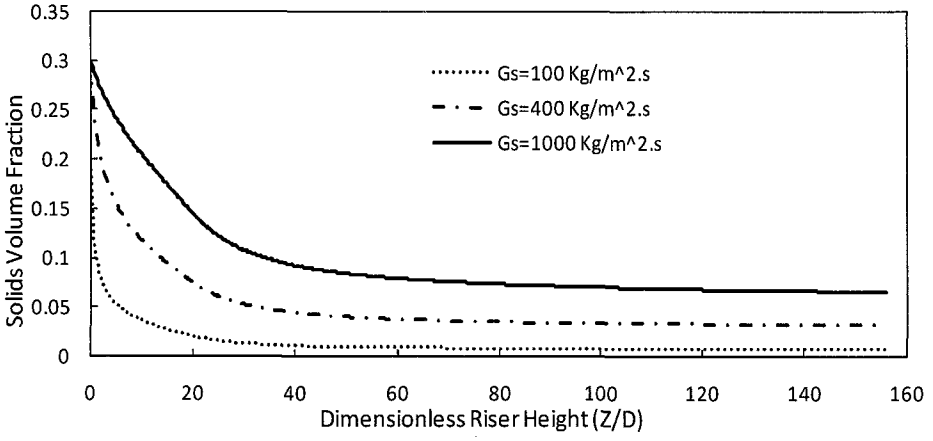

(b) Solid volume fraction

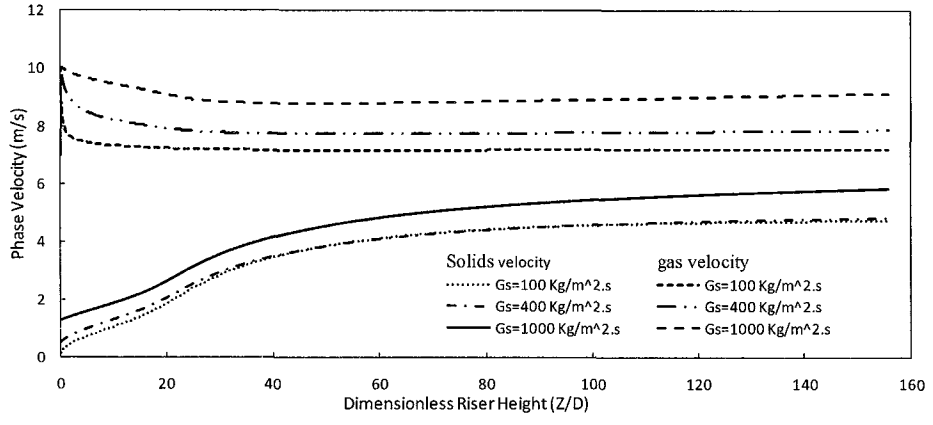

(c) Gas and Solid velocity

Figure 2.16 Effect of Solid mass flux variation on flow pattern (Continued).

Figure 2.16 shows the effect of solid mass flux variation on flow patterns. The gas velocity is kept at 7 m/s and the solid mass flux are at 100, 400 and 1000 kg/m^{2}s respectively. It reveals that, increasing in the solids mass flux causes higher pressure drop in the dense and acceleration regime if other parameters are kept unchanged, which is because of more intensive inter-particle collision. Regarding with the solid volume fraction and solid velocity, both of them still present the same S-shape as shown in Figure 2.16(b) and 2.16(c). The solid volume fraction decreases very fast with decrease of solids mass flux in the dense phase region. The solid volume fraction

in the dilute phase regime remains constant but decreases with decrease in solids mass flux, which is shown in Figure 2.16 (b).

2.3 New Understanding of Solids Back-Mixing

When the gas-solid riser flow is in the state of fast fluidization, the flow structure typical is so called "wall-annulus" region as shown in Figure 2.17(a). The solids volume fraction and solids velocity are typical S-shaped distribution over the whole length of the riser at then center of the riser, with a back-mixing solids film near the wall in which solids concentration may be quite high. Under some circumstances, the instantaneous solids volume fraction can be equal to minimum fluidization volume fraction. Furthermore, the solids flow in this near-wall region move downward, which will enter the main steam flow at the bottom mixing region. In this part of study, an attempt has been made to characterize the back-mixing solids flow and center upward flow.

2.3.1 Correlations for Solids Back-Mixing and Upward Flow

As we know, both the amount of solids back-mixing and wall region thickness are heavily dependent of riser operation conditions and riser geometry, such as solids circulating rate, gas velocity, riser diameters, and etc. Besides, they also the strong function of riser height. Although their importance on the riser flow structure has been recognized for a long time, there is no specific approach to quantify them.

From the Figure 2.17(b), we can easily understand that the solids mass flow rate in the center upward flow is far more than the pure input solids circulation rate,

however, it is the combined values of back-mixing flow rate and circulation rate. The effective cross section area for the upward flow will be total riser cross-section area subtracting wall region area.

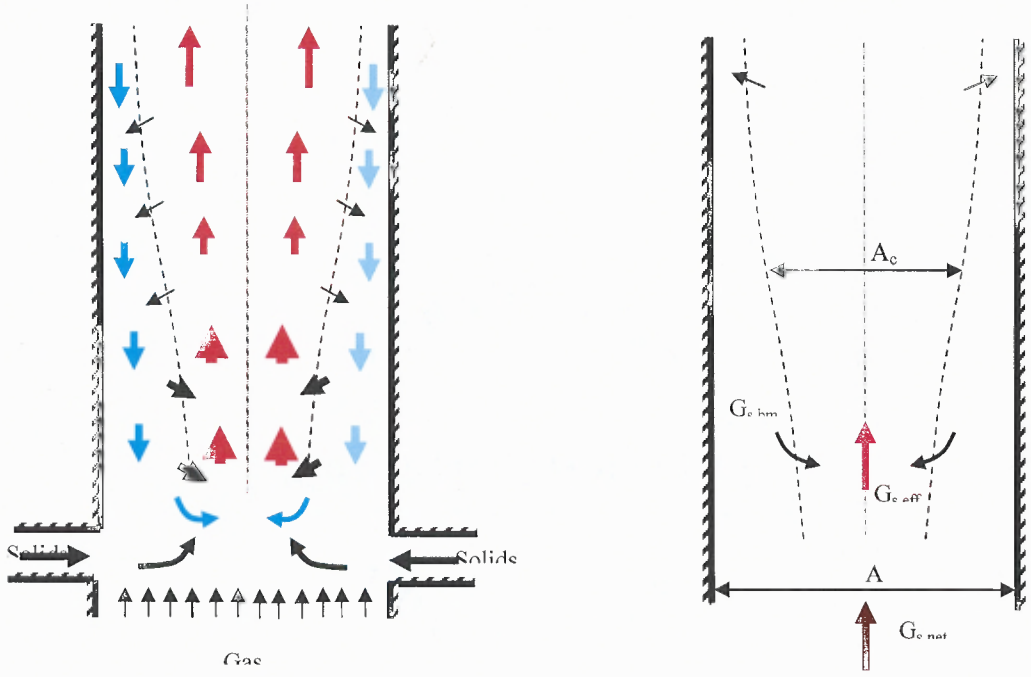

(a) (b)

Figure 2.17 Solids flow structure in riser.

Let's define R as the back-mixing ratio, which means the ratio of back-mixing mass flux over input solids mass flux.

$$R = \frac{\dot{m}_{s,bm}}{\dot{m}_{s,net}} \tag{2.38}$$

where $\dot{m}_{s,bm} = \alpha_s \rho_s U_s A_w$

$\dot{m}_{s,net} = \alpha_g \rho_g U_g A_c$

Considering the mass balance of solid phase, we have,

$$G_{s,eff} \cdot A_c = \left(G_{s,net} \cdot A + G_{s,bm} \cdot A_W\right) = (R+1) \cdot G_{s,net} \cdot A \tag{2.39}$$

Here, R is a function of input solids mass flow rate and riser height.

Since we don't have enough information to determine the center upward flow cross section area, as the first attempt to address this problem, we can use a three-order polynomial expression to characterize this cross section area which is assumed to be the function of riser height only.

The boundaries conditions used to determined the polynomial correlations are listed as following,

$$A_c\big|_{z=0} = \frac{A_0}{4}, \qquad A_c'\big|_{z=0} = 0$$
$$A_c\big|_{z=top} = \frac{9A_0}{16}, \qquad A_c'\big|_{z=top} = 0 \tag{2.40}$$

Based on above four boundary conditions, the three-order polynomial correlation can be defined as

$$A_c = \frac{A_0}{4} + \frac{15A_0}{16z_{top}^{\ 2}}z^2 - \frac{5A_0}{8Z_{top}^{\ 3}}z^3 \tag{2.41}$$

Since the back-mixing ratio R is the strong function riser height and solids circulation rate, we can predefine the correlation as:

$$R(G_{s,net}, z) = a(G_s)^{-n} \cdot (k_0 + k_1 z + k_2 z^2 + k_3 z^3) \tag{2.42}$$

All the boundaries used to determine the above predefine correlation are listed below:

$$R(G_{s,net}, z)\big|_{z=0} = R(G_{s,net}), \qquad \left.\frac{dR(G_{s,net}, z)}{dz}\right|_{z=0} = 0$$
$$R(G_{s,net}, z)\big|_{z=top} = 0, \qquad \left.\frac{dR(G_{s,net}, z)}{dz}\right|_{z=top} = 0$$
$$R(G_{s,net}, z)\big|_{G_{s,net}=400} = 0.3, \qquad R(G_{s,net}, z)\big|_{G_{s,net}=30} = 50 \tag{2.43}$$

After simple mathematical derivation, the expression of the back-mixing ratio

$R(G_{s,net},z)$ can be defined as:

$$R(G_s,z)=170547\cdot G_s^{-2.21}\cdot(1-\frac{3Z^2}{Z_1^2}+\frac{2Z^3}{Z_1^3}) \tag{2.44}$$

Once we have the correlations to quantify the upward flow cross-section area and back-mixing flow mass flow rate, we can revise the continuity equation of mass balance as:

$$\frac{d(\alpha_s\rho_s U_s A_c)}{dz}=\frac{m_{net}}{\rho_s}\cdot\frac{dR(G_s,z)}{dz} \tag{2.45}$$

$$\frac{d(\alpha_g\rho_g U_g A_c)}{dz}=0 \tag{2.46}$$

As combined with the momentum equation in previous riser hydrodynamic model, the model prediction results can be improved, especially for the low solid mass circulation rate conditions.

2.3.2 Model Prediction Comparison and Validation

The experiment data used for validating our model prediction is from literature (Schlichthaerle & Werther, 1999). The solids circulation rate in this experiment is as low as 23 kg/m^{2}s and gas velocity is about 4 m/s. Figure 2.18 gives the comparison among this improved model prediction, previous model prediction, and experimental measurement.

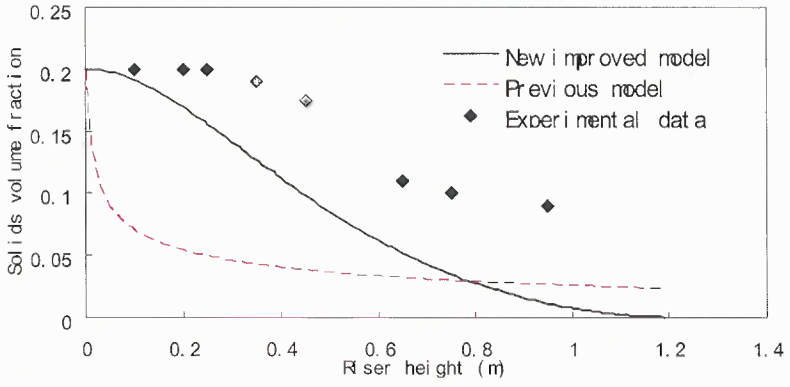

Figure 2.18 Model predictions vs. experimental measurement.

We can notice from the above Figure 2.18 that the new improved model prediction of solids volume fraction matches with the experimental measurement data much better than the previous along the whole riser, especially in the lower dense phase region. Under this extreme low solid circulation rate conditions, without the consideration of strong solids back-mixing from the wall region and the effective upward flow cross section area changes, the model can't give the reason prediction on the flow hydrodynamics.

CHAPTER 3

HETEROGENEOUS STRUCTURE OF RISER FLOW W/O REACTION

With the further understanding of solid collision and acceleration, in order to soundly interpret the well-known "core-annulus" two-zone flow structure and newly discovered "core-annulus-wall" 3-zone structure, a comprehensive modeling of continuous gas-solids flow structure both in radial and axial directions has been presented. In order to investigate the different riser inlet configuration's effects on gas-solid mixing in dense region and improve the uniform inlet condition assumption in above models, a systemically study regarding with different inlet conditions have been done based on commercial package- Fluent. Upon further understanding in the inlet condition's effect, outputs of FLUENT simulation are directly combined with model approach in order to yield better results.

3.1 Formation Mechanism of Heterogeneous Flow Structure

Let us examine the phenomenological structures of gas-solids riser flows with uniform inlet flow conditions, as shown in Figure 3.1. The commonly understood parts of the heterogeneous flow structure consist a dilute phase transport in the core-annulus region near the top of the riser, a dense phase transport in the core-annulus region near the bottom of the riser, a layer of downwards moving solids near the wall for most part of the riser except for the entrance region, and a uniform upwards moving gas-solids flow at the riser inlet. The parts of the heterogeneous flow structure that require further explanation include the detailed flow structural and behavioral information right after the flow entrance, the counter-flow mixing between the downwards moving solids and the

upwards moving solids in the wall region near the entrance, the structural transition in the solids acceleration region, and the flow structure dependency of the pressure drop distribution.

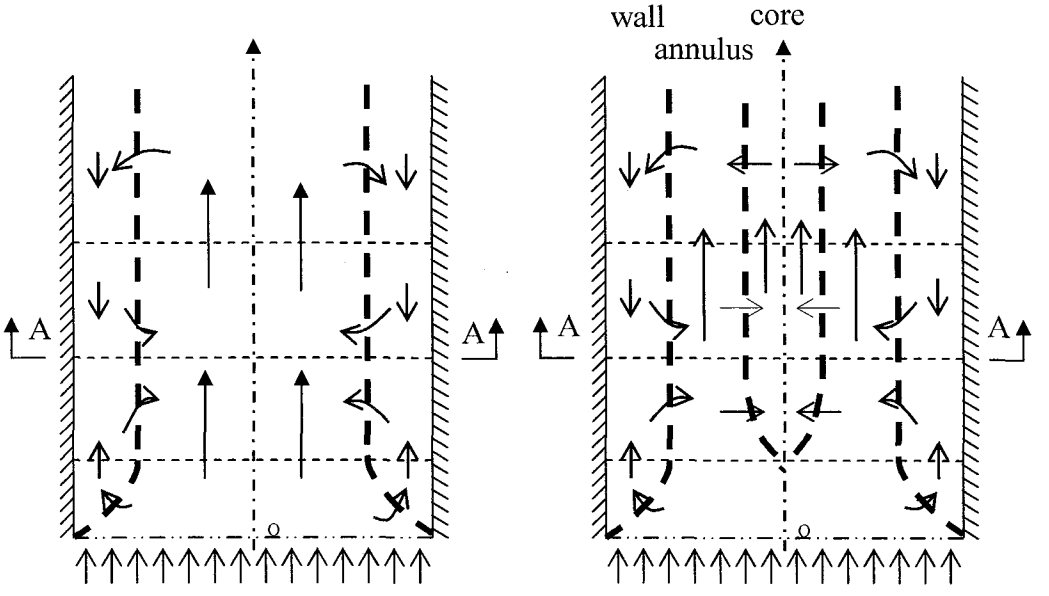

(a) Core-annulus (wall) model (b) Core-annulus-wall model

Figure 3.1 Heterogeneous flow structures in risers.

From the phenomenological consideration, a wall region of dense solids concentration has to be developed from the riser bottom because the averaged gas velocity in the wall region becomes too low to support upward moving solids due to the friction between riser wall and gas-solids flow. At a certain bed height, the solids in the wall region have to exhaust all their initial upward momentum and begin to fall due to gravity. At this location the averaged solids velocity in the wall region is null. Thus, in the bed section near this height, all solids from the upper wall region or from the lower wall region are forced to migrate inwardly towards the riser column center (Rhodes, et al. 1994). In a high convection riser flow (i.e., at a high fluidization velocity and low solids

loading) with little or moderate backflow of solids, the inwardly migrating solids are all entrained into the flow with few residual solids reaching the center of the riser. In this case, the flow pattern is commonly known as "core-annulus" two-region flow, where the radial solids concentration gradually decreases towards the centerline of riser, as illustrated in Figure 3.1(a).

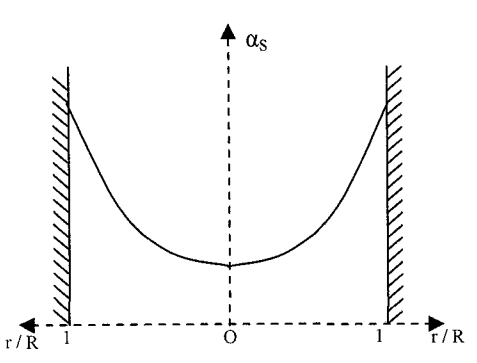

(c) solids concentration (core-annulus)

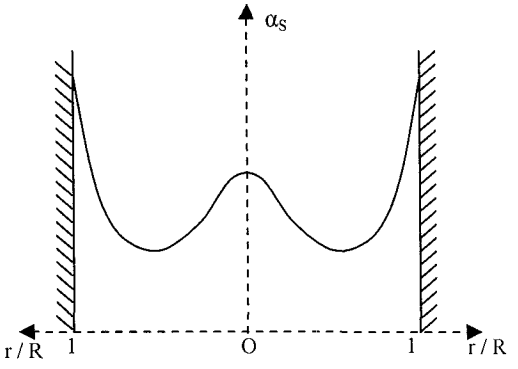

(d) solids concentration (wall-core-annulus)

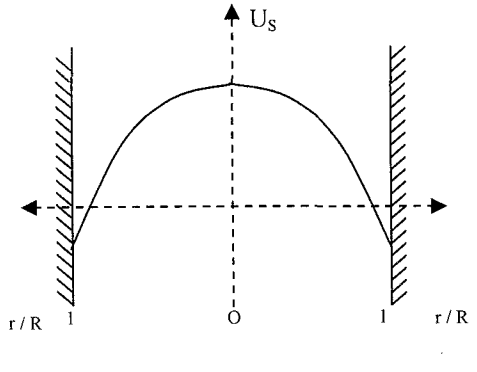

(e) solids velocity (core-annulus)

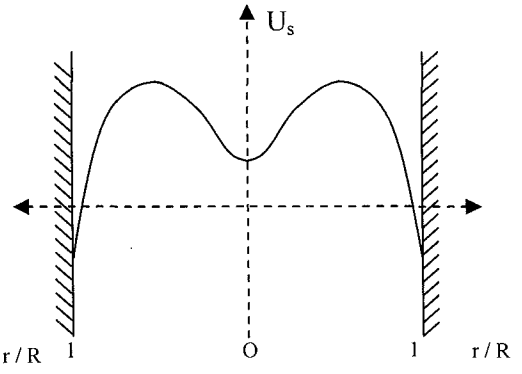

(f) solids velocity (wall-core-annulus)

Figure 3.1 Heterogeneous flow structures in risers (in A-A plane) (continued).

In other cases, especially with low fluidization velocities, part of the inwardly migrating solids may reach the central axis of riser. Due to the axial symmetry of a cylindrical riser, a dense core region must be formed, as shown in Figure 3.1(b). Required by a nearly-equal axial pressure gradient in all regions at the same bed height, the gas

velocity in the core tends to be lower than that in the annulus where the solids concentration is relatively leaner. The slower moving gas in the core results in a lower acceleration of solids in the core region, and hence preserves this core-annulus-wall structure with a relatively higher solids concentration at the core along the riser. In the mean time, based on the mass balance of solids, the downwards moving solids in the wall region in the upper part of a riser must come from those solids in the annulus and core. Hence, in the upper part of the riser, the solids migration into the wall yields depletion in solids concentration, which is severer in the core than in the annulus. Therefore, near the top of a riser, a core-annulus-wall structure technically still exists, yet it resembles the commonly known core-annulus two-zone structure. Thus, the formation mechanisms of the core-annulus and core-annulus-wall structures can be fully explained.

Figure 3.1 also shows the schematic radial distributions of solids concentrations and solids velocities at an imaginary A-A plane in Figure 3.1(a) and 3.1(b). The core-annulus structure has a typical paraboloidal distribution of solids concentration at any cross section, with the solid concentration in the wall region much higher than that in the core, as shown in Figure 3.2(c). Whereas, for the new revealed wall-core-annulus structure, there is a peak in solid concentration in the core region. Even with the peak in the core, the solids concentration in the wall may still be the highest in the cross section, as shown in Figure 3.2(d). Accordingly, the radial distributions solids velocities are illustrated in Figures 3.2(e) and 3.2(f), respectively, for cases of core-annular structure and core-annulus-wall structure. It is noted that, due to the wall friction and effect of boundary layers, the solid velocity close to the wall in both structures is not only much lower than that in central of the riser, but also downwards moving under gravity. In a

$$F_C = -\frac{\Gamma - (U_g - U_s)(-\frac{dP}{dz})}{U_s} \tag{3.6}$$

where, Γ represents the energy dissipations due to inter-phase frictional and inter-particle collision.

$$\Gamma \approx \sum_{j=0}^{N} k_j \alpha_s^j \tag{3.7}$$

τ_w and τ_{sw} are respectively the friction stresses between the wall and the gas phase and the solids phase.

For radically uniform flow, the integrals in above equation could be replaced by an averaged value; the closure of the problem for axially heterogeneous flow structure is fulfilled.

3.3 Simplified Three-Zone Model with Uniform Inlet Conditions

3.3.1 Three-Zone Modeling

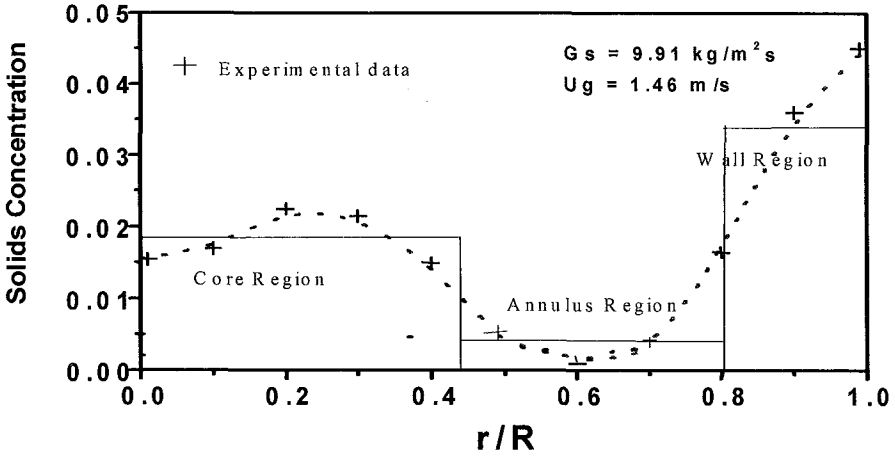

Figure 3.2 Three-zone representation of solids concentration distribution.

flow with the core-annulus structure, the highest solid velocity is located in the center of the riser flow, whereas for a flow with the wall-core-annulus structure, solid velocities in both wall and core region are lower than that in the annulus region.

3.2 General Model Approach

Basically, the flow in a riser could be described with following governing equations based on the mass and momentum conservation of each phase.

$$\frac{d}{dz}(\int_A \alpha_g \rho_g U_g dA) = 0 \tag{3.1}$$

$$\frac{d}{dz}(\int_A \alpha_s \rho_s U_s dA) = 0 \tag{3.2}$$

$$-\frac{d(\int_A P dA)}{dz} = \tau_w l_w + \int_A \alpha_g \rho_g g dA + \frac{d(\int_A \alpha_g \rho_g U_g^2 dA)}{dz} + \int_A F_D dA \tag{3.3}$$

$$\frac{d(\int_A \alpha_s \rho_s U_s^2 dA)}{dz} = \int_A F_D dA - \tau_{sw} l_w - \int_A \alpha_s \rho_s g dA - \int_A F_C dA \tag{3.4}$$

With the volumetric fraction relations of gas and solids phase and the equation of state of gas phase: $\alpha_g + \alpha_s = 1$ and $\rho_g = \frac{P}{RT}$.

where, FD is the drag force which is given by Richard-Zaki equation (Richardson and Zaki (1954)),

$$F_D = \frac{18\mu}{d_s^2} \frac{\alpha_s}{(1-\alpha_s)^L} \cdot (U_g - U_s) \tag{3.5}$$

F_C is the solid momentum transport due to energy dissipation in the dense and acceleration region (Zhu and You (2006)) which is

In reality the solids concentration distributions in both radial and axial directions should be continuous, which indicates that a set of partial differential equations of variants with respect to both radial and axial coordinates must be dealt with in a complete hydrodynamic modeling of gas-solids riser flows. A typical radial profile of solids concentration based on the optical probe measurements is shown in Figure 3.2, which demonstrates that, although the actual radial distribution is continuous, the profile can also be approximated, for the sake of simplicity, by a simple piecewise-uniform distribution in a three-zone structure. Based on this approximation as well as observations from ECT measurements, we further assume that the basic form of piecewise-uniform radial distribution is not only applicable to the entire riser but also applicable to all gas-solid flow properties, so that the hydrodynamic model can be approximated by a set of ordinary differential equations that depend only upon the axial coordinate of riser.

Based on the core-annulus-wall flow structure with piecewise-uniform radial distributions, independent governing equations now can be established for gas velocities, solid velocities and solid volume fractions in the entire region of riser. A summary of these equations are given as follows. Notations are referred to the section of List of Symbols.

Geometric relations and Equation of State:

$$A = A_c + A_a + A_w \tag{3.8}$$

$$\rho = \frac{p}{RT} \tag{3.9}$$

$$\alpha_i + \alpha_{si} = 1, \ i = a, c, w \tag{3.10}$$

Mass Balance of Solids

Overall balance: $$G_s A = \rho_s \alpha_{sc} U_{sc} A_c + \rho_s \alpha_{sa} U_{sa} A_a + \rho_s \alpha_{sw} U_{sw} A_w \quad (3.11)$$

Core-region: $$\frac{d}{dz}(\alpha_{sc} \rho_s U_{sc} A_c) = \dot{m}_{sc} \quad (3.12)$$

Annulus region: $$\frac{d}{dz}(\alpha_{sa} \rho_s U_{sa} A_a) = \dot{m}_{sw} - \dot{m}_{sc} \quad (3.13)$$

Wall region: $$\frac{d}{dz}(\alpha_{sw} \rho_s U_{sw} A_w) = -\dot{m}_{sw} \quad (3.14)$$

Mass Balance of Gas

$$GA = \rho \alpha_c U_c A_c + \rho \alpha_a U_a A_a + \rho \alpha_w U_w A_w \quad (3.15)$$

Gas Momentum Balance

Overall $$\frac{d}{dz}(\sum_{i=a,c,w} \alpha_i \rho U_i^2 A_i) = -\frac{dp}{dz} A - \sum_{i=a,c,w} F_{Di} A_i - \sum_{i=a,c,w} \alpha_i \rho g A_i - F_{fww} \quad (3.16)$$

Core-region: $$\frac{d}{dz}(\alpha_c \rho U_c^2 A_c) = -\frac{dp}{dz} A_c - F_{DC} A_c - \alpha_c \rho g A_c - F_{fac} \quad (3.17)$$

Annulus-region $$\frac{d}{dz}(\alpha_A \rho U_A^2 A_A) = -\frac{dp}{dz} A_A - F_{DA} A_A - \alpha_A \rho g A_A + F_{fac} - F_{faw} \quad (3.18)$$

Wall region: $$\frac{d}{dz}(\alpha_w \rho U_w^2 A_w) = -\frac{dp}{dz} A_w - F_{DW} A_W - \alpha_w \rho g A_w - F_{fww} + F_{faw} \quad (3.19)$$

Momentum Balance of Solids

$$\frac{d}{dz}(\sum_{i=a,c,w} \alpha_{si} \rho_s U_{si}^2 A_i) = \sum_{i=a,c,w} F_{Di} A_i - \sum_{i=a,c,w} \alpha_{si} \rho_s g A_i + \sum_{i=a,c,w} \frac{d}{dz}(C_{ppi} \frac{dU_{si}}{dz}) - F_{fsw} \quad (3.20)$$

Core-region: $$\frac{d}{dz}(\alpha_{sc} \rho_s U_{sc}{}^2 A_c) = F_{DC} A_c - \alpha_{sc} A_c \rho_s g + \frac{d}{dz}(C_{ppc} \frac{dU_{sc}}{dz}) + \dot{m}_{sc} U_{sc} \quad (3.21)$$

Annu.-region: $$\frac{d}{dz}(\alpha_{sa} \rho_s U_{sa}{}^2 A_a) = F_{DA} A_a - \alpha_{sa} A_a \rho_s g + \frac{d}{dz}(C_{ppa} \frac{dU_{sa}}{dz}) - \dot{m}_{sc} U_{sa} + \dot{m}_{sw} U_{sw} \quad (3.22)$$

Wall: $$\frac{d}{dz}(\alpha_{sw} \rho_s U_{sw}{}^2 A_w) = F_{DW} A_w - \alpha_{sw} A_w \rho_s g + \frac{d}{dz}(C_{ppw} \frac{dU_{sw}}{dz}) - \dot{m}_{sw} U_{sw} - F_{fsw} \quad (3.23)$$

Definition of Regional Boundaries

Based on the ECT measurements (Du., et al. 2004), the zone areas appear to have little variation along the riser, so that we may assume that

$$\frac{dA_w}{dz} = 0 \tag{3.24}$$

$$\frac{A_c}{A_a} = \text{constant} \tag{3.25}$$

In summary, for a complete description of the core-annulus-wall model of gas-solid riser flows, we have fourteen independent equations (3.8), (3.8), (3.10), (3.11), (3.12), (3.13),(3.15) - (3.18) for fourteen independent variables (A_c, A_w, A_a, U_{sc}, U_{sa}, U_{sw}, α_{sc}, α_{sa}, α_{sw}, U_c, U_a, U_w, p, ρ). Hence, the problem is closed. However, in order to solve for a specific gas-solid riser flow application, the detailed flow boundary conditions and flow operation conditions, as well as intrinsic correlations for inter-zone transport (e.g., F_f's), multiphase interactions (e.g., F_D's) and transport coefficients within the same phase (e.g., C_p's), must be specified.

3.3.2 Simplified Three-Zone Model

To further simplify the problem, we adopt the one-way flow coupling between the wall region and the core-annulus region. Namely, the gas-solid flows in the wall region are predetermined from wall boundary conditions and de-coupled from the governing equations of the core and annulus region. Why do we need to adopt this approach? First, there is no mature hydrodynamic model to describe the complicated mechanisms of gas-solids-wall friction and multiphase interactions in the wall boundary layer region where a dense layer of moving solids is present. Second, the distribution of solids backflow in the all region along the riser is difficult to determine due to the lack of sufficient

measurements and little understanding about turbulent transport of solids across the wall boundary layer. Third, little has been modeled on the hydrodynamics of gas flow in the wall boundary layer with a dense solids suspension. With such a one-way coupling simplification, the coupled set of ordinary differential equations becomes associated only with a core-annulus gas-solid flow and with a given axial distribution of solids migration from the wall region along the riser. Hence the complexity of the problem is greatly reduced.

3.3.2.1 Flow Characteristics in the Wall Region. Schematic distributions of the solids flow in the wall region along a riser are depicted in Figure 3.3, with (a) for the cross-section area of wall zone, (b) for the solids volume fraction, (c) for the solids mass flux across the wall-annulus boundary, (d) for the solids velocity, and (e) for the wall-entrance region. The characteristic heights of Z_e, Z_1, Z_2 and Z_3 denote, respectively, the end location of entrance regime, the end location of upwards moving solids in the wall region, the end location of radial-inwards migrating solids in the wall region, and the height of riser.

Based on the mass continuity and flow characteristics, the distributions of solids mass flux across the wall-annulus boundary must satisfy the following conditions:

$$\int_{z_1}^{z_2} \dot{m}_{sw} dz = \int_{z_2}^{z_3} \dot{m}_{sw} dz \tag{3.26}$$

$$\int_{Z_0}^{Z_1} \dot{m}_{sw}(z) dz = \int_{Z_e}^{Z_1} \dot{m}_{sw}(z) dz = G_{swe} \cdot A_w \tag{3.27}$$

$$\int_{z_1}^{z_2} m_{sw}\, dz = \int_{z_2}^{z_\infty} m_{sw}\, dz = G_{sB} A_w \tag{3.28}$$

The distribution of solids velocity must satisfy the following conditions:

$$U_{sw}\big|_{z=Z_1} = 0 \quad \text{and} \quad \left.\frac{dU_{sw}}{dz}\right|_{z=Z_1} < 0 \tag{3.29}$$

$$\dot{m}_{sw}\big|_{z=0} = \dot{m}_{sw}\big|_{z=Z_e} = \dot{m}_{sw}\big|_{z=Z_2} = 0 \tag{3.30}$$

$$\left.\frac{d\dot{m}_{sw}}{dz}\right|_{z=Z_e} > 0 \quad \text{and} \quad \left.\frac{d\dot{m}_{sw}}{dz}\right|_{z=Z_2} < 0 \tag{3.31}$$

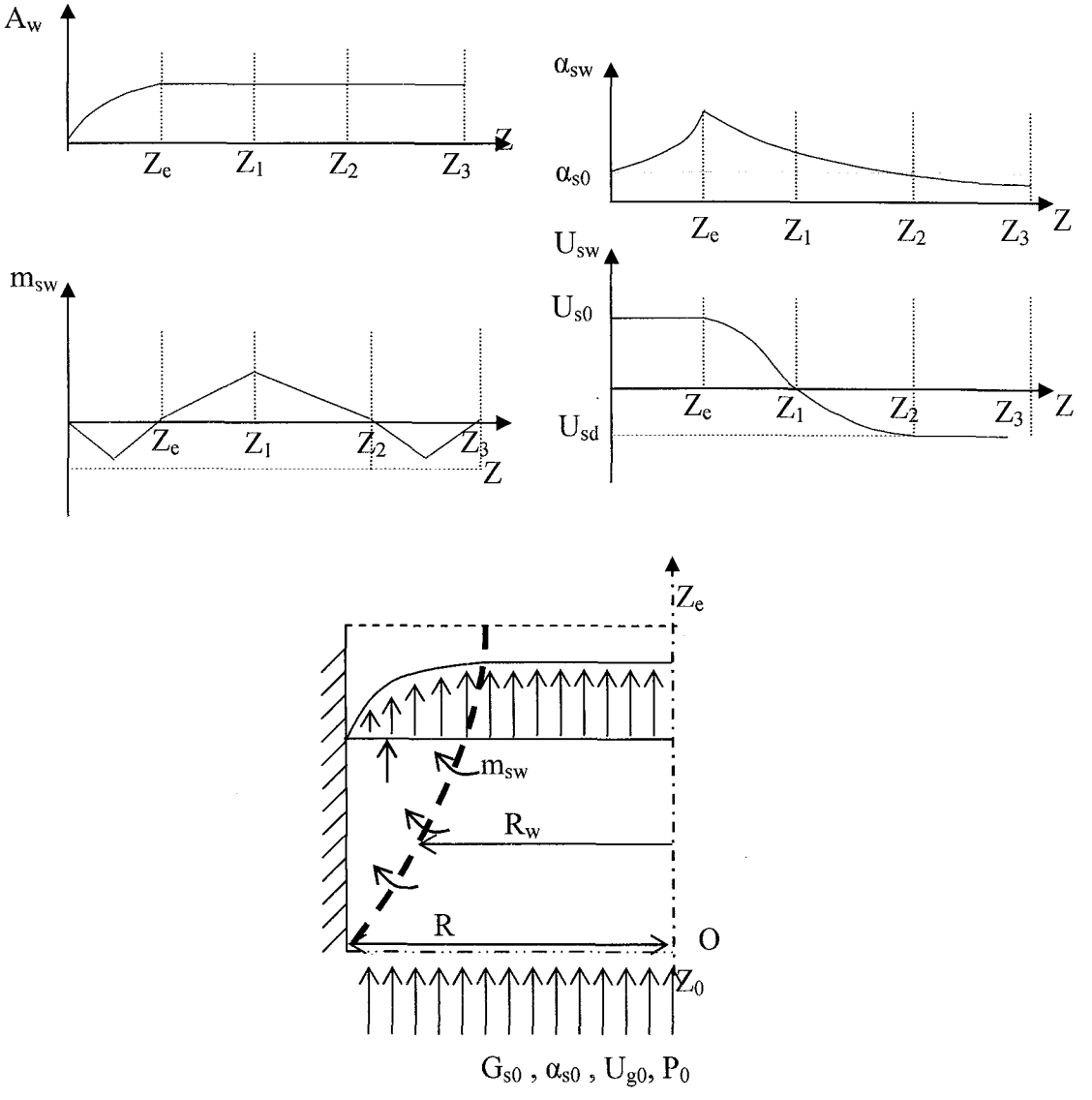

(e) wall-entrance region

Figure 3.3 Schematic profiles of solids flow in the wall region.

It is noted that the distributions of cross-section area of wall zone, solids concentration, solids velocity, and solids mass flux across the wall-annulus boundary are not independent of each other. Once three of them are determined, the remaining one can be deduced from the mass conservation of solids. In this study, we choose to predefine the distributions of cross-section area of wall zone, solids velocity and solids mass flux across the wall-annulus boundary whereas the distribution of the solid concentration is derived from the other three. This kind of selection has the advantage that, the derived solids concentration distribution with the available experimental data (such as from ECT measurement can be checked and validated or determined through common sense at the bulk range.

The distributions of solids velocity and solids mass flux across the wall-annulus boundary are assumed as follows, which satisfy the integral or boundary conditions of Eqs.(3.26) – (3.31).

$$U_{sw} = \begin{cases} U_{s0}\left[-1+e^{-U_{sd}(\frac{Z_1}{z}-1)}\right] & 0 \le z \le Z_1 \\ U_{sd}\left[-1+e^{-U_{s0}(\frac{z}{Z_1}-1)}\right] & Z_1 \le z \le Z_3 \end{cases} \tag{3.32}$$

$$\dot{m}_{sw}(z)=\begin{cases}\dfrac{4(G_{swe}-G_{s0})A_{we}z}{z_e^{\,2}} & 0<z<\dfrac{Z_e}{2}\\[2ex] \dfrac{4(G_{swe}-G_{s0})A_{we}(Z_e-z)}{z_e^{\,2}} & \dfrac{Z_e}{2}<z<Z_e\\[2ex] \dfrac{2(G_{swe}-G_{s0})\cdot A_w\cdot(z-Z_e)}{(Z_1-Z_e)^2} & Z_e\le z\le Z_1\\[2ex] \dfrac{2(G_{sB}-G_{s0})\cdot A_w\cdot(Z_2-z)}{(Z_2-Z_1)^2} & Z_1\le z\le Z_2\\[2ex] \dfrac{4(G_{sB}-G_{s0})\cdot A_w\cdot(z-Z_2)}{(Z_3-Z_2)^2} & Z_2\le z\le\dfrac{(Z_2+Z_3)}{2}\\[2ex] \dfrac{4(G_{sB}-G_{s0})\cdot A_w\cdot(Z_3-z)}{(Z_3-Z_2)^2} & \dfrac{(Z_2+Z_3)}{2}\le z\le Z_3\end{cases} \tag{3.33}$$

Now we need to determine the gas velocity distribution in the wall region. In the wall-entrance region where $0 < z < Z_e$, the following boundary conditions can be imposed:

$$U_w\big|_{r=R}=0,\quad U_w\big|_{r=R_w}=U_{ac},\quad \left.\frac{dU_w}{dr}\right|_{r=R_w}=0 \tag{3.34}$$

which defines a second-order polynomial for the radial distribution of gas velocity as

$$U_w=\frac{U_{ac}R(R-2R_w)}{(R-R_w)^2}+\frac{2U_{ac}R_w}{(R-R_w)^2}r-\frac{U_{ac}}{(R-R_w)^2}r^2 \tag{3.35}$$

The averaged interstitial gas velocity in the wall region can thus be obtained as

$$U_w=\frac{U_{ac}R(R-2R_w)}{(R-R_w)^2}+\frac{4}{3}\frac{U_{ac}R_w}{(R-R_w)^2}(R^2+RR_w+R_w^2)-\frac{U_{ac}}{2(R-R_w)^2}(R^2+R_w^2) \tag{3.36}$$

In the wall region above the entrance, we ignore any mass transfer of gas between the wall and core-annulus regions.

3.3.2.2 Intrinsic Correlations. As mentioned earlier, the intrinsic correlations for inter-zone transport (e.g., F_f's), multiphase interactions (e.g., F_D's) and transport coefficients within the same phase (e.g., C_p's), must be specified in order to solve the coupled set of governing equations. For simplicity, in the consideration of inter-zone

momentum transfer, we only consider the cross-boundary momentum transfer that results from the radial migration of solids whereas the other interfacial momentum transports (such as F_f's) are ignored. Such simplification may be partially justified by the fact that the actual radial distributions of solids phase momentum are continuous.

The momentum transfer between the gas and solids phases in each zone is modeled based on the Richard -Zaki equation (Richardson and Zaki, 1954), so that

$$F_{Di} = \frac{18\mu}{d_{si}^2} \cdot \frac{\alpha_{si}}{(1-\alpha_{si})^L} \cdot (U_i - U_{si}) \tag{3.37}$$

To account for the effect of the inter-phase frictional and inter-particle collision, an additional term must be included in the momentum equation of solids for solids flows in the dense and acceleration region, which is estimated by [Zhu and You, 2007]

$$\frac{d}{dz}(C_{ppi}\frac{dU_{si}}{dz}) = -\frac{A_i}{U_{si}}\left(\Gamma_i - (U_i - U_{si})(-\frac{dP}{dz})\right) \tag{3.38}$$

The energy dissipation function Γ_i can be further expressed in terms of the solids flow characteristics at minimum transport [Zhu and You, 2007]:

$$\Gamma_i \approx \sum_{j=0}^{N} k_j \alpha_{si}^j \tag{3.39}$$

3.3.2.3 Simplified Three-Zone Model After the implementation of the wall flow model (section 3.3.2.1) and the intrinsic correlations (section 3.3.2.2) into the Three-Zone Model (section 3), we can obtain a simplified three-zone model that is summarized as follows:

Mass Balance of Solids

Core-region:
$$\frac{d}{dz}(\alpha_{sc}U_{sc}) = \frac{\dot{m}_{sac}}{\rho_s A_c} \tag{3.40}$$

Annulus region:
$$\frac{d}{dz}(\alpha_{sa}U_{sa}) = \frac{\dot{m}_{swa} - \dot{m}_{sc}}{\rho_s A_a} \tag{3.41}$$

Mass Balance of Gas

$$GA - \rho\alpha_w U_w A_w = \rho\alpha_c U_c A_c + \rho\alpha_a U_a A_a \tag{3.42}$$

Momentum Balance of Gas

Core-region:
$$\frac{d}{dz}(\alpha_c U_c^2) = \frac{1}{\rho}\cdot\left[-\frac{dp}{dz} - F_{DC} - \alpha_c\rho g\right] \tag{3.43}$$

Annulus-region
$$\frac{d}{dz}(\alpha_a U_a^2) = \frac{1}{\rho}\cdot\left[-\frac{dp}{dz} - F_{DA} - \alpha_a\rho g\right] \tag{3.44}$$

Momentum Balance of Solids

Core-region:
$$\frac{d}{dz}(\alpha_{sc}U_{sc}^{\,2}) = \frac{1}{\rho_s}\left[\lambda_c F_{DC} - \alpha_{sc}\rho_s g + \frac{\dot{m}_{sc}U_{sc}}{A_c}\right] \tag{3.45}$$

Annulus-region
$$\frac{d}{dz}(\alpha_{sa}U_{sa}^{\,2}) = \frac{1}{\rho_s}\left[\lambda_c F_{DA} - \alpha_{sa}\rho_s g + \frac{\dot{m}_{sw}U_{sw} - \dot{m}_{sc}U_{sa}}{A_c}\right] \tag{3.46}$$

Hence we have seven independent equations ((3.40)-(3.46)) for seven independent variables (U_{sc}, U_{sa}, α_{sc}, α_{sa}, U_c, U_a, P) in the annulus and core regions.

3.3.3 Model Validation and Discussion

3.3.3.1 Experimental Approach. The experimental study provides the experimental data base for validating the proposed three-zone model. Specifically, measurements are made for distributions of solids concentration in all three zones along the tested riser as well as the associated pressure drop distribution along the riser. The solids concentrations are determined from the ECT measurements (with a double check by optical probe measurements), whereas the pressure drops are measured by a set of differential pressure transducers along the riser.

The riser is an integrated part of a circulating fluidized bed system used in our previous studies [Du, et al. 2004], as shown in Figure 3.4, with an I.D. of 0.1 m and a height of 6.32 m. The solids circulation rate is measured by timing the falling distance of tracer particles in the standpipe. The superficial air velocity is measured by a flow meter. The fluidized particles are FCC catalysts.

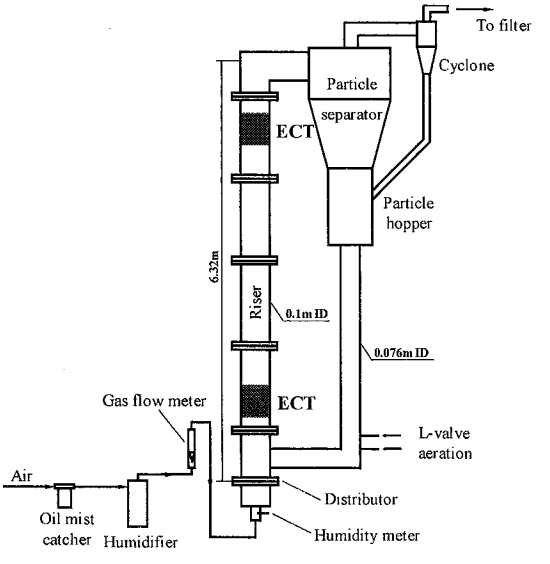

Figure 3.4 Schematic diagram of the riser system (CFB).

3.3.3.2 Model Predictions versus Measurements. To validate our model, the model predictions of solids concentration distributions and pressure distributions are directly compared against the ECT measurements and the pressure drop measurements under the same flow conditions. In this part, two cases of different solids loadings at the same gas velocity are investigated. Specifically, the solids circulation rate is controlled at 1.32 kg/m^2s or 2.30 kg/m^2s whereas the inlet gas velocity is maintained at 0.97 m/s. The averaged solids concentrations in the three zones were measured at five different heights along the riser.

As shown in Figures 3.5(a) and 3.5(b), both measurements and model predictions suggest that the core-annulus-wall structure is built up at the bottom part of the riser and kept stable along the riser. The solid concentrations in each zone at the same height of riser are not only significantly different but also quite different in their distributions along the riser, indicating a fundamental change in hydrodynamic characteristics of solids in different zones. The solid concentrations in the core and annulus regions decrease much faster than that in the wall region in the lower part of the riser. It is interesting to notice that, in the wall region, our model suggests that there exists a peak in solids concentration before it decreases quickly, possibly due to the collision effect between the downwards moving solids from back flow and upwards moving solids from the entrance. Comparison of solids concentration distributions between measurements and model predictions shows the model is quite successful, not only giving excellent qualitative solids distributions of all regions but also yielding very reasonable quantitative results in most of these regions. Figure 3.6 illustrates the comparison of axial distributions of pressure between the

measurements and model predictions, which also shows a very good quantitative agreement.

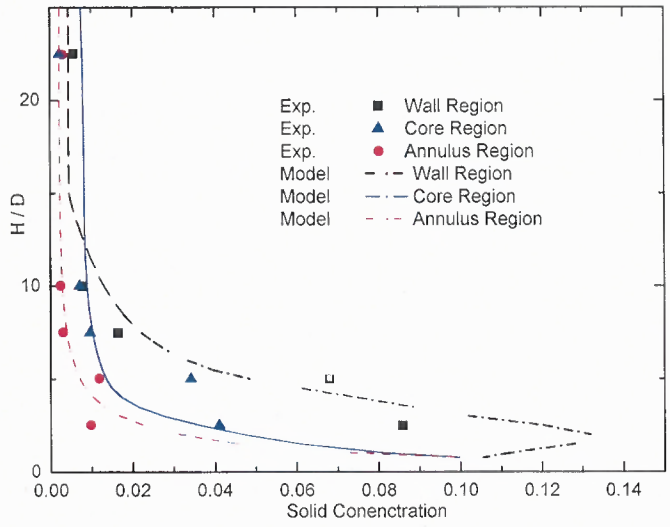

(a) G_s=1.32 kg/m^{2}s

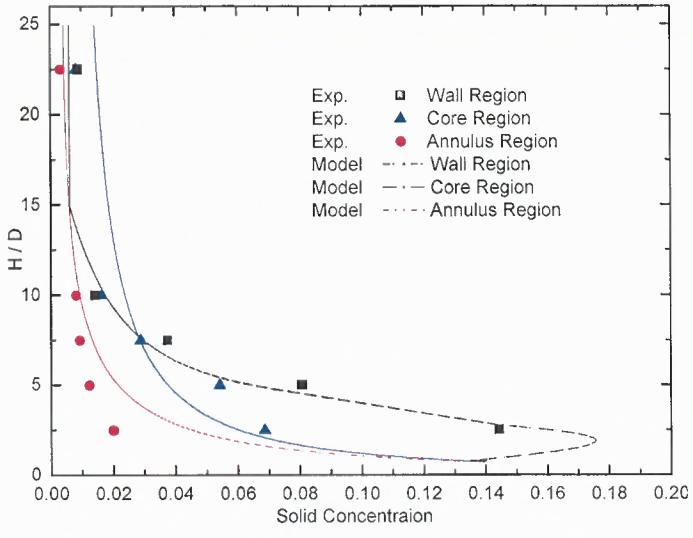

(b) G_s=2.30 kg/m^{2}s

Figure 3.5 Comparisons of Solid Concentration Distributions (U =0.97m/s).

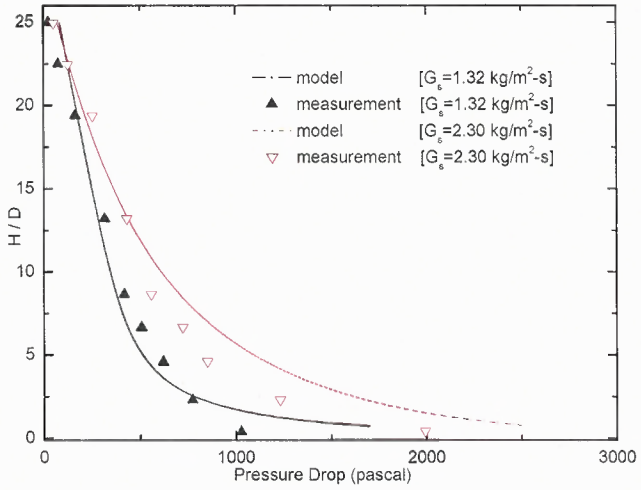

Figure 3.6 Comparisons of axial pressure distributions.

3.3.3.3 Effect of Solids Mass Flow rate on Flow Structure. As mentioned earlier, in the riser flow with a low solids mass flow rate, the inwardly migrating solids are all entrained into the flow without any residual solids reaching to the center of the riser. In this case, the riser flow has the familiar "core-annulus" two-zone structure. However, if the solids mass flow rate is increased to such an extent so that some inwardly migrating solids can reach to the center of the riser, the riser flow becomes the "core-annulus-wall" three-zone structure. In order to illustrate the effect of solid circulation rate on flow structure, various riser flows at the same gas velocity but with different solid mass flow rates have been predicted.

Figure 3.7 shows the flow structures of riser flows at a gas velocity of 5 m/s and the solids mass flow rate varying from 4 to 50 kg/m^2-s. As shown in Figure 3.7(a) with a low solids mass flow rate (4 kg/m^2-s), the riser flow clearly shows a "core-annulus" two-zone structure, with little difference in solids concentration distributions between the core and annulus regions.

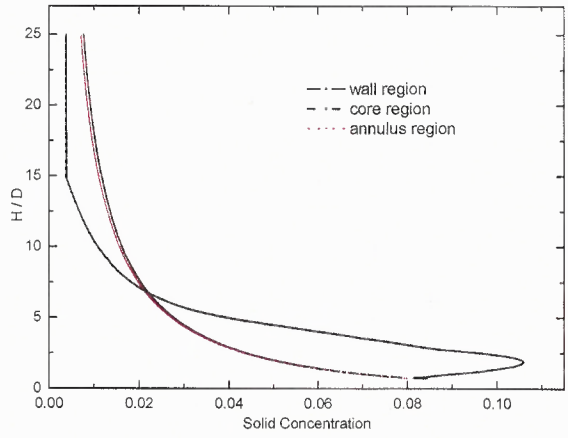

(a) two-zone structure [G_s=4 kg/m^2-s]

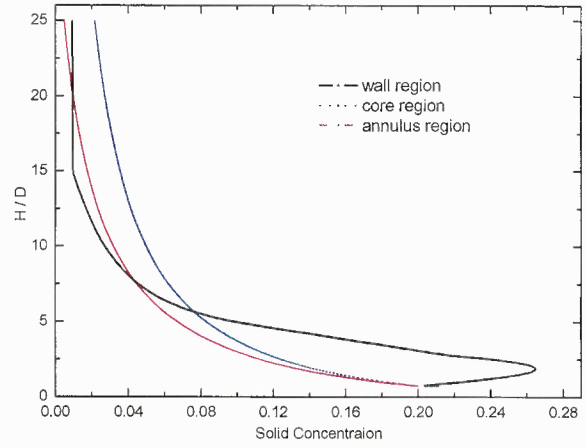

(b) three-zone structure [G_s=10 kg/m^2-s]

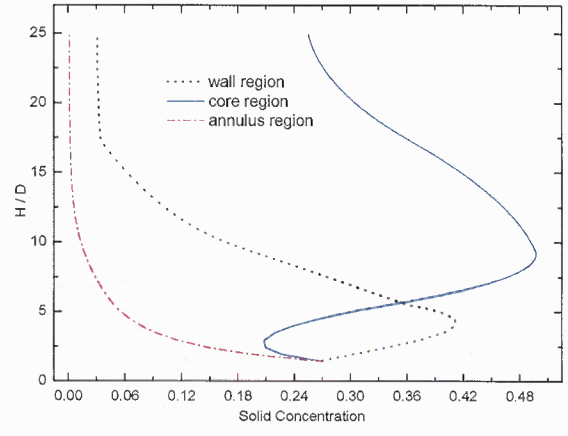

(c) Solid concentration reversal in the core region [G_s=50 kg/m^2-s]

Figure 3.7 Effect of solid mass flow rate on flow structure.

With a moderate solids mass flow rate (e.g., 10 kg/m^2-s), however, the riser flow becomes a "core-annulus-wall" three-zone structure, with distinct differences in solids concentration distributions among the core, annulus and wall regions, as shown in Figure 3.7(b). The "wall-core-annulus" three-zone structure starts from the entrance of the riser and exits throughout the entire riser. In the dilute transport regime, however, the difference in solids concentration distributions between the core and annulus regions becomes much insignificant, compared to that in the dense transport regime at the bottom of the riser. With a significant increase in solids mass flow rate (e.g., 50 kg/m^2-s), as shown in Figure 3.7(c), a reversal-hump-shaped distribution of solids concentration occurs in the core region. The initial decrease of solids concentration is due to the entrance effect on wall boundary layer development, whereas the hump results from a combined effect of a strong immigration of solids to the core region and a much reduced acceleration of the solids in the core region. The formation of the peak solids concentration in the core region can trigger the instability of the "core-annulus-wall" three-zone structure. When the peak solids concentration is high enough, the flow-induced particle-particle interactions (such as wake-induced collisions) will lead to the collapse of the stable structure of solids in the core region, like choking.

Figure 3.8 shows the effect of solids mass flow rate on the axial distributions of pressure. It is interesting to note that, at high solids loadings, even with the solids concentration reversal in the core, there is no reversal in the pressure distribution in a riser flow. This is due to the fact that, in a riser flow, the solids motion is governed by the hydrodynamic driving force (drag force or pressure) rather than inertia.

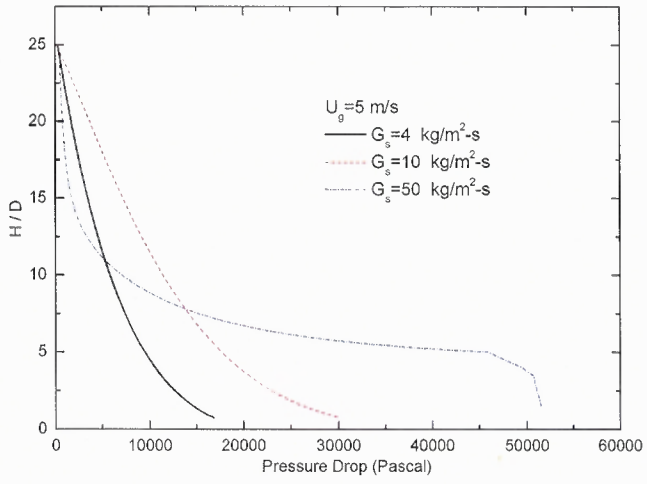

Figure 3.8 Effect of solids mass flow rate on axial pressure distribution.

3.3.3.4 Effect of Inlet Gas Velocity on Flow Structure. Besides the solid circulation rate, the gas velocity is another important controlling parameter on the riser flow structure. For riser flows with a given solids mass flow rate, high gas velocities can yield the "core-annulus" two-zone structure whereas low gas velocities tend to cause the "wall-core-annulus" three-zone structure, even the choking.

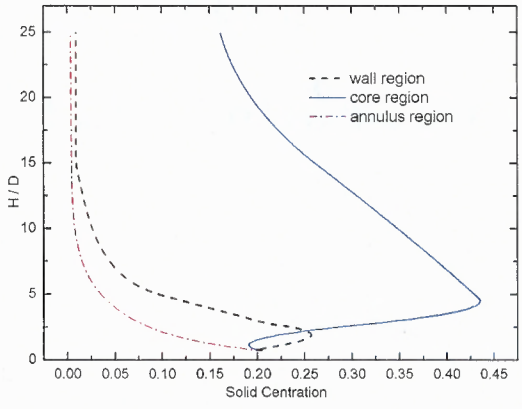

(a) Solid concentration reversal in the core (U=1 m/s).

Figure 3.9 Effect of gas inlet velocity on solids concentration structures.

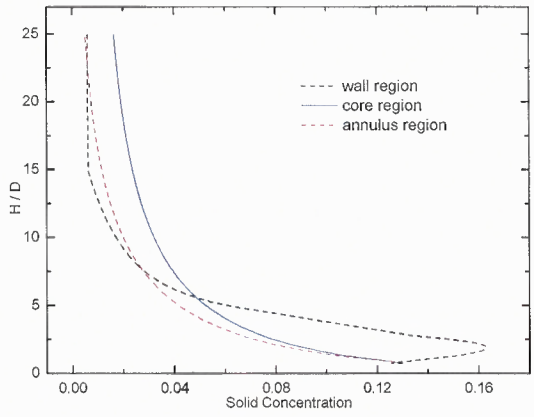

(b) three-zone structure (U=6 m/s).

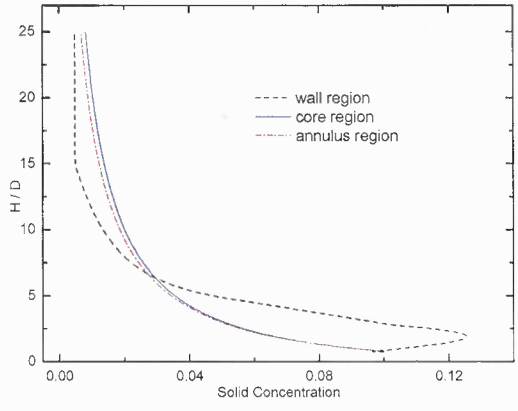

(c) two-zone structure (U = 10 m/s)

Figure 3.9 Effect of gas inlet velocity on solids concentration structures (Continued).

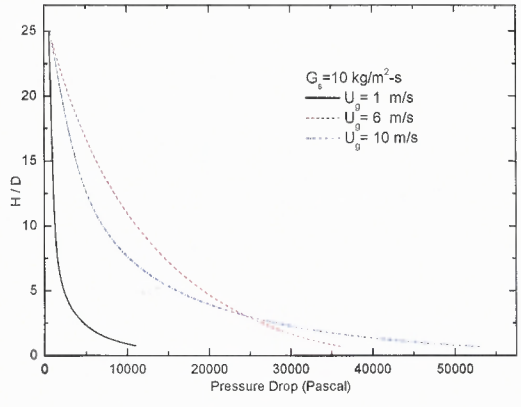

Figure 3.10 Effect of gas velocity on axial distributions of pressure.

Figure 3.9 shows the riser flow structures at the solids mass flow rate of 10 kg/m^2-s and the gas velocity varying from 1 to 10 m/s. As shown in Figure 3.9 (a) with a low gas velocity (e.g., 1 m/s), the riser flow shows a reversal-hump-shaped distribution of solids concentration occurring in the core region, which is similar to Figure 3.7(c). In this case, the gas velocity is too low to deliver the necessary dilution (or acceleration) of solids against the inwardly migrating solids from the wall. Figure 3.9 (b) shows that, with an increased gas velocity (e.g., 5 m/s), the riser flow becomes stable with a "wall-core-annulus" three-zone structure. Further increase in gas velocity (e.g., 10 m/s) yields a sufficient hydrodynamic power, not only to make a proper dilution or acceleration of solids but also a sufficient entrainment and dilution of solids emigrated from the wall region. Such hydrodynamic power of gas leads to little difference in solids concentration distributions between the core and annulus regions. Figure 3.10 shows the effect of gas velocity on axial distributions of pressure.

This portion of study presents a simplified three-zone modeling approach to understand the general heterogeneous flow structure in gas-solid riser flow, especially the "core-annulus-wall" three-zone flow structure and the unstable flow structure that leads to choking. The model prediction results are directly compared with experimental measurement using ECT technology, which shows a fairly good agreement. The proposed mechanisms and corresponding mathematical modeling yield a reasonable explanation for the formation and flow conditions of various heterogeneous structures. Effects of critical flow parameters such as solids mass flow rate and gas inlet velocity have also been illustrated. Simulation results show that the well-known "core-annulus" two-zone structure is easily formed at high gas velocity and/or low solids mass flow rate,

and the "core-annulus-wall " three-zone structure always happens at low gas inlet velocity and/or high solids mass flow rate. The formation of reversal solids concentration profiles along the riser in the core region may be the underlying cause of choking.

3.4 Simplified Three-Zone Model with Entrance Effect

Our previous research, which is capable of providing qualitative predictions of hydrodynamic characteristic of both structures, already gave us a preliminary understand of the formation mechanisms of the heterogeneous flow structure throughout the entire riser region.

However, the quantification of core-annulus-wall structure near the riser bottom (entrance region) is particularly difficult to handle, since it dependents heavily upon the inlet flow conditions, which varies for risers with different solid/gas feeding devices (such as L-valve, J-bend, or varies fluidization bed distributors) as well as at different solids loadings. In this part, special concerns focused on the flow hydrodynamic characteristic in the entrance region under various inlet flow conditions. With the help of commercial package (Fluent), the different entrance conditions are directly coupled with our current model, which, in the first stage and for the purpose of simplicity, assumes a uniform inlet condition. In addition to theoretically studies, our simulation results are directly compared with available ECT measurement and fairly good agreement achieved.

The parts study shows that the flow structure in the entrance region can be strongly affected by the selection of solids feeding patterns but weakly dependent upon the operation conditions. The flow structure in the main riser region, however, is weakly

dependent upon the selection of solids feeding patterns but strongly affected by the operation conditions. The riser characteristic length of entrance region is nearly independent of the gas inlet velocity and solids mass flow rate; however it is moderately influenced by the solid feeding pattern. As part of model validation, some simulation results are directly compared with available experimental measurements, with a reasonably good agreement.

3.4.1 Modeling Methodology

A riser flow can be conceptually divided into three regions, namely, the entrance region, the main region, and the exit region. In both entrance and exit regions the flow is multi-dimensional structure, where as in the main region the flow can be approximated as one-dimensional. Due to the dominant effect of convection, the exit region is constantly assumed to have a weak impact on the flow structure in the main and entrance regions. Thus, for simplicity in the study of entrance effect, the overall flow structure is considered only in the entrance and main regions, as shown in Figure 3.11.

Other key approximations in this study include the axial symmetry of the riser flow and the dispersed phase of solids (i.e., no clusters or agglomerates). These are introduced for the simplicity of mechanistic modeling and for the computer capacity limitation in the numerical simulation, especially with the consideration of gas-solid flows in the entrance region of a complex geometry. Thus, the flow in the entrance region is first investigated by means of a fine-grid 2-D numerical simulation approach, from which the characteristic length of entrance region (at the end of which the flow becomes one-dimensional) can be defined and the radial distributions of phase transport properties (velocity and volume fractions) at the end the entrance region can be obtained.

Using these radial profiles as the flow inlet conditions, the flow structure in the rest part of the riser is then studied using a 1-D multi-zone mechanistic model, based on which the flow stability can be further assessed.

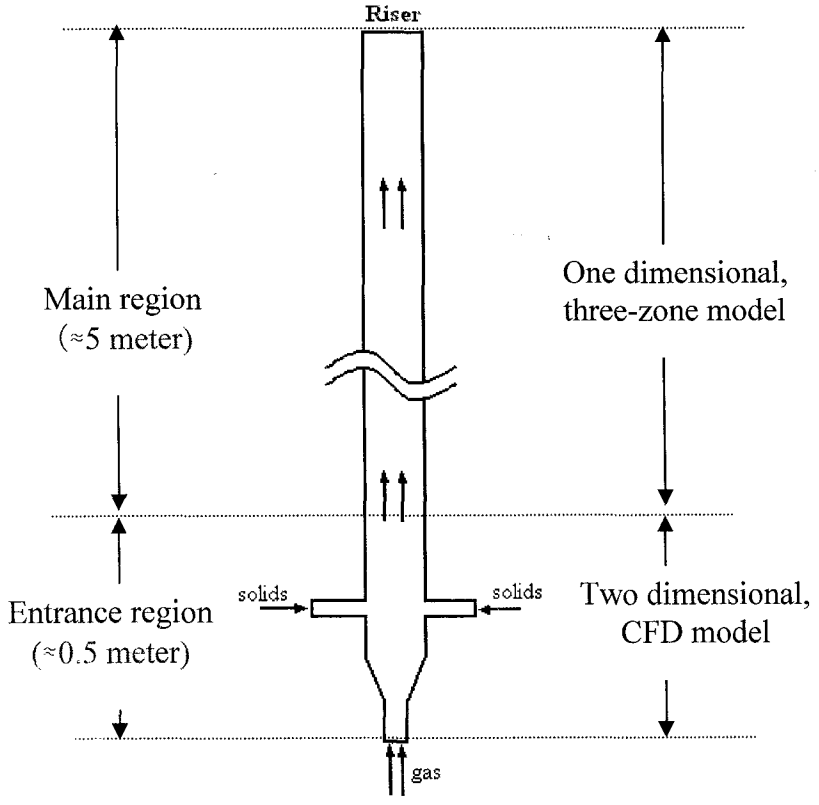

Figure 3.11 Two-region approximation for riser flow study of entrance effect.

The general approach is firstly to study the flow hydrodynamics near the riser bottom (entrance region) based on commercial package "FLUENT" simulation. Then the simulation results will pre-processed after extracted from "FLUENT". Once ready, they will serve as input data for the three-zone structure model simulation. This idea is shown in figure 3.12.

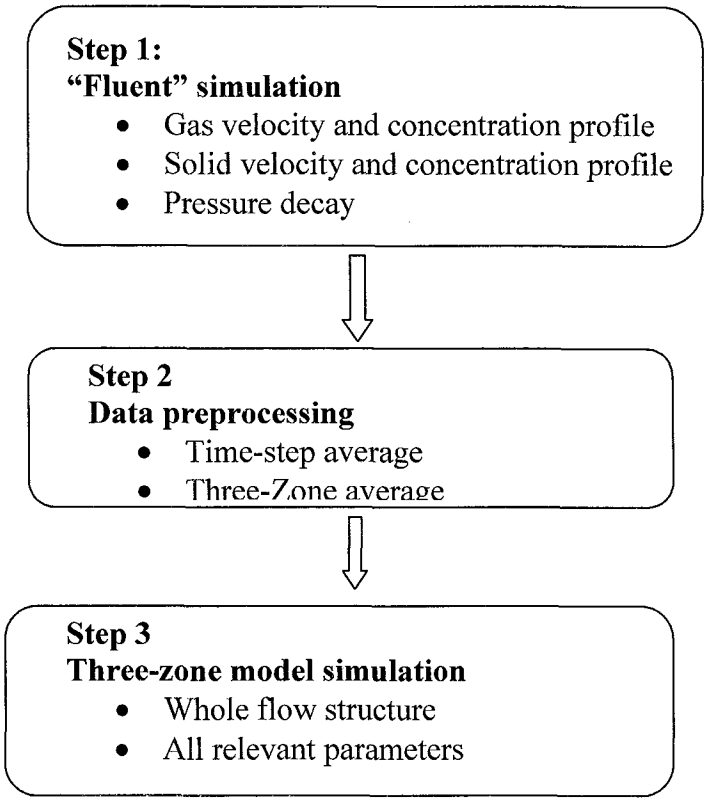

Figure 3.12 Entrance effect simulation flow chart.

The FLUENT modeling is based on the three-dimensional conversation equation for mass, momentum and energy. The differential equations are discretized by the Finite Volume Method and are solved by the SIMPLE algorithm. The FLUENT code utilizes an unstructured non-uniform mesh, on which the conservation equation for mass, momentum and energy are discretized. In our simulation, the Eulerian model is adopted. The Eulerian model is the most complex of the multiphase models (in FLUENT). It solves a set of n momentum and continuity equations for each phase. Coupling is achieved through the pressure and interphase exchange coefficients. The manner in which this coupling is handled depends upon the type of phases involved; granular flows, the properties are obtained from application of kinetic theory. Momentum exchange between the phases is also dependent upon the type of mixture being modeled. (FLUENT's user-

defined functions allow you to customize the calculation of the momentum exchange). Tables 3.1 gives the main settings used in the simulation and some parts of the main parameters of gas and solid phase are also listed in Table 3.2.

Table 3.1 List of FLUENT Models Setup in Simulation

Model	**Setting**
Space	Axisymmetric
Time	Unsteady
Multiphase model	Eulerian
Viscous	Standard K-epsilon turbulence model
Wall treatment	Standard wall functions
phase interaction	User-defined function

Table 3.2 Main Parameters Used in Simulation

Parameter	**Range of values**
Riser Dimensions	R=0.1 m H=1 m
Side Entrance	r=0.025 m
Properties of particle	Density: 1400 kg m-3
	Diameter: 6e-5 m
	Granular viscosity: Syamlal-obrien
Properties of air	Density: 1.225 kg m-3
	Viscosity: 1.79e-5 kgm-1s-1
Gas velocity	0.97 ~ 2m/s
Solid circulation rate	1.32~26 kg/m2s

The prediction of pressure drop in an uniformly fluidized bed is a problem of long standing interest in the process industry. The Eulerian models in FLUENT provide an important modeling tool for studying dense phase particulate flow involving complex inter-phase momentum transfer. Despite rigorous mathematical modeling of the associated physics, the drag laws used in the model continue to be semi-empirical in nature. Therefore, it is crucial to use a drag law that correctly predicts the incipient or minimum fluidization conditions where the bed of particles is essentially in a state of suspension as a result of the balance between interfacial drag and body forces.

The default Syamlal-O'brien is as follows:

The gas-solid exchange coefficient:

$$K_{sl} = \frac{3\alpha_s \alpha_g \rho_g}{4U_{r,s}^2 d_s} C_D\left(\frac{\mathrm{Re}_s}{v_{r,s}}\right)\left|\overrightarrow{U_s} - \overrightarrow{U_g}\right| \tag{3.47}$$

where $U_{r,s}^2$ is the terminal velocity coefficient for the solid phase.

$$U_{r,s} = 0.5(A - 0.06\mathrm{Re}_s + \sqrt{(0.06\mathrm{Re}_s)^2 + 0.12\mathrm{Re}_s(2B - A) + A^2}) \tag{3.48}$$

where A= $\alpha_s^{4.14}$ and B=0.8 $\alpha_s^{1.28}$ for $\alpha_s \leq 0.85$ and with B= $\alpha_s^{2.65}$ for $\alpha_s \succ 0.85$. Therefore these values have to be used to predict the correct bed behavior and are passed to the code through user-defined functions. The user-defined functions are realized using C language.

Considering the complexity of dense gas-solid riser flow near the entrance region and the reality of availability of large computation capacity, 2D approximation would be a good compromise for the present study though it may lose some 3D characteristics of entrance region. To provide a comprehensive physical model for gas-solids riser flows in the entrance region, one must consider the following mechanistic natures of the problem:

1. two phase flow
2. turbulent flow
3. inter-particle collision dominated flow (granular flow theory)
4. multi-scale size of feeding tube and riser
5. complicated geometry (such as taped) riser entrances
6. transient flow approach (for numerical solving stability).

Table 3.3 Quick summary of 2D and 3D simulation

		2-Dimensional	3-Dimension	
			Coarse mesh	Fine mesh
Equations need to solve:	Total:	11	18	
	Mass:	1	1	1
	Momentum:	4	6	6
	k-ε model:	2	2	2
	Granular theory	4	5	5
Total grid:		6624	30185	761464
Computation time:		6 hours*	51 hours*	> 1500 hours**

* Computation time on a computer with 3.5 Ghz Pentium Dual-Core CPU and 3 GB memory
** Estimated calculation time

In order to compare the effects of mesh size on the simulation, two kind of mesh strategy was adopted in our simulation. One is coarse mesh and another one is fine mesh. Detailed comparison is listed in following Figure 3.13.

A detailed comparison of computation capacities needed by 2D and 3D simulations is listed in Table 3.3. As a result, a 2D approximation has to be adopted to accommodate all these requirements because of impractically long simulation time of 3D

simulation with relatively reasonable grid amount. In order to provide concrete comparison and check the rationality of 2D simulation, one of 3D simulation based on fairly coarse mesh has been conducted and compared with 2D simulation. Figure 3.14 presents the solids velocity and volume fraction profiles of medium-plane of 3D simulation and 2D simulation. It could be observed that the two simulations bear certain similar patterns for both the velocity and volume fraction profiles. Hence, the 2D simulation may provide similar characteristic descriptions of flow transport to that from 3D simulation in the entrance region of gas-solid riser flows.

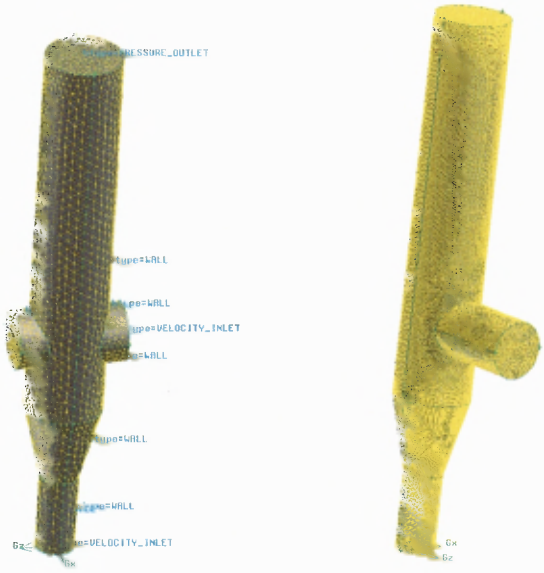

Figure 3.13 Fine mesh vs. coarse mesh.

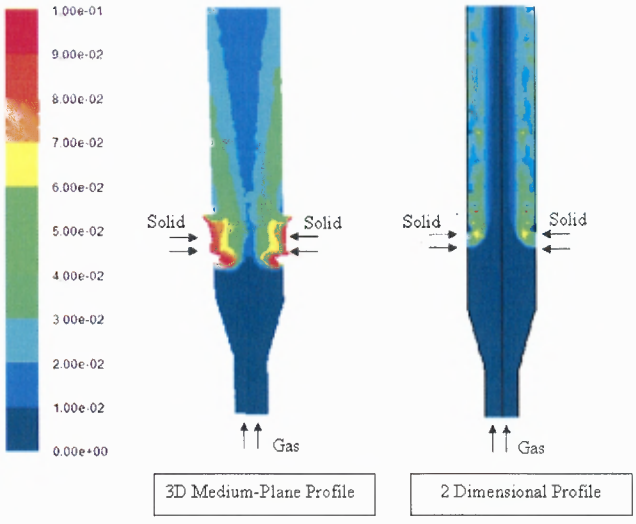

(a) Solids volume fraction

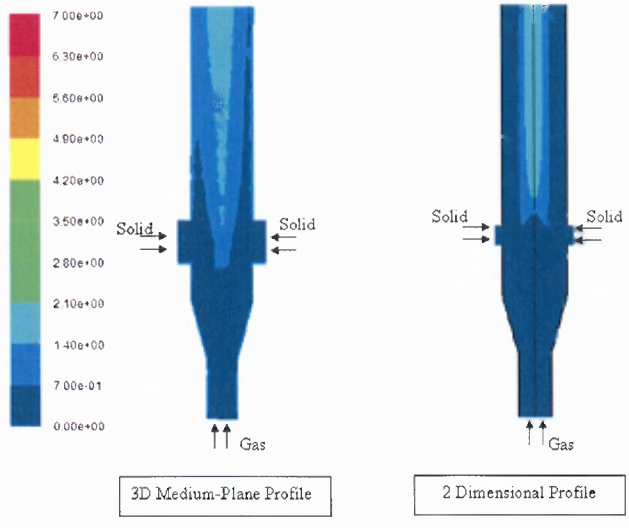

(b) Solids velocity

Figure 3.14 Comparison of 3D vs. 2D simulation results in entrance region. (U_g=1.94m/s, G_s=11.9 kg/m^2-s, 0.1 meter I.D.)

3.4.2 Selection of Typical Entrance Patterns

In order to examine the solids feeding pattern effects on the flow structure and hydrodynamic characteristics of the riser, certain types of the entrance feeding patterns should be decided to conduct the numerical simulation since in industrial facilities a wide

variety of feeding patterns are adopted. Our selection concerns are mainly based on the availability of experimental validation and the representation of common solids feeding devices. Figure 3.15(a) illustrates some typical solids feeding pattern widely used in industrial applications and laboratory experiments, including (a) J-bend feeder, (b) L-valve feeder above a flow distributor, (c) L-valve feeder with an internal baffle, and (d) L-valve feeder after an expansion section. For the convenience of analysis and validation of our simulation without losing generality, three axial symmetric feeding patterns are selected, as shown in Figure 3.15(b), representing (a) J-bend feeder or any feeders with a uniform solids flow at the bottom of riser, (b) annular ring of L-valve feeders above a flow distributor, and (3) annular ring of L-valve feeders after an expansion section.

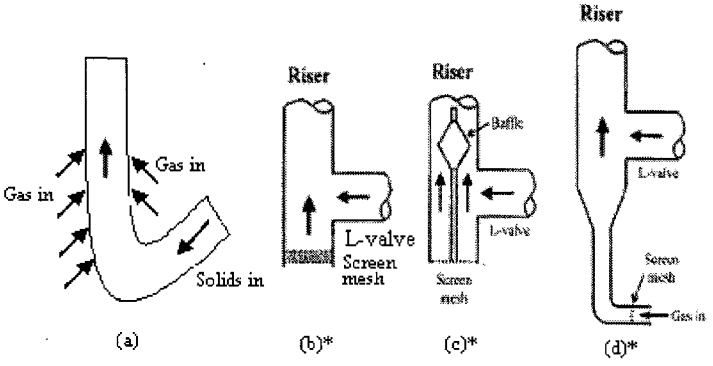

(a) Solids feeding patterns used in the experiment (* from Du et al. 2004).

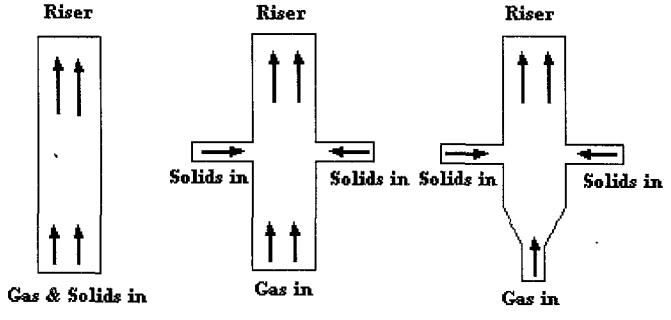

(b) Axial symmetric solids feeding patterns used in 2-D simulations

Figure 3.15 Selection of solids feeding patterns

3.4.3 Modeling of Gas-solid Flow in Entrance Region

Gas-solid flow in the entrance region of a riser is not only multi-dimensional and multiphase but also transient in phase transport due to turbulence, phase instability (such as cluster formation and destruction) and inter-particle collisions. Modeling of such a multiphase flow system is typically based on the volume-time averaging approach, described in either Lagrangian or Eulerian coordinates (Bolton LW, et al. 1988). In this study, we adopt the Eulerian modeling for both gas and solids phases. For steady-state, non-reactive and isothermal gas-solid flows, the general volume-time averaged equations can be expressed, respectively based on the mass and momentum conservation laws, as:

$$\nabla \cdot (\alpha_i \rho_i \mathbf{U}_i) = 0 \qquad i = s, g \tag{3.49}$$

$$\nabla \cdot (\alpha_i \rho_i \mathbf{U}_i \mathbf{U}_i) = -\nabla p \delta_{ig} + \nabla \cdot \boldsymbol{\tau}_i + \alpha_i \rho_i \mathbf{g} + \mathbf{F}_{Ai} \qquad i = s, g \tag{3.50}$$

In Equation (3.50), F_A stands for the averaged interfacial momentum transfer or generalized drag force; τ_g is the averaged shear stress of gas or turbulence stress, and τ_s is the total solids stress due to inter-particle collisions. In this modeling, the k-ε model is used to account for the turbulence effect, whereas the granular kinetic theory is used to account for the inter-particle collision effect. As for the boundary conditions for the geometries in Figure 3.15(b), the entrance region exit is set as outflow since the details of the flow velocity and pressure are not known prior to solution of the flow problem, and velocity inlet is set for the gas and solids inlets.

3.4.4 Modeling of Gas-Solid Flow in Main Region

Volume-time averaged gas-solid flow in the main region of a riser can be approximated as steady and one-dimensional. However, due to the wall boundary effect, the radial distributions of phase transport properties are typically non-uniform, which nevertheless may be simplified by a three-zone representation, as illustrated in Figure 3.16. A schematic pattern of these three zones (namely, core, annulus and wall zones) in the main region is shown in Figure 3.1(b), with a uniform inlet flow condition. A mechanistic model to describe such a three-zone flow structure has already been developed by our research group (Halow JS., et al. 1993).

In the current study of entrance effect, we apply this three-zone model to the cases with non-uniform inlet flow conditions predetermined from the modeling of entrance region. The length of the main region is estimated from the difference between the riser height and the characteristic length of entrance region (also determined from the modeling of entrance region).

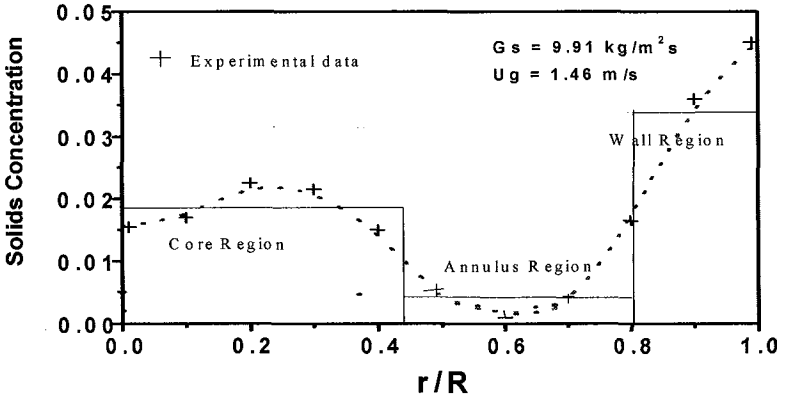

Figure 3.16 Three-zone representation of solids concentration distribution.

Based on the core-annulus-wall flow structure with piecewise-uniform radial distributions, independent governing equations can be established, from mass and momentum conservations of each phase in each zone, as

$$G_g A = \sum_i \rho_g \alpha_{gi} U_{gi} A_i \qquad i = a, c, w \tag{3.51}$$

$$\frac{d}{dz}(\alpha_{si} \rho_s U_{si} A_i) = \dot{m}_{si} \qquad i = a, c, w \tag{3.52}$$

$$\frac{d}{dz}(\alpha_{gi} \rho_g U_{gi}^2 A_i) = -\frac{dp}{dz} A_i - F_{Di} A_i - \alpha_{gi} \rho_g g A_i + \sum_{j \neq i} F_{fij}, \qquad i, j = a, c, w \tag{3.53}$$

$$\frac{d}{dz}(\alpha_{si} \rho_s U_{si}{}^2 A_i) = F_{Di} A_i - \alpha_{si} A_i \rho_s g + \frac{d}{dz}(C_{ppi} \frac{dU_{si}}{dz}) + \dot{M}_{si} + F_{fsi} \qquad i = a, c, w \tag{3.54}$$

3.4.5 Model Results and Discussion

In this section, the modeling results of flow structure are presented and discussed, in sequence, for the entrance effect in the entrance and main regions. First the simulations results are validated against the experimental results under comparable entrance and flow conditions. Then a series of parametrical studies are performed to investigate the entrance effect on the characteristics length of the region and radial distributions of phase transport properties at the end of the entrance region, with various entrance and flow operation conditions. Finally, the flow structure in the main region and its variation at different entrance flow conditions are presented. Discussions are also extended to the parametric effects of entrance on the flow instability such as the possible occurrence of choking.

3.4.5.1 Flow Structure in Entrance Region. Numerical simulation of flow in the entrance region has been performed using the commercial code of FLUENT®6.3. The geometry and mesh are generated using GAMBIT® where the quad/triangle types of element are used in the mesh generation process. In the basic setting of FLUENT®, the axial-symmetric Eulerian multiphase model is selected. To capture the transient features of flow dynamics, the unsteady solver is adopted. The standard k-ε model is employed to describe the turbulence transport. In order to correctly predict the incipient or minimum fluidization conditions, the Syamlal-O'Brien empirical correlations for momentum transfer across the fluid-solid interfaces is introduced via a user-defined function. For the boundary conditions at the exit of entrance region, it is set as outflow since the details of the flow velocity and pressure are not known prior to solution of the flow. For the boundary conditions at the inlet of entrance region, uniform velocity profile is set for the gas, whereas the mass flow rate condition is given for the solids.

(A) Typical Flow Structure and Modeling Validation

During the unsteady simulation, the time step size is set as 0.001s and total of time steps is 100000. Figure 3.17 illustrates the typical transient flow structure of phase transport properties in the entrance region, with the entrance of annular ring of L-valve feeders above a flow distributor that simulates the case (a) in Du et al. 2004. Figure 3.17(a) indicates that the transient spatial distribution of solids concentration may not be continuous, coupled with the formation and destruction of clusters. The transient flow structures in phase velocity however are relatively stable, as demonstrated in Figure 3.17(b) and (c). A time-averaged flow structure can be obtained by averaging the

transient results over a period of time that is longer than the integral characteristic time scale of the flow system.

It is realized that the published experimental data of phase distributions of transport properties in the entrance region are very scarce, which very much limits the validation of our simulation both in the range and in the accuracy. Figure 3.18 gives an example for the comparison of the time-averaged radial solids concentration distribution between the simulation results and the tomographic measurements from (Du Bin, et al. 2004). The riser inner diameter used in the experiment is 0.1 meter, and the fluidized particles are FCC catalysts with a mean diameter of 60μm and particle density of 1400 kg/m^3. The gas is fed from riser bottom and solids are fed through the L-valve aeration on the side wall. The comparison indicates that the numerical simulation agrees reasonably well with the experimental measurements, which partially validates the simulation.

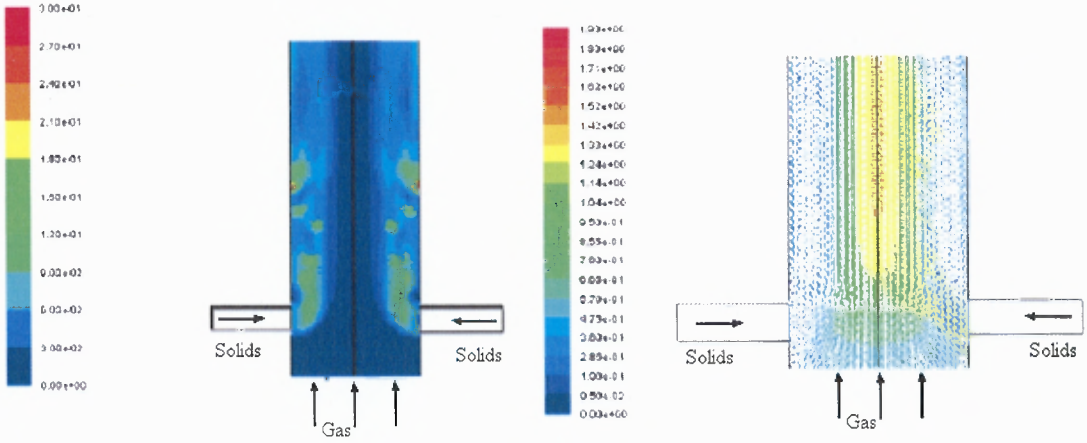

(a) Solids volume fraction profile (b) Gas velocity profile

Figure 3.17 Transient flow structures in entrance region.
(U_g=0.97m/s, G_s=1.32 kg/m^2-s, 0.1 meter I.D.)

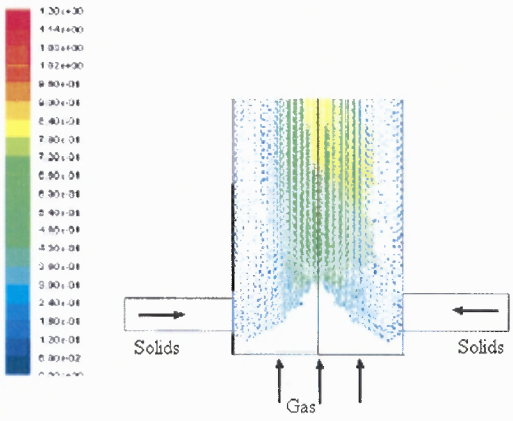

(c) Solids velocity profile

Figure 3.17 Transient flow structures in entrance region (Continued). (U_g=0.97m/s, G_s=1.32 kg/m^2-s, 0.1 meter I.D.)

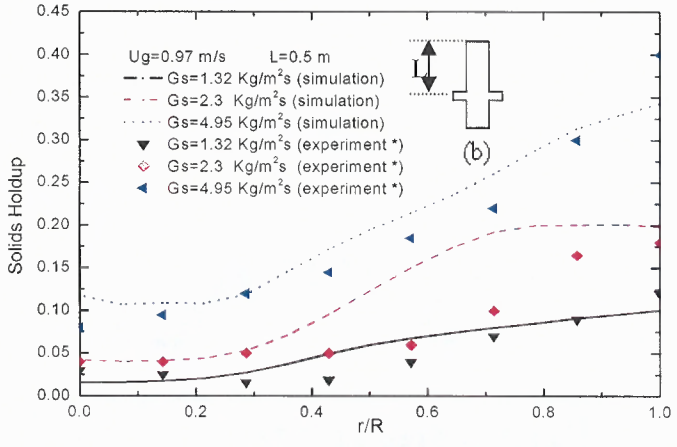

(a) Gas velocity of 0.97 m/s

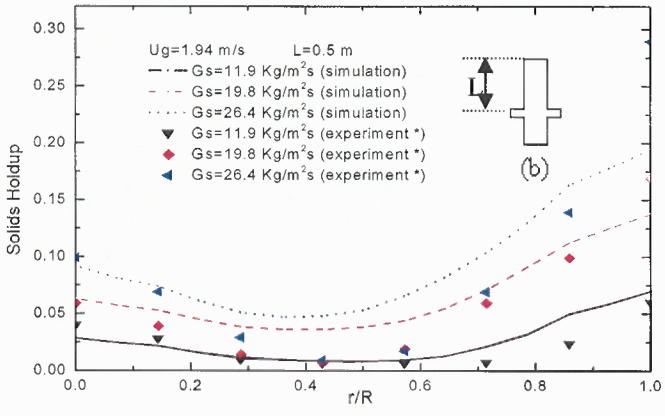

(b) Gas velocity of 1.94 m/s

Figure 3.18 Radial distribution of solids concentration. (* data are from Du et al. 2004).

(B) Effect of Solids Feeding Patterns

For the convenience of investigating the effect of solids feeding patterns, the radial distributions of phase transport properties (i.e., solids concentration, solids velocity and gas velocity) under various feeding patterns and operation conditions are compared in risers of the same diameter and at the same height above the level of solids entrance, as illustrated in Figure 3.19 and Figure 3.20. Figure 3.19(a) shows that there exists a clear difference in solids concentration profiles with three different solids feeding patterns. For instance, the solids feeding type (a) leads to a very much even profile of solids concentration than those by other two types, whereas the cross-flow feedings may lead to sever solids accumulation near the wall. It is noticed that there is a moderate difference in all profiles between the feeding patterns (b) and (c), which indicates a limited role of the taper section in the pattern (c). Figure 3.19(b) shows much weaker gas velocities with the feeding patterns (b) and (c) near the wall, indicating a strong damp effect by the high solids concentrations near the wall. It is interesting to note that, as shown in Figure 3.19(c), there is some backflow mixing with the feeding pattern (c), whereas no backflow mixing occurs with other two feeding patterns at this level. This is probably due to the effect of taper section that weakens the gas flow near the wall, as shown in gas velocity profile in Figure 3.19(b). Figure 3.20 shows the effect of solids feeding patterns on flow structures in the entrance regions, with an elevated solids mass flow rate and at an elevated gas velocity under otherwise similar operating conditions in Figure 3.19. Overall both Figure 3.19 and Figure 3.20 present similar radial distribution profiles of phase transport properties, which indicates that the effect of solids feeding patterns in the entrance regions is strongly dependent upon the type of solids feeding mode (such as

cross-flow feeding and concurrent flow feeding) but is weakly dependent upon the solids mass flow rate and gas velocity.

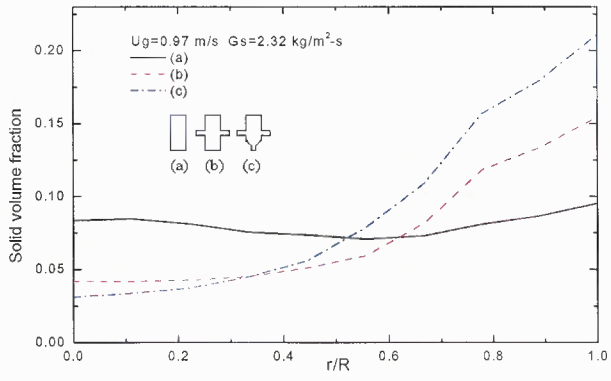

(a) Radial distributions of solid volume concentration.

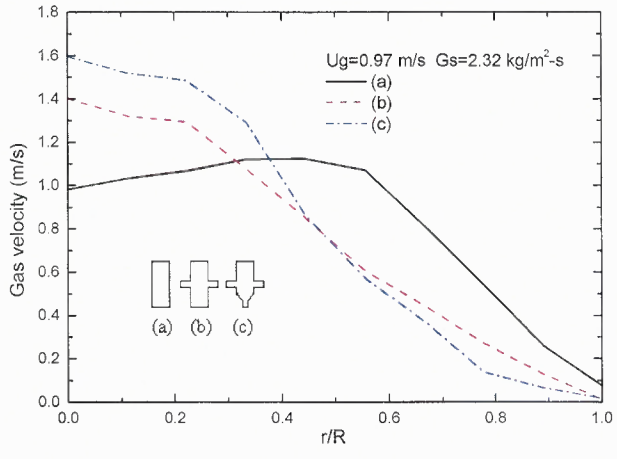

(b) Radial distributions of gas velocity

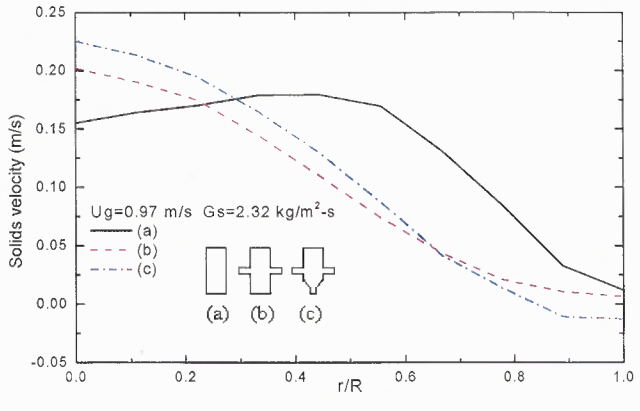

(c) Radial distributions of solids velocity

Figure 3.19 Effect of solids feeding patterns on radial profiles. (U_g=0.97m/s, G_s=2.32 kg/m^2-s, z=0.3 m)

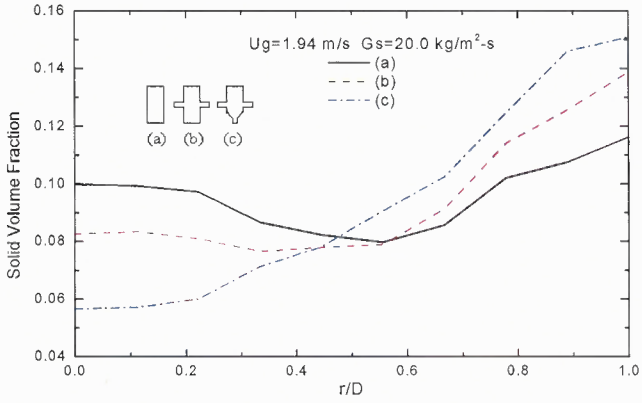

(a) Radial distributions of solid volume concentration

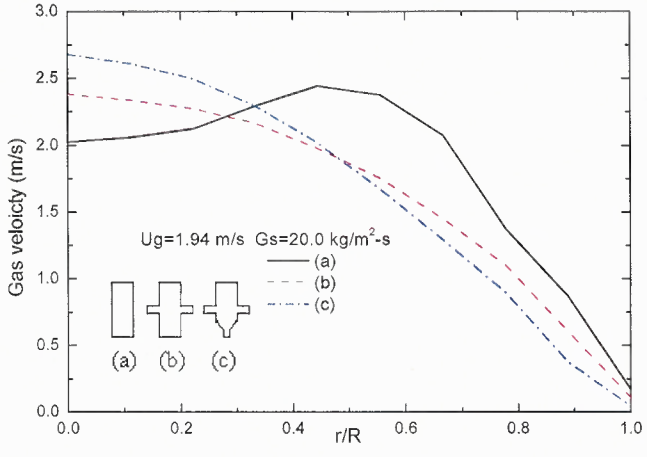

(b) Radial distributions of gas velocity

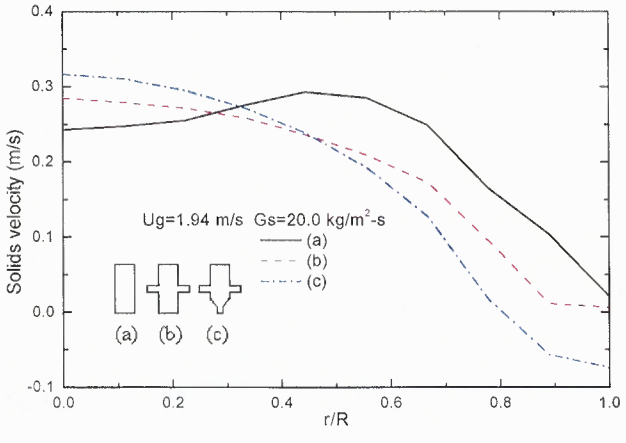

(c) Radial distributions of solids

Figure 3.20 Effect of solids feeding patterns on radial profiles. (U_g=1.94m/s, G_s=20.0 kg/m^2-s, Z=0.3 m)

(C) Characteristic Length of Entrance Region

For a solids flow in the entrance region, a wall region of dense solids concentration has to be developed from the riser bottom because, due to the wall boundary effect, the averaged gas velocity in the wall region becomes too low to support upward moving solids. At a certain height, the solids in the wall region have to exhaust all their initial upward momentum against gravity as well as against the backflow mixing. At this location the averaged solids velocity in the wall region is null and, beyond this characteristic height, solids in the wall region start to move downward (a phenomenon known as backflow mixing). The head-on impact of upward moving solids and backflow mixing solids is believed to be the major mechanism leading to the radial-inward moving migration of solids. The distance between the entrance location of solids feeding and this characteristic height (which is the turning point of the solid velocity) is defined in this paper as *Characteristic Length of Entrance Region.* There is no well-established theory of determining the characteristic length for the flow pattern transition from the multi-dimensional flow in the entrance to the approximated one-dimensional flow. In our paper, the characteristic length of entrance region is defined as the distance from the entrance of the riser to the point where the solid velocity at the wall decreases from entrance velocity to zero. Beyond this point, the flow pattern may be approximately characterized as one-dimensional. This definition is schematically illustrated in Figure 3.21. This characteristic length may also be used as a demarcation position for the flow pattern transition between the multi-dimensional flow in the entrance and one-dimensional flow approximation in the following main region of riser.

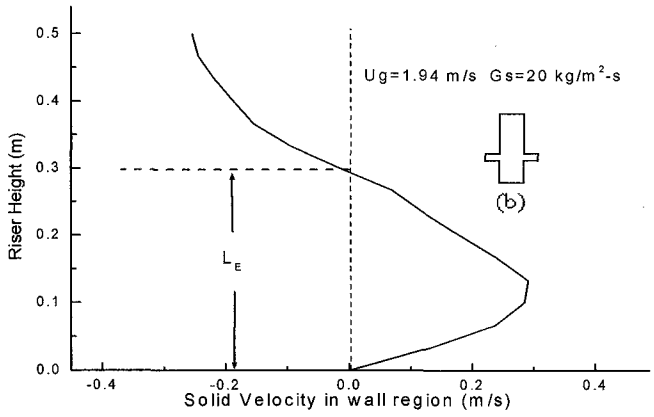

Figure 3.21 Definition of characteristic length of entrance region (L_E).

Figure 3.22 shows the effects of solids feeding patterns on this characteristic length of entrance region at various solids mass flow rates and gas velocities. It is noted that the characteristic length of entrance region is quite independent of solids mass flow rate and gas velocity, however it is strongly dependent on the solids feeding pattern. After comparison we can see that solids feeding type A has the largest characteristic length of entrance region, and the characteristic length of solids feeding pattern C is the smallest. Using a tracing technique, from the simulation, it can be observed that, starting from the solids entrance, solid moves upward with the very low initial axial velocity for all three cases. Once entering the riser, all solids including those very close to the wall, experience a short period of acceleration then quickly exhaust their inertia possibly by inter-particle collisions. Beyond some certain height of riser, the solids near the wall begin to move downward. Figure 3.22(a) shows that the characteristic lengths of entrance region are 0.35 m, 0.31 m and 0.26 m, respectively, for the three feeding patterns in this study.

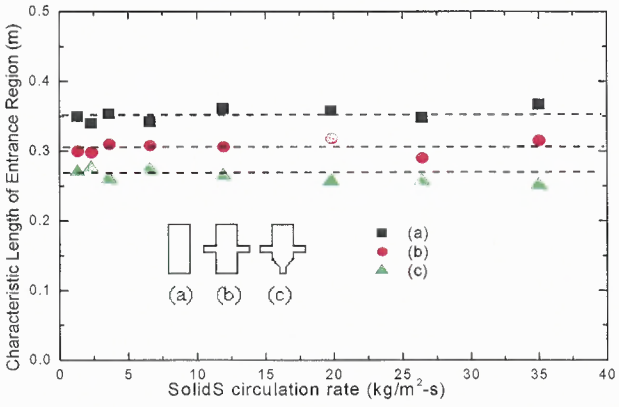

(a) Effect of solids mass flow rate

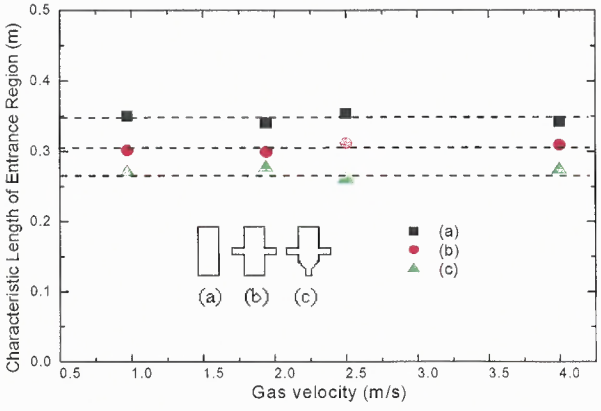

(b) Effect of gas velocity effect

Figure 3.22 Variable characteristic length of entrance region.

In the wall region of all three simulated solid feeding patterns, due to the solids-wall interactions and the non-slip of gas velocity at the wall, the drag force from gas phase is insufficient to overcome the gravity and frictional forces of the solids, thus solids near the wall will gradually lose their inertia and eventually their velocity will decrease to zero. So, the characteristic length of entrance region is basically decided by two factors: the solid initial momentum and averaged gas velocity in the wall region. Pattern A represents a configuration with a higher solids initial momentum and a relatively smaller slip velocity, which leads to a longer characteristic length of entrance region. Whereas Pattern C has a relatively lower solids initial axial velocity and the smallest gas velocity

in the wall region due to the expansion section of the riser, it has the smallest characteristic length of all three configurations considered.

3.4.5.2 Flow Structure in Main Region. As described in modeling methodology, the flow structure simulation in the main riser region is based on a modified mechanistic model originally developed by our research group (Halow JS., et al. 1993). Basic assumptions or requirements of this mechanics model include (1) one-dimensional flow; (2) three-zone flow structure, with predefined zone boundary or correlation; (3) neglect of inter-zone transport of gas phase; and (4) given radial distributions of phase transport properties at the inlet. The length of main riser region is the difference between the riser height and the characteristic length of entrance region.

(A) Three-Zone Approximation of Inlet Flow Conditions

Based on the flow structure simulation in the entrance region, the time-averaged radial distributions of phase transport properties at the end of the entrance region can be obtained, as exemplified in Figure 3.20. However, the mechanistic model of flow structure is currently based on a three-zone approximation, which calls for the zone-averaging over these continuous-based radial profiles, as exemplified in Figure 3.23. It should be pointed out that the selection of the three-zone boundary is not rigorously based on a scientific definition, rather based on the rough estimation from tomographic measurements of solids concentration [You, et al. 2008]. The r/R=0.8 for the wall region is our conservative estimation based on many reported radial distributions in velocity and solids concentration measurement in dilute regime (although the extension into dense regime near the riser entrance may be questionable), and r/R=0.45 is our best estimation based on concentration transition from ECT measurements. This approximation is agreed

with ECT findings. We understand these ratios could be dependent upon the riser flow characteristics such as riser size, transport regime and overall flow conditions, which needs to be considered in the future modeling.

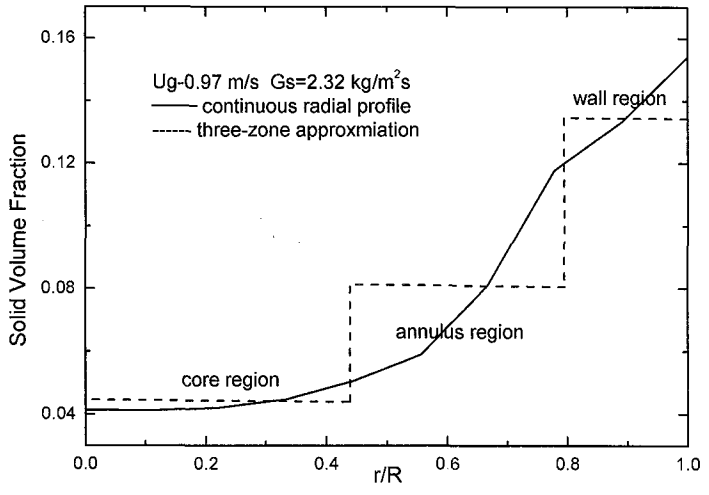

Figure 3.23 Three-zone approximation of inlet condition.

(B) Effect of Entrance on Flow Structure

Figure 3.24 gives the effect of solids feeding pattern on the axial distributions of solid concentrations of each zone in the main riser region. It is shown that, at the same operation conditions, the use of different solids feeding patterns has no significant impact on the basic flow structures along the riser, namely the axial distributions in each zone is weakly dependent on the type of solids feeding. Figure 3.24(a) shows that, with a low solids mass flow rate, there is little difference in solids concentration distributions between the core and annulus regions, indicating a two-zone flow structure. In the wall zone near the inlet of main region, there exists a peak in the axial distribution of solids concentration. This may reflect the relatively delayed effect of solids acceleration near the wall as well as the strong coupling between the wall and annulus region. Beyond a certain height (say, z/D > 10), the axial distribution of solids concentrations becomes

independent of the axial coordinate, indicating the fully developed state of flow structure. Figure 3.24(b) shows that, with a high solids mass flow rate, there is a clear three-zone flow structure throughout the entire main region. Similar to the case of low solids mass flow rate, beyond a certain height (in this case, z/D > 15), the flow reaches a fully developed state. In Figure 3.24(a), the solids concentrations are also compared with available experiment measurement in each region, and it shows a fairly good agreement.

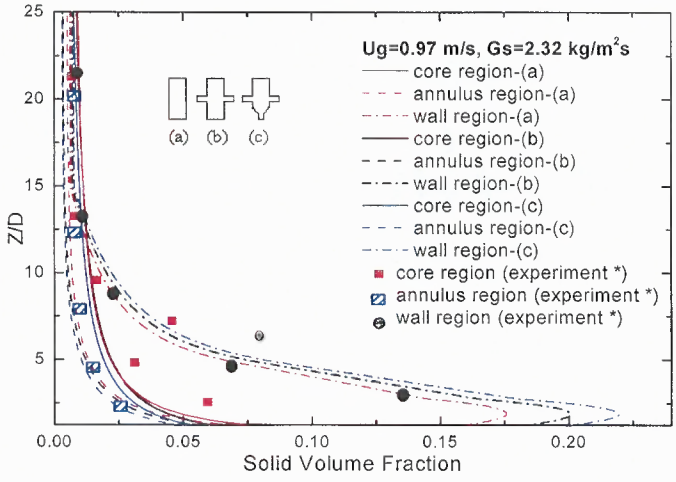

(a) Example of low solids mass flow (Ug=0.97m/s, Gs=2.32 kg/m2-s)
(* data are from Halow JS, et al. 1993)

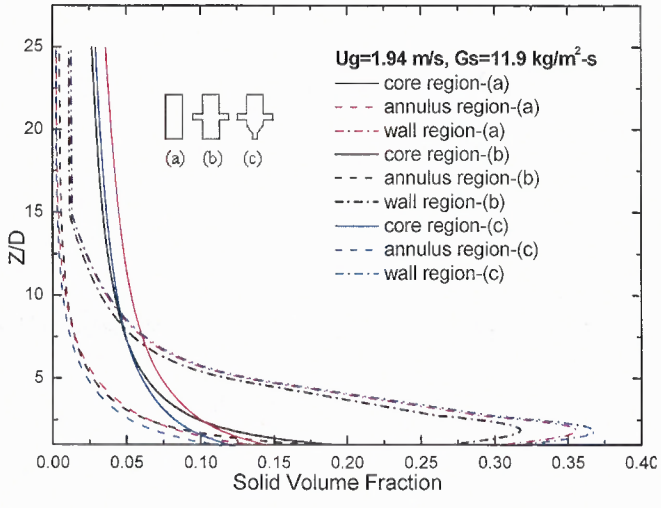

(b) Example of high solids mass flow rate (Ug=1.94m/s, Gs=11.9 kg/m2-s)

Figure 3.24 Effect of solids feeding patterns on solids concentration.

Figure 3.25 demonstrated the effect of solids feeding pattern on the axial distributions of solids velocity of each zone in the main riser region. Similar conclusion can be drawn from Figure 3.25(a) and 3.24(b) that different solids feeding patterns has no significant impact on the basic flow structure in the riser. In both Figure 3.25(a) and (b), it can be seen that in the core region, there is even smaller impacts coming from the solids feeding patterns when compared with those impacts in annulus and wall region. It is interesting to notice that the solids velocity in the annulus region reaches its peak value at the height of H/D=15 and then keep this velocity through the rest of the riser, while in the core region, it is not true. The solids in the core region keep accelerating in the entire of the riser and its value are is always lower than that in the annulus region. As for the solids in the wall region, it seems that there are no significant changes for the solids velocity and it always moves downward. Besides, in this wall region the impacts coming from solids feeding patterns are still very weak.

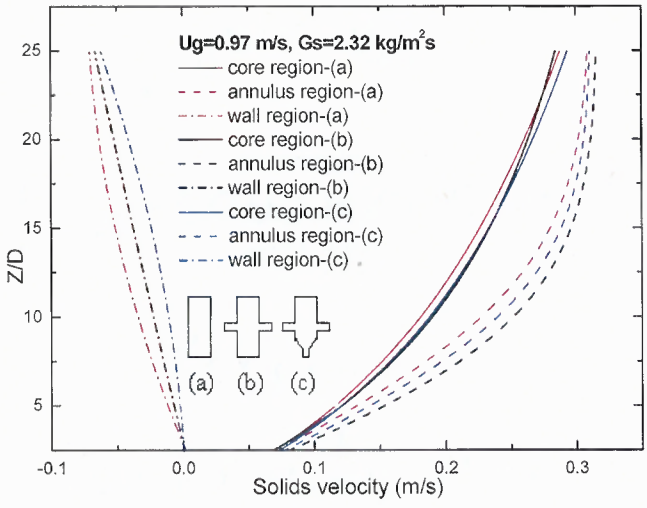

(a) Example of low solids mass flow (U_g=0.97m/s, G_s=2.32 kg/m^2-s)

Figure 3.25 Effect of solids feeding patterns on solids velocity.

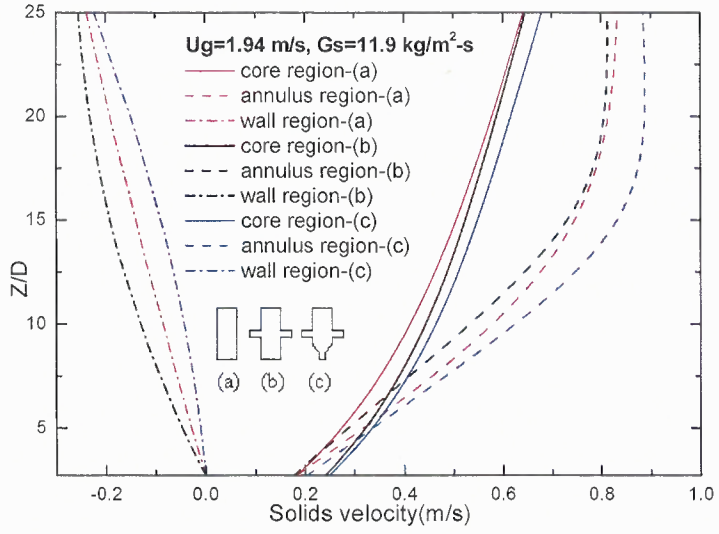

(b) Example of high solids mass flow rate (U_g=1.94m/s, G_s=11.9 kg/m^2-s)

Figure 3.25 Effect of solids feeding patterns on solids velocity (Continued).

(C) Effect of Operation Conditions

So far our simulation is limited to the operating conditions similar to those in the published experiment study in Du et al. 2004. It is interesting to speculate the effect of entrance on flow structure under other operation conditions, as illustrated in Figure 3.26 for the axial distribution of solids concentration. Figure 3.26(a) represents the case of low solids mass flow rate at a high gas velocity; whereas Figure 3.26(b) shows the typical case of high solids mass flow rate at a low gas velocity. Both cases suggest that the basic flow structure is weakly influenced by the type of solids feeding but strongly dependent on the operations conditions. With a significant increase in solids mass flow rate, as shown in Figure 3.26(b), a reversal-hump-shaped distribution of solids concentration occurs in the core region. The initial decrease of solids concentration is due to the entrance effect on wall boundary layer development, whereas the hump results from a combined effect of a strong immigration of solids to the core region and a much reduced acceleration of the solids in the core region. The

formation of the peak solids concentration in the core region can trigger the instability of the "core-annulus-wall" three-zone structure, as observed in Du et al. 2004. When the peak solids concentration is high enough, the flow-induced particle-particle interactions (such as wake-induced collisions) will lead to the collapse of the stable structure of solids in the core region, like choking, and hence the destruction of the entire flow structure in the riser.

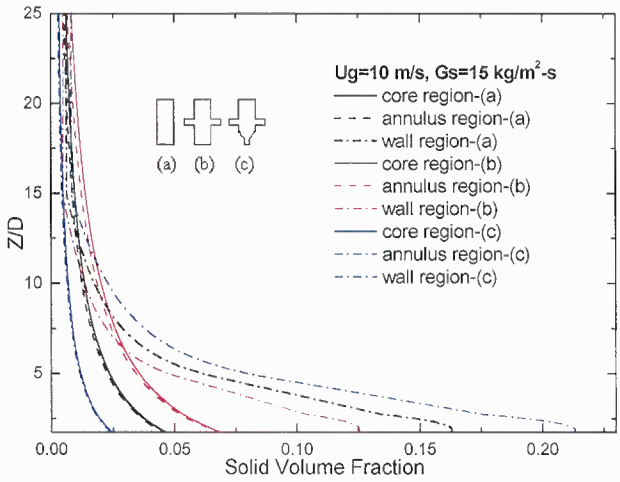

(a) High gas velocity and low solids mass flow rate

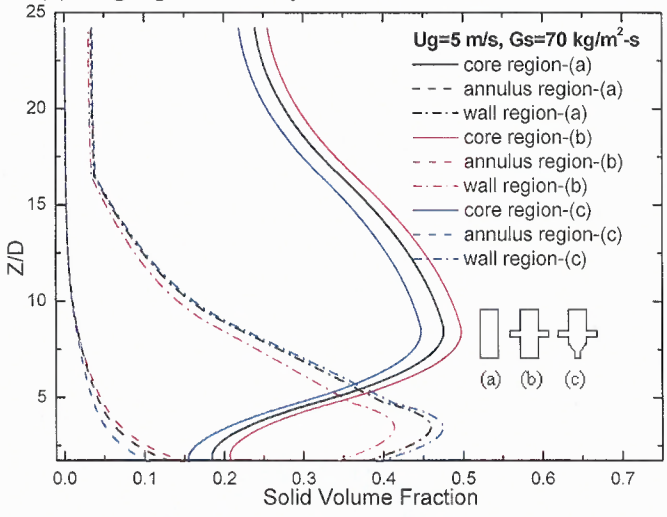

(b) Low gas velocity and high solids mass flow rate

Figure 3.26 Parametric study of effects of entrance region.

Till now, we have investigated the effect of various riser entrances on the overall flow structure and its stability at different operation conditions. Three riser entrances are selected to simulate the common solids feeding devices of risers, namely, the J-bend feeder, the L-valve feeder with a fluidized bed distributor, and the L-valve feeder after a taper section. For the purpose of validation, some simulation results are directly compared with available experimental measurements and reasonably good agreements are reached. It was concluded that the riser characteristic length of entrance region is almost independent of gas inlet velocities and solids mass flow rates; however it is moderately influenced by the solid feeding patterns. The study also shows that the flow structure in the entrance region can be strongly affected by the selection of solids feeding patterns but weakly dependent upon the operation conditions. According to the results of riser main region simulation, it is shown that, at the same operation conditions, the use of different solids feeding patterns has no significant impact on the basic flow structures along the riser, namely the axial distributions in each zone is weakly dependent on the type of solids feeding. Besides, it can also be concluded from the study that even the flow stability will not be significantly affected by the types of solids feeding patterns.

CHAPTER 4

MODEL OF GAS-SOLIDS TRANSPORT WITH CHEMICAL REACTION

While commercial FCC riser reactor converts heavy hydrocarbon petroleum fractions into a slate of more usable products, there, in nature, exist strong inter-coupling between gas-solids transport flow hydrodynamics and chemical reaction kinetics. On one hand, as quantified by the rate law of each reaction, reaction rates are heavily related to the local flow hydrodynamics, such as local temperature and concentrations of catalyst involved in reactions. On the other hand, the local flow hydrodynamics will also be significantly influenced by the momentum transfer, heat and mass transfer and even phase transfer due to chemical reactions.

Unfortunately most of published literature either focused too much on the FCC process itself, or only coupled the FCC process with oversimplified plug flow hydrodynamic model, which obviously neglect the significant influence of multiphase flow hydrodynamics on the cracking kinetics and certainly cannot truly reflect the strong interaction behavior between them.

In order to accurately predict the multiphase phase flow hydrodynamic coupled with FCC reaction kinetics occurred in the riser reactor, special attention should be given to the strong inter-coupling between gas-solids transport flow hydrodynamics and chemical reaction kinetics. The aim of this work is to develop a generic modeling approach which can fully incorporate multiphase flow hydrodynamics with FCC process. The emphasis of this model is to develop a framework to simultaneously simulate the multiphase flow hydrodynamics, cracking reaction and their inter-coupling characteristics in a riser reactor. This modeling

approach opens up new dimensions for making generic models suitable for the analysis and control studies of FCC units. Predictions of the model are compared with the yield pattern of industrial scale plant data reported in published literatures.

4.1 Governing Equations of Hydrodynamic Model with Reaction

The aim of this work is to develop a modeling approach which can incorporate gas-solids multiphase flow hydrodynamics with FCC reaction process, and consider the effects of local temperature and catalyst local concentration on reaction rates. In order to simplify the model equations, following commonly used assumptions are made.

1. It is assumed that the small amount of steam and by-product H_2 are neglected in the mixture of vapor, so all the gas phase will only be composed of the compounds in the four-lump model.

2. It is assumed that, at the riser inlet, hydrocarbon feed instantly vaporizes when comes in contact with the hot catalyst coming from the regenerator (taking away latent heat and sensible heat from the hot catalyst). The vapor formed moves upward in thermal equilibrium with the catalyst. Under this assumption, the complex multiphase flow which includes gas, solid and liquid become gas-solids flow.

3. The wall of the riser is assumed to be adiabatic and there is no heat loss to environment from the rise. The temperature of the reaction mixture (hydrocarbon vapors and catalyst) falls only because of the endothermic cracking reactions.

4. Ideal gas law is assumed to hold while calculating gas phase density variation on account of molar expansion due to cracking and gas phase temperature.

5. Temperature of gas phase and solids phase is assumed to the same in local thermal equilibrium, and heat and mass transfer resistances are assumed to be negligible. In this way, it is much easier to calculate total energy balance inside the riser reactor. The initial temperature setup for model simulation will be estimated upon initial feed temperatures of catalyst and VGO.

6. In addition, all coke (one of the productions of the cracking reaction) is assumed to attach on the catalyst particles surface and the change of catalyst particles dimension is neglected.

As a first step of this study, in order to simplify the mathematical derivation, four-lump reaction scheme developed by Lee *et al.* (1989) is used to simulate the cracking reactions.

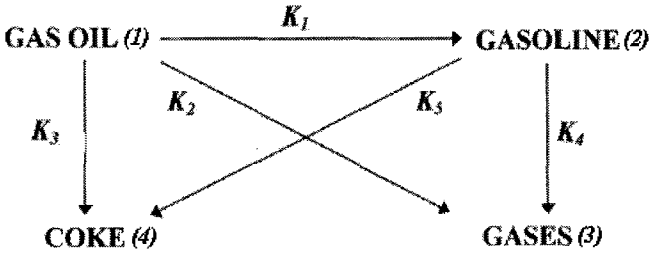

Figure 4.1 Four lumps model for gas oil cracking reactions

Figure 4.1 gives the typical four-lump model used in our modeling approach. It is assumed that the VGO (vacuum gas oil) is cracked into the most desired gasoline, by-products of gases and coke. Since the FCC reactor is operating at very high temperature (about 700~900K), there is secondary cracking reaction occurs in which some gasoline cracks into coke and gases. There is no inter-reaction between coke and gases.

The solid catalyst and gas oil are fed from the bottom of the riser reactor and the governing equations are discussed below.

The mass balance of gas and solid phase can be described by Equation (4.1) and (4.2).

Solid phase:
$$\frac{d(\alpha_s \rho_s U_s)}{dz} = (r_3 + r_5)M_4 \tag{4.1}$$

Gas phase:
$$\frac{d(\alpha_g \bar{\rho}_g U_g)}{dz} = -(r_3 + r_5)M_4 \tag{4.2}$$

Here the average gas density can be calculated from the ideal gas law as:

$$\bar{\rho}_g = \frac{P \cdot \sum_{i=1}^{3}(C_i \cdot M_i)}{RT \sum_{i=1}^{3} C_i} \tag{4.3}$$

The term in the left hand side of the above equations represents the coke mass amount, which is the mass transfer between gas and solid phases when coke deposits on the surface of the solid catalyst.

Based on the force balance of each control volume, the momentum equation of solid and gas phase can be derived as:

$$-\frac{dP}{dz} = \bar{\alpha}_g \rho_g g + \bar{\alpha}_g \rho_g U_g \frac{dU_g}{dz} + F_D \tag{4.4}$$

Which shows that, pressure gradient is balanced against gravitational force, acceleration of gas phase and gas-solid interfacial force between gas and solids.

The momentum equation of solids phase can be expressed as (You et al. 2008):

$$F_D = \bar{\alpha}_s \rho_s g + G_s \frac{dU_s}{dZ} + \gamma \tag{4.5}$$

The particle-fluid interfacial force balances against the gravitational force, solids acceleration and the solids axial compact momentum due to inter-particle collisions. In Equation (4.4), F_D is the drag force per unit volume. It is obtained by multiplying the drag force on a single particle by the number of particle per unit volume. In this model, Richard-Zaki equation is still utilized to consider the averaged drag force (You et al. 2008):

$$F_D = \frac{18\mu}{d_s^2} \cdot \frac{\alpha_s}{(1-\alpha_s)^4} \cdot (U_g - U_s) \tag{4.6}$$

In the solids acceleration regime, the stabilized wake effect becomes very important (Zhu *et al.*, 1994; Joseph, 1993), which leads to reduction in drag force of trailing particles of colliding pair. Hence, the modified drag force may be expressed as:

$$F_D = \zeta_1 F_{D0} \tag{4.7}$$

ζ_1 is the coefficient of wake effect of the neighboring particles on the particle-fluid interfacial force (Zhu *et al.*, 1994), which is represented as:

$$\zeta_1 = 1-(1-K_A)\exp\left[K_B\cdot\left(\sqrt[3]{\frac{\pi}{6\bar{\alpha}_s}}-1\right)\right] \tag{4.8}$$

where

$$K_A = 1-\exp(-0.483+3.45\times10^{-3}\,\mathrm{Re}-1.07\times10^{-5}\,\mathrm{Re}^2) \tag{4.9}$$

$$K_B = -0.115-8.75\times10^{-4}\,\mathrm{Re}-5.61\times10^{-7}\,\mathrm{Re}^2) \tag{4.10}$$

Then the corrected drag force should be expressed as:

$$F_D^{'} = \zeta_1\cdot F_D \tag{4.11}$$

With the assumption of instantaneous vaporization of the gas oil, the steady-state continuity equations for the components and lumps in the gas phase can be written as Equations (4.12), (4.13) and (4.14):

$$U_g\frac{dC_1}{dz}+C_1\frac{dU_g}{dz} = -(k_1+k_2+k_3)C_1 \tag{4.12}$$

$$U_g\frac{dC_2}{dz}+C_2\frac{dU_g}{dz} = mk_1C_1-(k_4+k_5)C_2 \tag{4.13}$$

$$U_g\frac{dC_3}{dz}+C_3\frac{dU_g}{dz} = nk_2C_1+qk_4C_2 \tag{4.14}$$

While the continuity equation for the coke on the catalyst is represented by

$$U_s\frac{dC_4}{dz}+C_4\frac{dU_s}{dz} = k_3C_1+k_5C_2 \tag{4.15}$$

In the cracking reaction described in Equation (4.12-4.15), the rate equation or rate law is a mathematical expression used in chemical kinetics to link the rate of a reaction to the concentration of each reactant.

$$k = \kappa(T)\cdot C_A^{n'}\cdot\alpha_s^{m'} \tag{4.16}$$

In this equation k(T) is the reaction rate coefficient or rate constant, however it is not really a constant, because it includes all the parameters that affect reaction rate. Of all the parameters described before, temperature is normally the most important one. The exponents n' and m' are called reaction orders and depend on the reaction mechanisms. Each reaction rate coefficient 'k' has a temperature dependency, which is usually given by the Arrhenius Equation:

$$\kappa(T) = F \cdot e^{-\frac{E_a}{RT}} \tag{4.17}$$

E_a is the activation energy and R is the gas constant. Since at temperature T the molecules have energies given by a Boltzmann distribution, one can expect the number of collisions with energy greater than E_a to be proportional to temperature. F is the pre-exponential factor or frequency factor. The values for A and E_a are dependent on the reaction.

Finally, the temperature dependency of kinetic parameters appearing in Equation (4.12)-(4.15) can be described by the Arrhenius expression:

$$k_i = (\frac{c}{o})_L \cdot \Phi_s k_{i0} \cdot e^{\frac{E_i}{R}(\frac{1}{T_0} - \frac{1}{T_i})} \tag{4.18}$$

In current plug flow model used by industries, an overall catalyst to oil ratio $[(c/o)_{overall}]$, which is defined as feed mass flow rate ratio of catalyst to oil, was used in Equation 4.18 instead of $(c/o)_L$, which we called localized catalyst to oil ratio. The overall catalyst to oil ratio is determined assuming plug flow, namely, it is solely determined by catalyst and oil feed mass flow rate at reactor inlet, and remains constant along the whole riser reactor. The plug flow assumption obviously contradicts to the rise flow characteristics where the catalyst concentration is diluted along the riser.

From reaction kinetics point of view, the cracking reaction rate will be greatly influenced by the contact area between catalyst and reactants, which should be mainly decided by local catalyst solids concentration. As a first endeavor to consider the significant mutual coupling between the flow hydrodynamics and cracking reaction, a localized catalyst to oil ratio $(c/o)_L$ is introduced in Equation 4.18, which is estimated by:

$$(\frac{c}{o})_L = \frac{\alpha_s}{\alpha_{s0}} \cdot (\frac{c}{o})_{overall} \tag{4.19}$$

Besides, the catalyst activity coefficient Φ_s represents the catalyst deactivation due to coke deposition. This coefficient depends on the coke concentration on the catalyst, and following correlation proposed by Pitault et al.(1994) will be adopted in this model.

$$\Phi_s = \frac{11.4}{10.4 + \exp(4.29 \cdot wt_{coke}\%)} \tag{4.20}$$

and

$$wt_{coke}\% = \frac{y_{coke} \cdot w}{m_c} \times 100 \tag{4..21}$$

Since it has been assumed that the gas phase is always in thermal equilibrium with the solid catalyst along the riser, and the heat transfer resistance between the catalyst and gas phases has been neglected, the evolution of the temperature along the riser is obtained from the enthalpy balance, which can be represented as:

$$\left(\alpha_s \rho_s c_{p,s} U_s + M_4 C_4 c_{p,coke} U_s + \alpha_g \overline{\rho}_g \overline{c}_{p,g} U_g\right) \frac{dT}{dz} = -\sum_{i=1}^{5} r_i \cdot \Delta H_i \tag{4.22}$$

The energy equation represents the combined change of internal energy of gas and solid phase.

In summary, for a complete description of this gas-solids flow hydrodynamics coupled with reaction model, we have total 10 independent Equations (4.1), (4.2), (4.3),(4.4), (4.5), (4.12), (4.13), (4.14), (4.15), (4.22) for total 10 independent variables (α_s, U_s, U_g, C_1, C_2, C_3, C_4, $\overline{\rho}_g$, T ,P), hence, the problem is closed.

4.2 Model Validation with FCC Plant data

In this proposed model, the material balance equations are combined with reaction kinetics and the hydrodynamic model equations to obtain the moles of each lumps at any height of the riser, thus, this model not only predicts the yield pattern along the riser height, but also predicts the temperature, pressure, phase velocities and phase concentrations along the whole riser.

The reaction kinetics of the FCC reactor depends on process variables and parameters such temperature, space velocity, ratio of catalyst circulation rate to oil mass flow rate, regenerator temperature, gas oil preheat temperature, physical properties of the gas oil and properties of the catalyst. Usually, feed and catalyst conditions do not change frequently. Thus they are not considered to be variable in this study. Among all possible variables, the most important is reactor temperature.

As a preliminary study of the proposed model, we used two operating cases reported in literature. Table 4.1 gives the basic parameters of the operating conditions. The reaction constants for the four-lump reaction at different temperature adopted in this study are given in Table 4.2.

Since the proposal model is a simplified one-dimensional model and based upon the assumption which the riser reactor has uniform inlet conditions, the starting location of the simulation is above the real riser reactor inlet, and the entrance region (You, et al, 2008) where most phase mixing and fast evaporating happen in the riser bottom is not within the simulation region. Hence, the initial conditions for this model simulation are slightly different from those conditions listed in Table 1. However, some simple derivation and calculation based on mass and energy balance will be necessary to reach the initial conditions for simulation based on the real conditions in Table 4.1.

The values of heat of reaction and part of the physical properties used in our simulation are also listed in Tables 4.3 and 4. 4.

Case study -1 Industrial FCC plant data reported by Ali *et al.* (1997) given in Table 4.1 are used in this case study for the purpose of validation of our model prediction.

Table 4.1 Operating Conditions of Industrial FCC Riser Reactors

Parameter	Ali et al. (1997) (Case study-1)	Derouin et al. (1997) (Case study-2)
Catalyst flux (kg/s)	144	470
CTO	7.2	5.5
VGO feed rate (kg/s)	20	85
Feed temperature (K)	496	650
Catalyst inlet temperature (K)	960	960
Riser inside diameter (m)	0.8	1
Riser height (m)	33	35
Droplet diameter (μm)	100	100
Riser pressure (atm)	2.9	3.15

Table 4.2 Reaction Rate Constants and Activation Energy

	Temperature (K)			K_0	E_a
	755	822	889	(hr^{-1})	(kJ/mol)
K_1	15.644	39.364	79.408	7.978e5	68.2495
K_2	1.297	3.302	6.012	3.765e4	64.5750
K_3	3.323	9.749	28.02	4.549e6	89.2164
K_4	0.411	0.393	1.364	7.957e1	115.458
K_5	0.711	1.730	2.470	3.255e3	52.7184

Table 4.3 Lump Components and Catalyst Physical Properties

Species	Molecular weight (kg/kmol)	Specific heat(J/kg K)
VGO	400	1040
Gasoline	100	1040
Gas	50	1040
Coke	400	1040
catalyst	1730 (density kg/m^3)	1000

Table 4.4 Heat of Reaction Used For the Simulation

Reaction	ΔH_r (J/kg)
VGO → Gasoline	195
VGO → Gas	670
VGO → Coke	745
Gasoline → Gas	512.5
Gasoline → Coke	550

Figure 4.2 gives the yield weight percentages at the exit of the riser reactor, which shows a fairly good agreement with model predictions. It also demonstrates reasonable tendency of each component along the whole riser height.

We can see from the comparison that, most of the cracking reaction occurs in lower part of the riser and the weight percentage of each component changes very violent. With the increase of the riser height, the gradient of each curve become smaller. The VGO conversion rate and gasoline yield predictions are demonstrated in Figure 4.3.

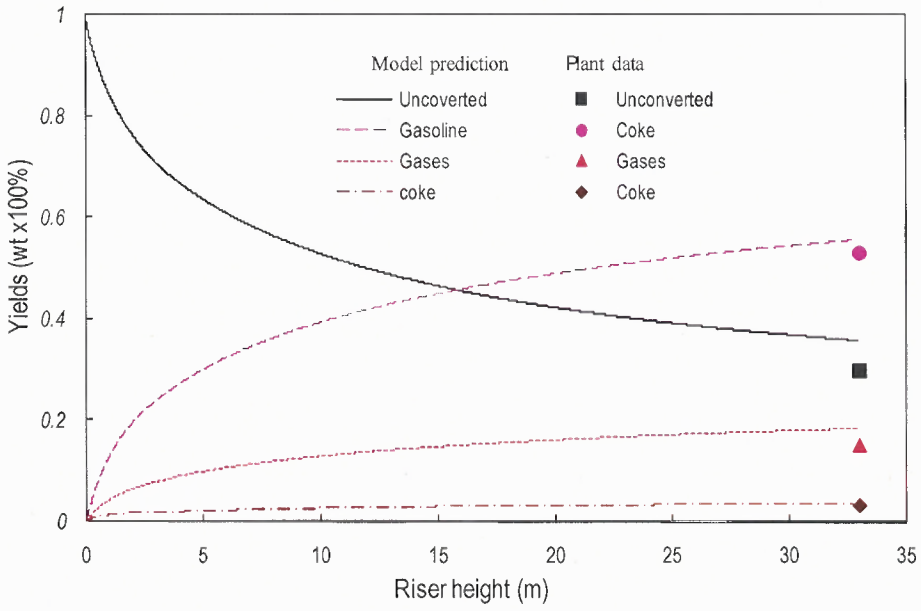

Figure 4.2 Case study 1- comparison with the data reported by Ali et al. (1997).

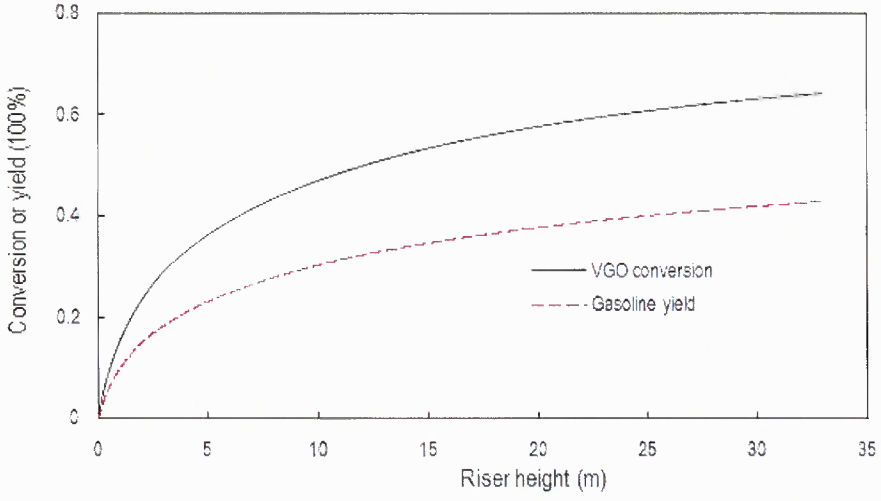

Figure 4.3 VGO conversion rate and gasoline yield prediction results.

From the Figure 4.3, very similar conclusion can be drawn as those from Figure 4.2. Under the circumstance of operation conditions listed in Table 4.1, the total VGO conversion rate is about 63% and gasoline yield is about 42% at the outlet of riser, respectively. However, the curve shows that, at the height of approximately 5 meter, the VGO conversion rate is about 35% and gasoline yield is about 22%, which

is more than half of the total results, indicating the riser bottom is the place where VGO cracks most violent.

Case study -2 In this case FCC plant data (in Table 4.1) reported by Derouin et al. (1997) was used to compare our model predictions. Authors reported the product data for gasoline yield and conversion at four different height positions along the riser. Figure 4.4 shows the comparison results for this case.

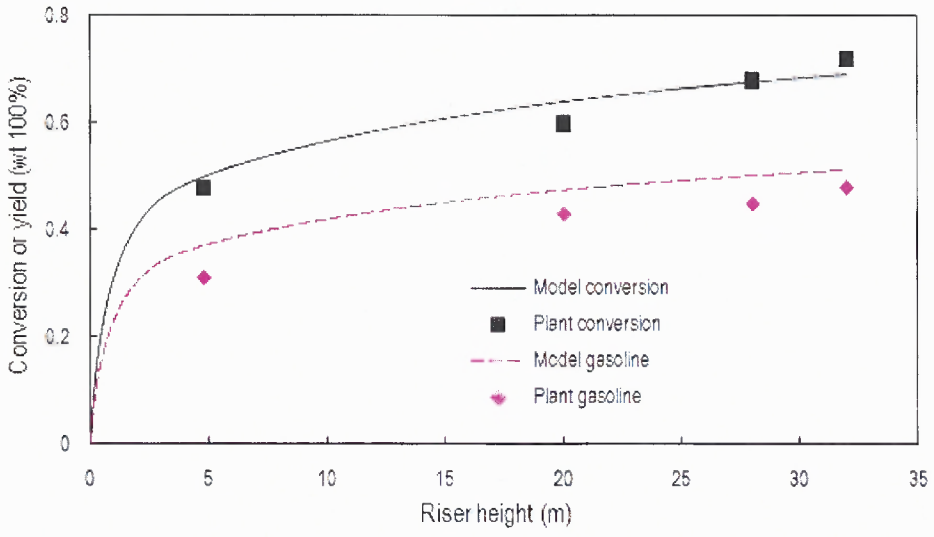

Figure 4.4 Case study 2- comparison with the data reported by Derouin et al. (1997).

From the comparison shown in Figure 4.4, the model prediction for the gasoline yield and VGO conversion along the riser height matches satisfactorily with the plant data. When comparing with the data in Figure 4.3, the gasoline yield in the lower part of the riser in case 2 even bigger than that in case 1. At the height about 5 meter, the VGO conversion and gasoline yield reach approximately two third of the total value, which implies much more violent cracking reaction in this region compare to the rest of the riser. Figure 4.5 gives the yield of all components in the cracking reaction.

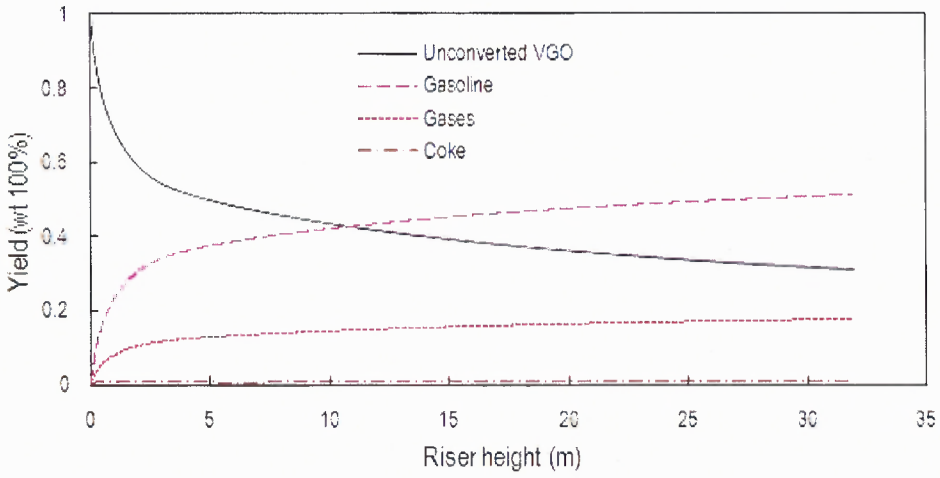

Figure 4.5 Model prediction of component yield.

The above Figure 4.4 and Figure 4.5 provide the comparison of model prediction of conversion and yield with FCC plant data reported in literatures and both of the cases shows that our model predictions match with FCC plant data satisfactorily. In the next part of the study, we will compare our model with traditional plug flow model predictions to find out how this coupled localized catalyst to oil ratio will influence the reaction patterns.

4.3 Comparison with Plug flow model

In order to compare our model prediction with traditional plug flow reaction model, we adopted a simple plug flow model from Ali, et al. (1997).

The riser bed acts as a transported bed, with a high combined stream velocity and a short residence time in the order of a few seconds. Thus it can be assumed that the dynamics of the riser in comparison with the coke burning and temperature changes in the dense phase of the riser are negligible. Therefore, the mass and energy balance equation in the riser are considered at quasi steady-state. In addition, the concentrations of various hydrocarbon gases in the riser are normalized with respect

to the gas oil feed concentration, and the temperature is normalized with respect to the steady-state dense phase temperature (T_{ref})

$$\frac{dy_1}{dz}+\frac{\Phi_s A_R \alpha_g L_R \rho_g}{F_g}\left(k_1+k_2+k_3\right)\cdot y_1=0 \tag{4.23}$$

$$\frac{dy_2}{dz}+\frac{\Phi_s A_R \alpha_g L_R \rho_g}{F_g}\left[(k_4+k_5)y_2-k_1 y_1\right]=0 \tag{4.24}$$

$$\frac{dy_3}{dz}-\frac{\Phi_s A_R \alpha_g L_R \rho_g}{F_g}\left(k_4 y_2+k_2 y_1\right)=0 \tag{4.25}$$

$$\frac{dy_4}{dz}-\frac{\Phi_s A_R \alpha_g L_R \rho_g}{F_g}\left(k_5 y_2+k_3 y_1\right)=0 \tag{4.26}$$

Energy balance:

$$\frac{dT_R}{dz}-\frac{\Phi_s A_R \alpha_g L_R \rho_g}{(F_g cp_g+F_s cp_s)}\cdot\left[y_1\cdot\left(k_1\Delta H_1+k_2\Delta H_2+k_3\Delta H_3\right)\right] + y_2\left(k_4\Delta H_4+k_5\Delta H_5\right)=0 \tag{4.27}$$

In this simple plug flow model, only five independent variables which are normalized lump weight percentage (y_1, y_2, y_3, y_4) and temperature (T). At the same time, based on the mass and energy balance, we also have five independent coupled differential equations, so this model is also self-closed.

In order to compare the predictions of those two different models, we still used the operation conditions listed in Table 4.1 to conduct the simulations. The first case is the operation data reported by Ali, et al., (1997).

Figure 4.5 gives the comparison of model predictions of yield of two different model approaches. One is our model approach which is based on localized catalyst to oil ratio, another one is plug flow model, in which the overall constant catalyst to oil ratio is used.

From the comparison illustrated in Figure 4.6, both of the models provide reasonable good prediction on the yield of different component and match with each other fairly good. However there are still various differences between two sets of data. In the lower part of the riser, the gradient of the yield changes in our model is quite

bigger than those in the plug flow model, which shows more intensive cracking reaction occurs in our model. The reasons behind of the phenomenon are because in our model, the localized catalyst to oil ratio are used instead of the overall catalyst to oil ratio. So in our model, in the bottom of the riser, the localized catalyst to oil ratio is larger than the average values, however, in the top region, the local valve is much less than the average one. Hence in our model prediction results, it always has larger yield gradient in the lower riser part, and small gradient in the upper riser part.

From the comparison in Figure 4.7, it can easier notice the result differences between these two different model approaches, which can further backup our conclusion drawn from Figure 4.6.

The second case we will use for the comparison is the operation conditions reported by Derouin et al. (1997). Figure 4.8 gives the comparison results on the yield along the riser reactor.

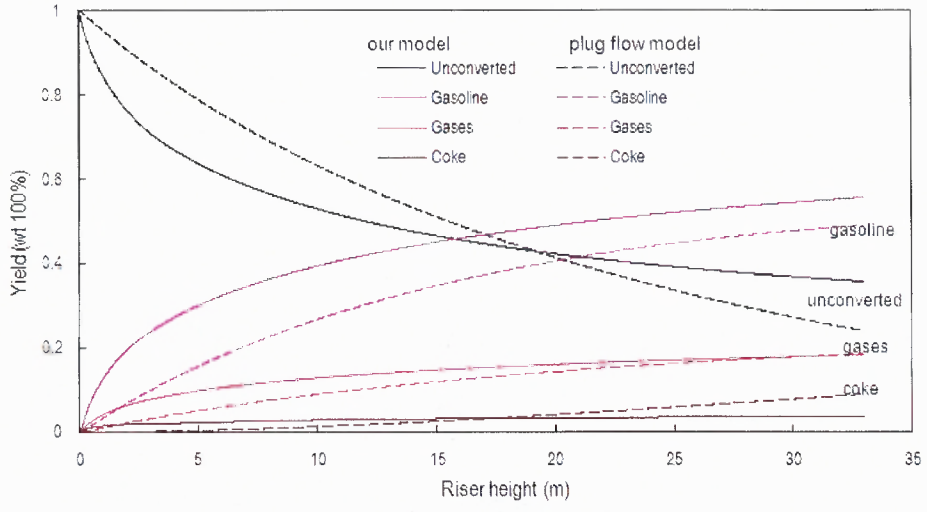

Figure 4.6 Comparison of two model prediction on yield of case 1.

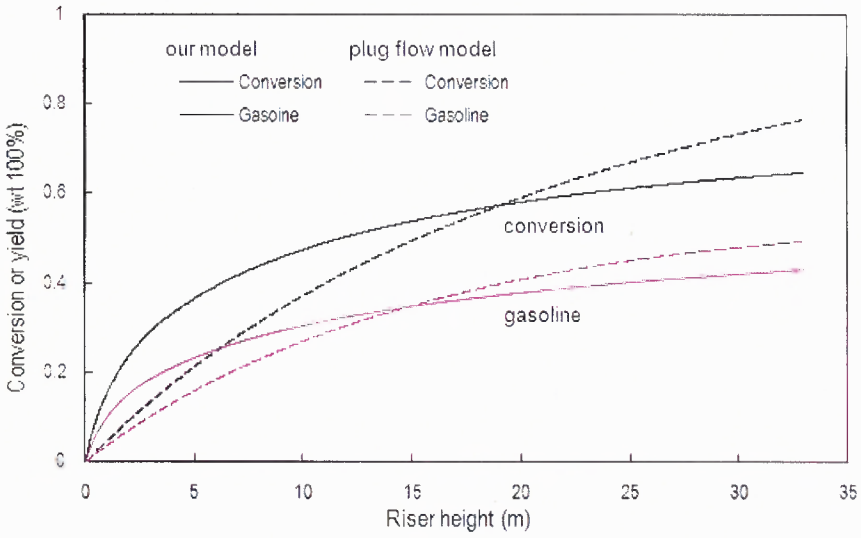

Figure 4.7 Comparison of two model prediction on conversion/yield of case 1.

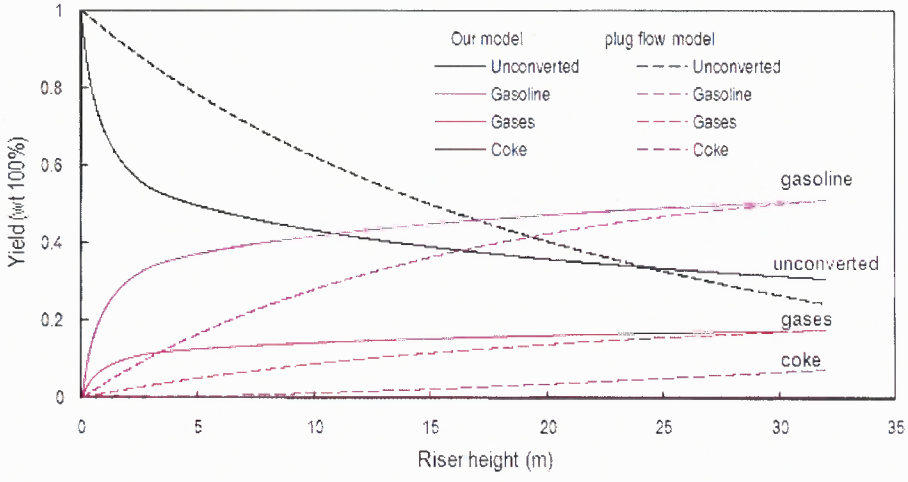

Figure 4.8 Comparison of two model prediction on yield of case 2.

As shown in Figure 4.8 and Figure 4.9, in the results of case 2, the differences between two models are more obvious. Although the calculated final yields based on the two models are in the same box range, the intermediate values of the yield are quite different. For instance, at the height of about 5 meter, the error of the gasoline yield and unconverted VGO is about 40% high.

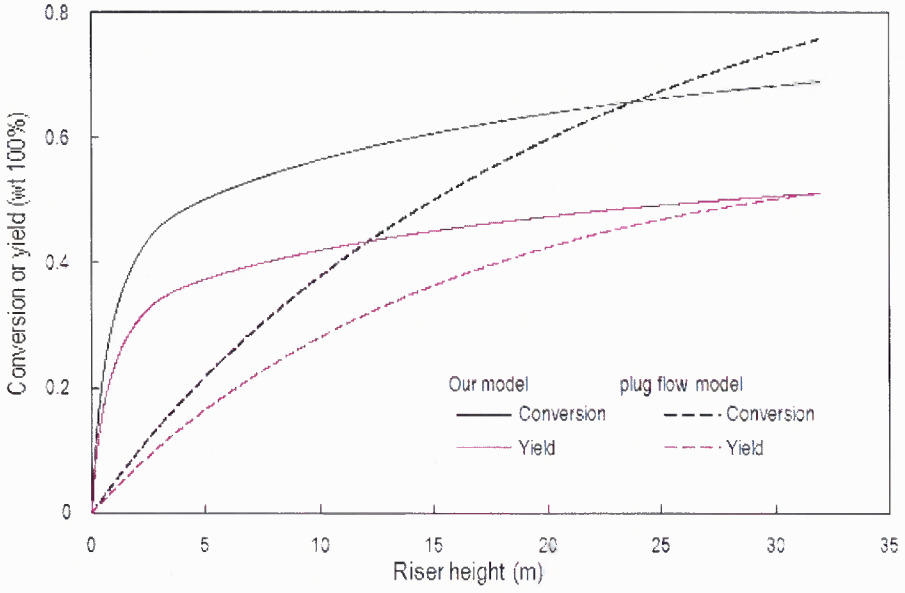

Figure 4.9 Comparison of two model prediction on yield/conversion of case 2.

From the comparison of above two cases, we realized that both of the models can give reasonable good prediction on the conversion and yield results, however, it is also shown that the change rate of the yield or conversion have significant difference, especially in the lower part of the riser. This difference will gradually diminish with the increase of the riser height. The reason to explain those differences is the difference between localized catalyst to oil and overall catalyst to oil ratio.

4.4 Typical predictions of our hydrodynamic model

In this part of study, we will present the typical predictions of our hydrodynamic model, which includes not only the cracking reaction related result, such as yield and conversion, but also the flow hydrodynamic parameters, e.g. phase velocity, phase volume fraction, riser temperature and averaged gas phase density.

The operation conditions will also be the one reported by Derouin et al.(1997) which is listed in Table 4.1-4.4.

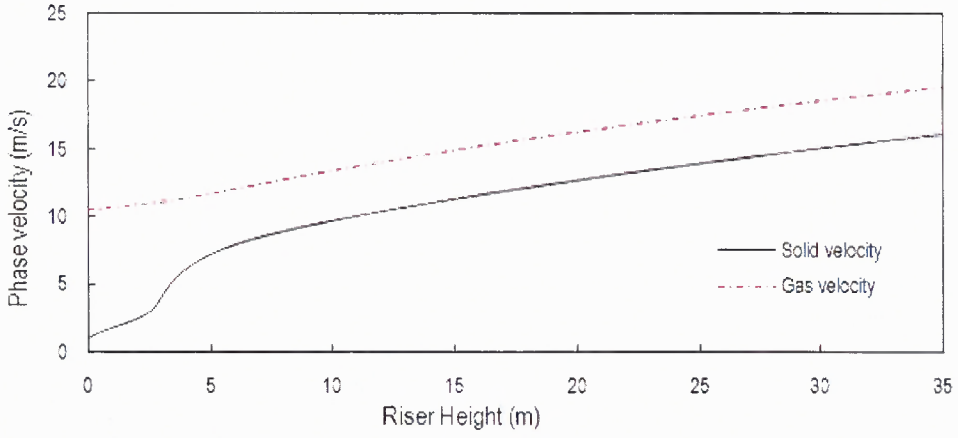

Figure 4.10 Model prediction of phase velocity.

Figure 4.10 illustrate the gas phase and solid phase velocity along the whole riser reactor. As shown in this figure, the overall tendency of the gas phase is increasing continuously, which is due to the cracking expansion of the VGO. It is also interested to notice that in the lower part of the riser, the increase rate is larger than the rest of the riser, because of more intensive cracking reaction. Although the volume fraction of the gas phase increase dramatically in the lower riser, which will cause the decrease of the gas velocity, the velocity increase due to cracking expansion take over this decrease, so the overall gas velocity still increase obviously in this region. With the slower reaction rate, and no significant change of volume fraction, the gas velocity keeps the increase trend. The catalyst velocity is the traditional S-shape in the whole riser which we have already given detailed description in chapter 2.

Figure 4.11 is the model prediction of the solids phase volume fraction. The solids phase starts from very dense region (about 0.32) quickly decrease to the steady dilute phase, which keeps volume faction at about 0.06. The overall shape is basically S-shape which is also given special attention in Chapter 1.

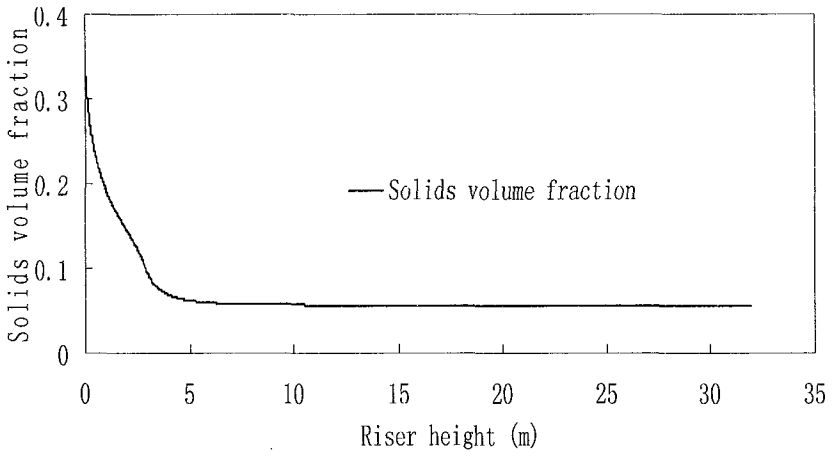

Figure 4.11 Model prediction of solids volume fraction.

Figure 4.12 gives the model prediction of gas and solid phase combined riser temperature. Since the identical temperature of gas and solid phase is one of the major assumption of our model, so we can not give the specially temperature for each phase. As demonstrated in Figure 4.12, due to the endothermic cracking reaction, the overall temperature drop from initial 810K to finally about 680K. Because the reaction constant is heavily dependent on temperature, so this is also a critical reason which cause the cracking reaction become slower in the upper of riser. Similarly, due to the more intensive cracking reaction, the temperature drops much faster in the lower part of riser than that in the upper riser.

Our model can also give the prediction the axial pressure profile along the whole riser which is shown in Figure 4.13. Starting at about 3.1atm at the beginning of the riser, the axial pressure decrease very fast in the dense phase region due to the intensive collision induced energy dissipation which has been given detailed explanation in Chapter 2. In the dilute phase of riser, the slow pressure decrease is mainly due to the solids phase gravity and pipe friction.

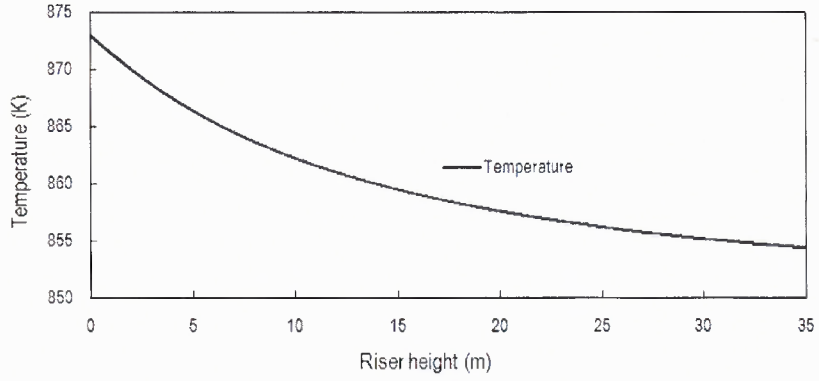

Figure 4.12 Model prediction of riser temperature.

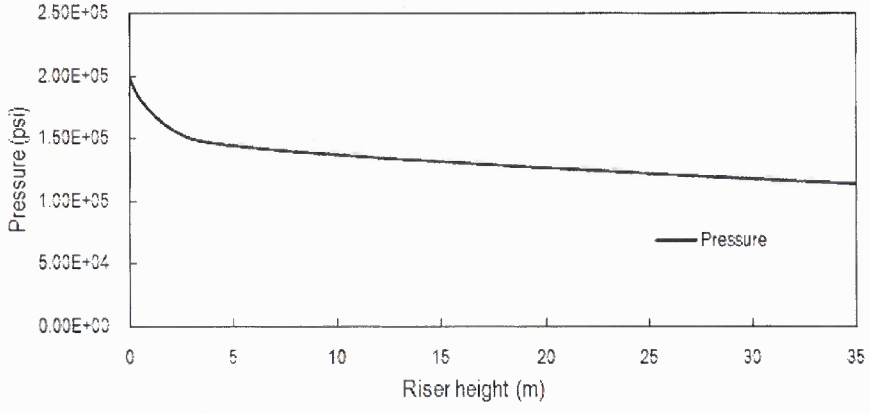

Figure 4.13 Model prediction of riser pressure.

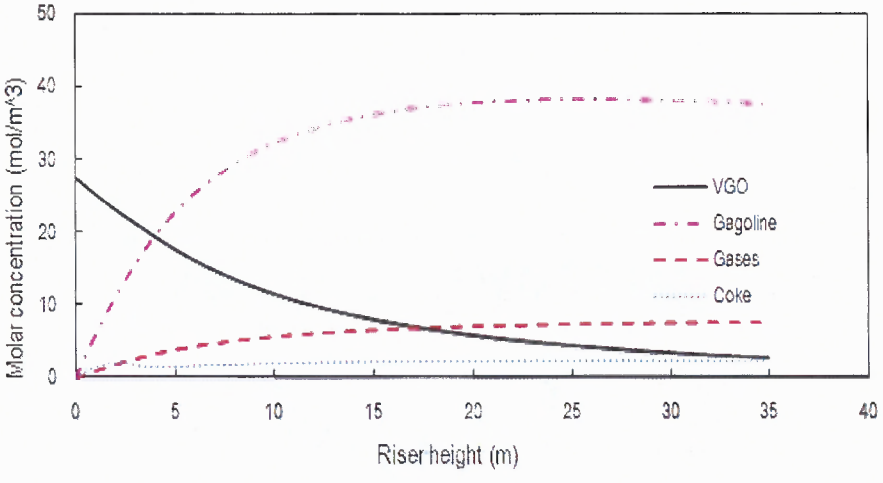

Figure 4.14 Model prediction of lump molar concentration.

In addition to giving conversion and yield, our model can also give the prediction of axial lump molar concentration along the riser. Although the weight percentage of the gases is much less than that of unconverted VGO, due to its much small molecular weight, its molar concentration even larger than unconverted VGO.

From above discussion, we have presented all typical outputs of our model, which include ten independent parameters. The prediction of all those detailed information can provide very useful input information for riser reactor design and control process optimization.

4.5 Parametrical Study of Reaction Coupled Hydrodynamic Model

Till now, we have already validated our model with two sets of FCC plant data, compared our model prediction with traditional plug flow model, and also presented all the typical prediction of both flow hydrodynamic parameters and reaction parameters, in the next part of this study, we are going to study the parametrical study of the model. We will investigate how the input catalyst to oil ratio and initial temperature will influence our model predictions.

Firstly we will conduct the parametrical study of the variable catalyst to oil ratio, since this catalyst to oil ratio is the most important input parameters which has significant impact on the cracking reaction.

In this part of parametrical study, we are going to change the initial catalyst to oil ratio from 5.5 to 8.0 or 2.5, and keep all other operation condition unchanged. The Figure 4.15 shows the model prediction result comparison between catalyst to oil ratio equaling to 5.5 and 8.0.

Table 4.5 Operating Conditions for Parametrical Study of C/O

Parameter	Derouin et al. (1997)	Higher CTO	Lower CTO
Catalyst flux (kg/s)	***470***	***680***	***212.5***
CTO	***5.5***	***8.0***	***2.5***
VGO feed rate (kg/s)	85	85	85
Feed temperature (K)	650	650	650
Catalyst inlet temperature (K)	960	960	960
Riser inside diameter (m)	1	1	1
Riser height (m)	35	35	35
Droplet diameter (μm)	100	100	100
Riser pressure (atm)	3.15	3.15	3.15

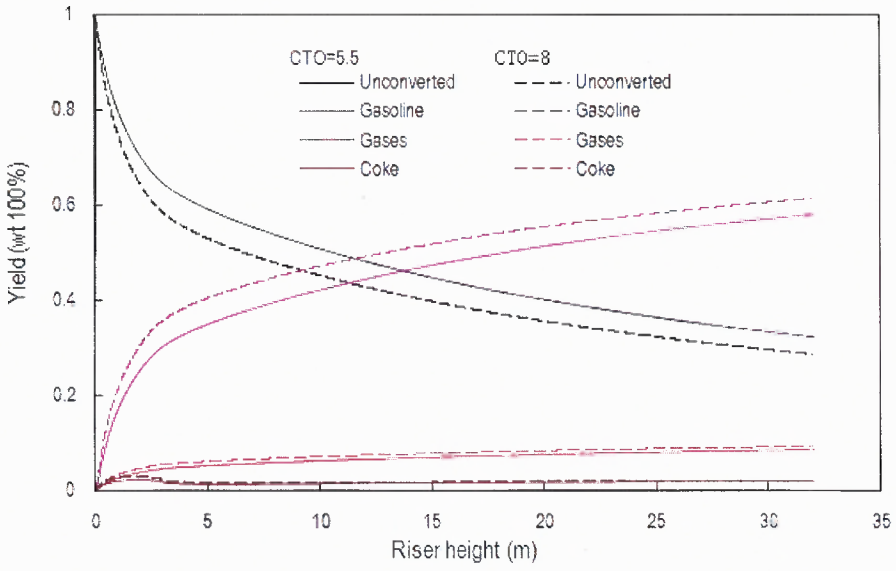

Figure 4.15 Parametrical study of catalyst to oil ratio (5.5 vs. 8.0).

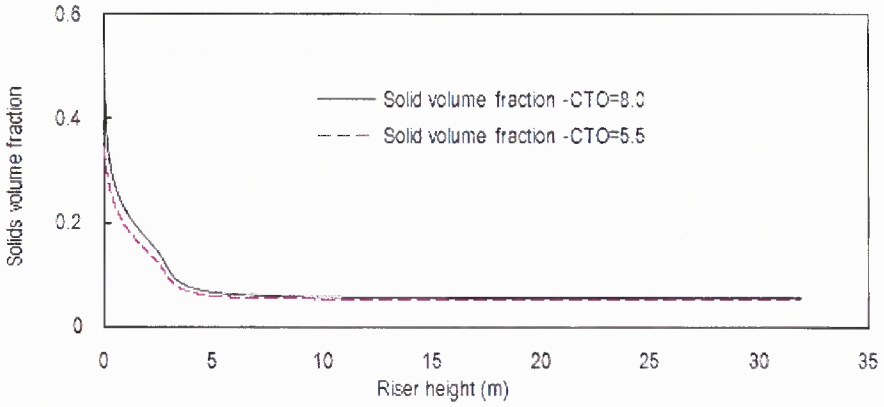

Figure 4.16 Catalyst volume fraction distributions (5.5 vs. 8.0).

As shown in Figure 4.15, with all other operating conditions unchanged, when the catalyst to oil ratio changes from 5.5 to 8.0 (catalyst mass flow rate from 470 to 680 kg/s), there is no significant difference in the yield of each components. Quantitative to say, with the catalyst mass flow rate increase about 50%, the gasoline yield increases about 5.9%. The only region where the difference is made is in the lower part of riser, whereas in the most part of the riser, the yield of each component has almost no change. In order to explain this, let's have a look of the Figure 4.16, which shows the axial catalyst volume fraction profiles of both cases. In Figure 4.16, we can notice that the solids volume fraction only has the difference in the very lower part of the riser, however, in the most part of the riser, both cases have very similar solids volume fractions, so the yield in those part of the riser didn't have much difference.

When we still keep all other operation conditions the same, and drop the initial catalyst to oil ratio from 5.5 to 2.5(catalyst mass flow rate from 470 to 212.5 kg/s), how the yield of each component will be influenced?

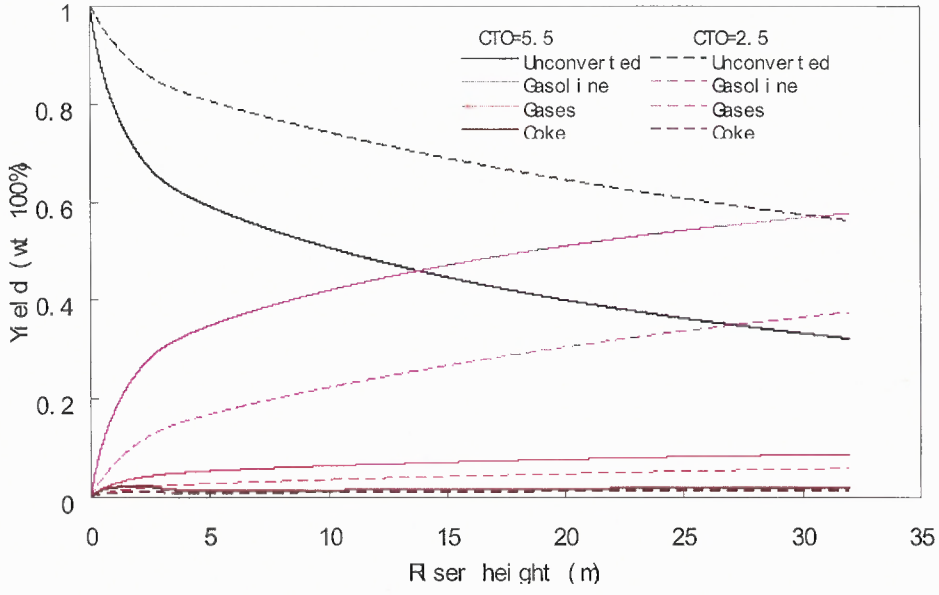

Figure 4.17 Parametrical study of catalyst to oil ratio (5.5 vs. 2.5).

In Figure 4.17, it shows that when inlet catalyst mass flow rate decrease about 55%, the gasoline yield at the riser outlet drops about 35%, which is much more than the 6% when catalyst to oil ratio equals to 8. This bigger drops also happens to gases yield which is about 33%. At the same time, the unconverted VGO increase about 74% which show the significance of the catalyst mass flow rate to the cracking reaction.

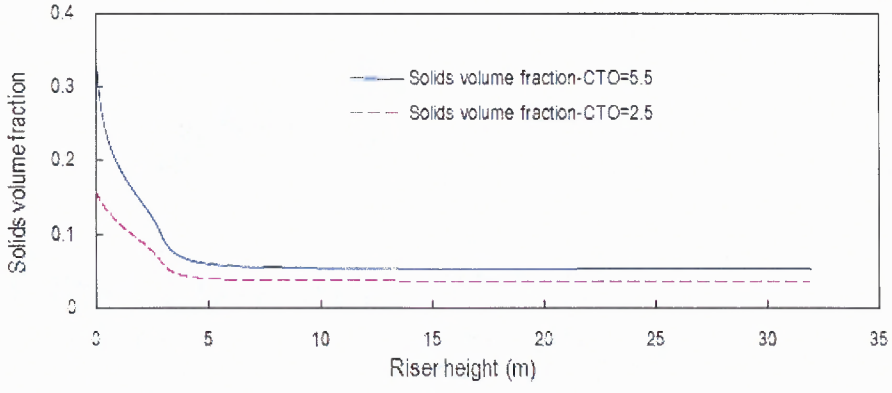

Figure 4.18 Catalyst volume fraction distributions (5.5 vs. 2.5).

From the catalyst volume fraction distribution along the whole riser shown in Figure 4.18, we can notice that not only the catalyst volume fraction in dense phase has obvious decrease, but also in dilute transport phase, the catalyst volume fraction drop quite much; this could explain the significant drop in component yields in above comparison.

In the next part of this study, we will conduct the parametrical study on riser temperature. Since the reaction constant is heavily dependent on reaction temperature, so the riser temperature has directly influence on the cracking reaction itself. Besides, the average gas density will also influence by the riser temperature, thus, the gas velocity and pressure will also change, correspondingly. It is very interested to find out how this temperature parameter will influence the cracking reaction.

Table 4.6 gives the operation condition for this temperature based parametrical study. In the three simulation cases, we keep all other condition the same, and solely adjust the temperature from 805K to 600K and 900K. The following Figure 4.19 gives the model predictions on production yields with the change of temperature.

Table 4.6 Operating Conditions for Parametrical Study of Temperature

Parameter	Derouin et al. (1997)	Higher Temperature	Lower Temperature
Catalyst flux (kg/s)	470	470	470
CTO	5.5	5.5	5.5
VGO feed rate (kg/s)	85	85	85
Riser temperature (K)	***805***	***900***	***600***
Riser inside diameter (m)	1	1	1
Riser height (m)	35	35	35
Droplet diameter (μm)	100	100	100
Riser pressure (atm)	3.15	3.15	3.15

Figure 4.19 clearly shows how the final component yields are influenced by riser initial temperature. When the temperature drops from 805K to 600K, the unconverted VGO and gasoline yield decrease approximately 61% and 38%, respectively. However, if the temperature increases from 805K to 900K, the two values also increase by about 26% and 16%.

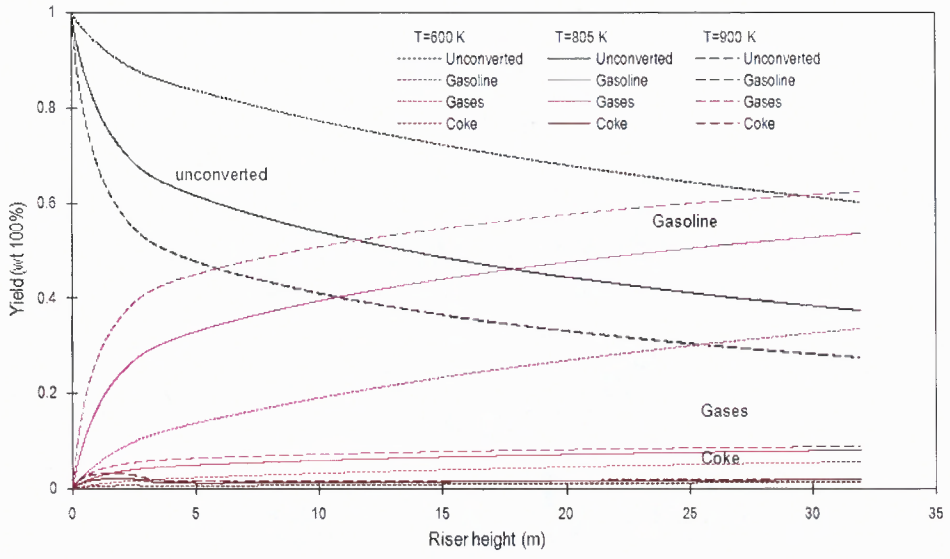

Figure 4.19 Parametrical study of temperature (805K vs. 600K and 900K).

Till now, we have conducted parametrical studies on both initial catalyst to oil ratio and temperature.

From the above parametrical study, we realize that both of the reaction temperature and catalyst to oil ratio have critical influence on final product yields. However due to complex flow hydrodynamics and reaction mechanism, the relationship among them is far more than some simple linear correlations. To take the best advantage of the facility and reach the maximum product yields, more specific and systematical parametrical study should be conducted.

CHAPTER 5

SUMMARY AND CONCLUSIONS

5.1 Major Contributions and Findings

- **New understanding on inter-particle collision force and energy dissipation**

In the first part of the study, most important physical mechanisms including inter-particle collision force, gas/solid interfacial force and wall boundary effects, which are believed to be most important aspects of the flow hydrodynamics, have been fully investigated. An energy-based mechanistic model was developed to analyze the partitions of the axial gradient of pressure by solids acceleration, collision-induced energy dissipation and solids holdup in gas-solid riser flows. Thought this part of study, important understanding of the inter-particle collision force (F_C), gas/solid interfacial force (F_D) inside the momentum equations and energy dissipation (Γ), especially in dense and acceleration region, has been reached. Our study shows that the transport energy is typically partitioned by three basic modes, namely, kinetic energy for solids acceleration, energy dissipation by collisions and frictions, and potential energy for solid lift-up. The traditional method of estimation of solid volume fraction directly from axial gradient of pressure leads to significant overestimation of solids volume fraction and underestimation of solid velocity in the solid acceleration and dense phase transport regimes.

- **Hydrodynamic model of riser flow**

A simple mechanistic model is developed in the second part of this Chapter, which describes the mechanism of neighboring particle compaction and collision's effect on drag force by modifying the traditional Richard-Zaki equation. An intrinsic

correlation for momentum transfer of solids is derived to account for the inter-particles collisions. This mechanistic model not only gives the prediction of solid volume fraction, gas and solid velocity, but also is capable of predicting the axial pressure distribution along the whole riser.

The model predictions are compared with the axial gradient of pressure and solid volume fraction for the experimental data of independent research groups. The model predictions show fairly good agreement with the experimental data in the bulk range. Moreover, systematic parametric studies have been conducted to demonstrate the effects of variation in gas velocity and solid mass flux on flow patterns.

In the last part of this chapter, an attempt has been made to quantify the solids back-mixing and upward flow cross section area, which is changing with the riser height. When combined this obtained correlations in the hydrodynamic model developed in previous section, the model prediction results was significantly improved, especially for the operating condition with very low solids circulation rate.

- **General mathematical model for heteronymous flow structure**

For the second part of study in chapter 3.1 and 3.2, we soundly explain the formation mechanism of traditional "core-annulus" two zone structures and newly found "core-annulus-wall" three zone structure. With the further understanding of solid collision and acceleration form the previous study, a comprehensive modeling of continuous gas-solids flow structure both in radial and axial directions has been presented. In order to simplify the problem and solve the set of coupled integral-differential equations, two separate sub-models based on different strategy have been developed to serve this purpose. First sub-model is called three-zone simplification and the second one is continuous approximation approach. Both of the sub-model

simulations are proofed to be successful and validated by direct comparisons against measurements in solids concentrations as well as in the pres

- **Simplified three-zone model to solve general flow structure model**

In the three-zone sum-model in chapter 3.3, a simplified three-zone modeling approach to understand the general heterogeneous flow structure in gas-solid riser flow, especially the "core-annulus-wall" three-zone flow structure and the unstable flow structure that leads to choking. The model prediction results are directly compared with experimental measurement using ECT technology, which shows a fairly good agreement. The proposed mechanisms and corresponding mathematical modeling yield a reasonable explanation for the formation and flow conditions of various heterogeneous structures. Effects of critical flow parameters such as solids mass flow rate and gas inlet velocity have also been illustrated. Simulation results show that the well-known "core-annulus" two-zone structure is easily formed at high gas velocity and/or low solids mass flow rate, and the "core-annulus-wall" three-zone structure always happens at low gas inlet velocity and/or high solids mass flow rate. The formation of reversal solids concentration profiles along the riser in the core region may be the underlying cause of choking.

- **Entrance effect for gas-solid flow structure**

This part of study investigates the effect of various riser entrances on the overall flow structure and its stability at different operation conditions. Three riser entrances are selected to simulate the common solids feeding devices of risers, namely, the J-bend feeder, the L-valve feeder with a fluidized bed distributor, and the L-valve feeder after a taper section. For the purpose of validation, some simulation results are directly

compared with available experimental measurements and reasonably good agreements are reached. It was concluded that the riser characteristic length of entrance region is almost independent of gas inlet velocities and solids mass flow rates; however it is moderately influenced by the solid feeding patterns. The study also shows that the flow structure in the entrance region can be strongly affected by the selection of solids feeding patterns but weakly dependent upon the operation conditions. According to the results of riser main region simulation, it is shown that, at the same operation conditions, the use of different solids feeding patterns has no significant impact on the basic flow structures along the riser, namely the axial distributions in each zone is weakly dependent on the type of solids feeding. Besides, it can also be concluded from the study that even the flow stability will not be significantly affected by the types of solids feeding patterns.

- **Model for Chemical Reaction Coupled Gas-solid transport**

In the last portion of the study of chapter 4, in order to consider the fluid dynamics of gas-solid two-phase flow which is very complex and strongly dominated by particle-particle interactions, and at the same time the gas-phase cracking reactions interacting with the complicated flow dynamic, it is necessary to develop a simplified mechanistic modeling approach which can describe both. The portion of study aims to develop a steady-state mechanistic riser model which can take into account flow hydrodynamics and catalytic cracking reactions. The emphasis was not on developing accurate flow model but was developing a framework to simultaneously simulate multi-phase flow and cracking reactions in riser reactor. A series of inter-coupled differential equations based on conservation of mass, momentum and energy and phase diffusion are developed which makes this mechanistic model closure. As a first

endeavor to consider the significant mutual coupling between the flow hydrodynamics and cracking reaction, a localized catalyst to oil ratio is introduced. The model was capable of quick evaluating the flow parameters including gas and solid phase velocity and concentration, temperature and reaction yield profiles as the function of riser height.

5.2 Proposed Future Study

Yet major part of the research topics listed in Figure 5.1 have been completed, however, either fundamental physical mechanism of gas-solid riser flow or chemical reaction coupled flow characteristics is far from fully understood. Hence, in this section, several research topics are suggested to further investigate in order to completely understand these phenomena and provide more solid mechanistic explanations.

- **Mechanism of gas-solid riser flow**

The fundamental mechanism of gas-solid flow can be summarized as three main aspects, which are inter-particle collision force, gas/solid interfacial force and wall effects. None of these three aspects has been fully understood, and how to accurately quantify them using mathematical modeling approach still have a lot of work to do. In our model approach, we recognize the importance of this collision force on solids phase momentum balance and, as a mathematical and compromised approach, we combined this collision force with the gas/solid interfacial force, which is far away from the perfect modeling approach. In order to accurately describe this critical force on solids phase, more studies need to be conducted to accomplish this goal.

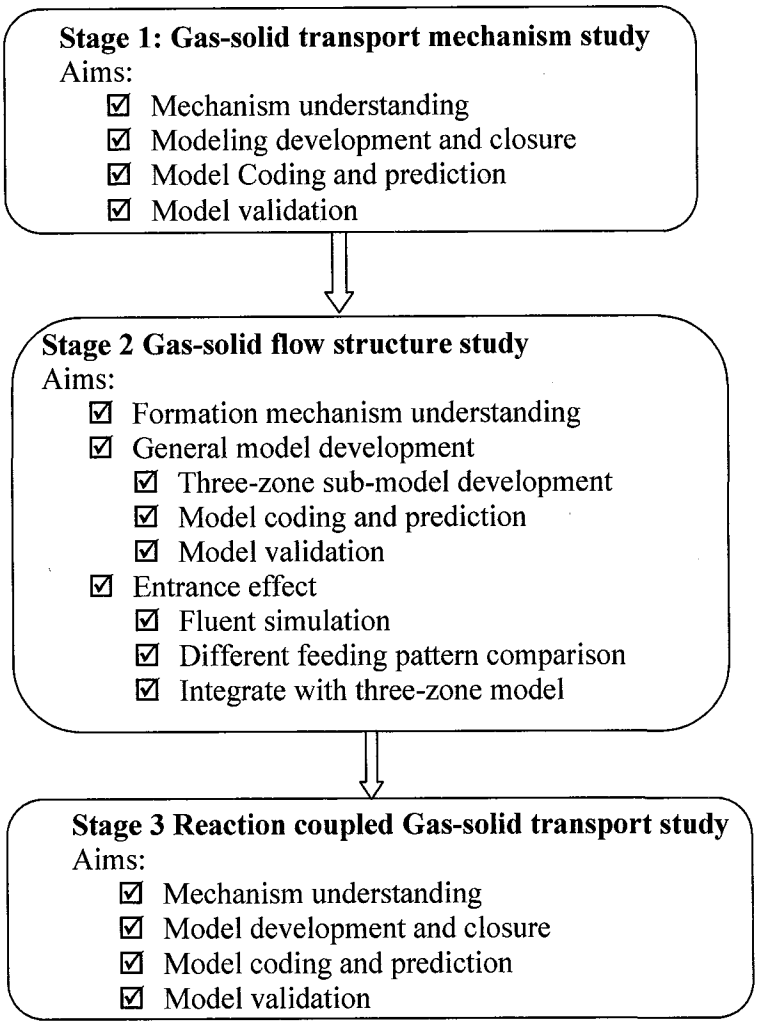

Figure 5.1 Overall research quick reviews.

In most of our studies, the gas/solids interfacial force is estimated based on traditional Richard-Zaki equation. However during our study, we realized it may not be the appropriate way to quantify this gas/solid interfacial force using this R-K equation. Because in many cases, especially in the dense and acceleration regime, this gas/solid interfacial force calculated from R-K equation is obviously much larger than the actual force imposed on particles. Since the R-K equation is only an empirical correlation derived to match with measured pressure drop values, it may not reflect the true gas/solid interfacial force imposed on the particles. Besides, the R-K

equation was developed in the creep flow regime, so it may not be able to apply into the fast fluidized riser flow. More detailed study need to be done toward the true mechanism of this gas/solid interfacial force, which are the most critical aspects of the hydrodynamic modeling of riser flow.

Another important feature of riser gas-solid hydrodynamic which has not been fully understood is solid back-mixing. As we know, both the amount of solids back-mixing and wall region thickness are heavily dependent of riser operation conditions and riser geometry, such as solids circulating rate, gas velocity, riser diameters, and etc. In our study, only some simple correlations have been presented. Considering the significant effect on flow hydrodynamics, more systematical study is recommended on this aspect.

- **Modeling for heterogeneous flow structure**

As the first step endeavor, the mechanism of heterogeneous flow structure has been explained by our simplified three-zone modeling approach. However, there are still many unknowns in detailed flow structures modeling, such as the intrinsic correlations for inter-zone transport (e.g., F_f' s) and transport coefficients for gas phase and solids phase. A very important issue, which has not been covered in our work, is how the wall boundary influences the flow structure. Although predefined zone wall boundaries are introduced in the modeling approach, it is not enough to fully consider the true effects the wall effects. In order to provide better and accurate prediction results, much more work need to be done.

- **Modeling for chemical reaction coupled flow hydrodynamic model**

As pioneer attempt to truly couple the chemical reaction mechanism into gas-solid hydrodynamic model, our emphasis was not trying to accurately predict flow and reaction parameters, but to develop a framework to simultaneously simulate multi-phase flow and cracking reactions in riser reactor.

As the next step study, there are many issues still need to be continuously investigated. First of all, a more completed and sophisticated gas-solid hydrodynamic model without reaction is the foundation of the coupling model with reaction, so more work should still be focused on the flow hydrodynamic itself without reaction.

Secondly, since the reaction constants are heavily dependent on the reaction temperature, the detailed heat transfer model between gas and solid phase need to be developed in order to accurately capture the inter-coupling influence between chemical reaction and flow hydrodynamics, instead of assuming identical temperature of gas and solids phase in current model.

Thirdly, the aging function of catalyst is one of the critical aspects which have significant influence on cracking reaction. In the current model, some empirical correlations from literatures were introduced. However, the catalyst aging function is directly related with flow structure and solid back-mixing, and the mechanism behind these relationships deserve a fully investigation.

At last, in order to avoid complicated mathematical derivation, a simple four-lump FCC reaction model was introduced, which may not represent most of complex chemical reactions in many industrial areas. In order to board our model application, more studies should be done toward the typical chemical reaction model and their different influences on local flow hydrodynamics.

REFERENCES

Bader, R., J. Findlay and T. M. Knowlton, Gas-solid flow patterns in a 30.5 cm diameter circulating fluidized bed, in P. Basu and J. F. Large (eds.), *Circulating Fluidized Bed Technology II*, Pergamon Press, New York, 123-137, 1988.

Bi, H.T. and L.S. Fan, Existence of turbulent regime in gas-solid fluidization, *AIChE J.*, 38, 297-305, 1992.

Berry, T., McKeen, T., Pugsley, T., Dalai, A., 2004. Two-dimensional reaction engineering model of the riser section of a fluid catalytic cracking unit. *Indus. & Eng. Chemistry Research,* 43, 5571-5581.

Bolton, L.W. and J.F. Davidson, Recirculation of Particles in Fast Fluidized Risers, In *Circulation Fluidized Bed Technology,* (Ed. Basu and Large), Toronto: Pergamon Press, 1988.

Buchanan, J.S., 1994. Analysis of heating and vaporization of feed droplet in fluidized catalytic cracking risers. *Indus. & Eng. Chemistry Research,* 33, 3104-3111.

Büssing, W. and L. Reh, On viscous momentum transfer by solids in gas–solids flow through risers, *Chem. Eng. Sci.*, 56, 3803-3813, 2001.

Brereton, C. M. H., and J. R. Grace, Microstructure aspects of the behavior of circulating fluidized beds, *Chem. Eng. Sci.*, 48(14), 2565, 1993.

Corella, J., Frances, E., 1991. Analysis of the riser reactor of a fluid catalytic cracking unit: model based on kinetics of cracking and deactivation from laboratory tests. In: Occelli, M.L. (Ed.), *Fluid Catalytic Cracking—II: Concepts in Catalyst Design, ACS Symposium Series,* vol. 452. American Chemical Society, Washington, 165-182.

Delhaye, J.M., Basic equations for two-phase flow modeling, in Bergles, Collier, Delhaye, Hewitt and Mayinger (eds.), *Two-Phase Flow and Heat Transfer in the Power and Process Indus.*, Hemisphere, Washington, 1981.

Das, A.K., De Wilde, J., Hegnderickx, G.J., Marin, G.B., Vierendeels, J., Dick, E., 2004. CFD simulation of dilute phase gas–solid riser reactors: Part I: a new solution method and flow model validation. *Chem. Eng. Sci.* 59, 167-186

Derouin, C., Nevicato, D., Forissier, M., Wild, G., Bernard, J., 1997, Hydrodynamics of riser units and their impact on FCC operation. *Indus. & Eng. Chem. Res.* 36, 4504-4515

Du, B., W. Warsito and L.S. Fan, ECT studies of the choking phenomenon in a gas-solid circulating fluidized bed, *AIChE J.*, 50(7), 1387, 2004.

Fan, L.S. and C. Zhu, Principles of Gas-solid Flows, Cambridge Univ. Press, London, 1998.

Farag, H. 1993. Catalytic cracking of hydrocarbons with novel metal traps. Ph.D. Dissertation, University of Western Ontario, London, Ontario, Canada.

Farag, H., Gianetto, A., Blasetti, A., de Lasa, H., 1994. FCC catalyst for reformulated gasolines. Kinetic modeling. *Indust. & Eng. Chemistry Res.*, 33, 3053.

Geldart, D. and M. J. Rhodes, From minimum fluidization to pneumatic transport: a critical review of the hydrodynamics, in P. Basu (eds.), *Circulating Fluidized Bed Technology*, Pergamon Press, Oxford, 193- 200, 1986

Grace, J.R., A.A. Avidan and T.M. Knowlton, Circulating Fluidized Beds, London, UK: Chapman & Hall, 1997.

Gao, J., Xu, C., Lin, S., Yang, G., 2001. Simulation of gas–Liquid–solid 3 phase flow and reaction in FCC Riser Reactors. *AIChE. Journal*,47, 677- 692.

Gupta, A., Subba Rao, D., 2003. Effect of feed atomization on FCC performance: Simulation of entire unit. *Chem. Eng. Sci.* 58, 4567- 4579.

Gupta, R.K., Kumar, K., Srivastava, V.K., A new generic approach for the modeling of fluid catalytic cracking (FCC) riser reactor, *Chem. Eng. Sci.*, 62, (2007), 4510-4528

Halow J.S., Fasching G.E., Nicoletti P., Spenik J.L., Observations of a fluidized bed using capacitance imaging, *Chem. Eng. Sci.* 48 (1993), 643-659

Han, I.S., Chung, C.B., Dynamic modeling and simulation of a fluidized catalytic cracking process, *Chem. Eng. Sci.*, 56, (2001), 1951-1971

He, Y. and V. Rudolph, The volume-average voidage in the riser of a circulating fluidized bed, *Powder Technology*, 89, 79-82, 1996.

Horio, M., & Kuroki, H. Three-dimensional visualization of dilutely dispersed solids in bubbling and circulating fluidized beds, *Chem. Eng. Sci.*, 49(15), 2413-2428. (1994).

Jacob, S.M., Gross, B., Voltz, S.E.,& Weekman, 1976, V.W., A lumping and reaction scheme for catalytic cracking, *AIChE Journal*, 22, 701-713.

Larocca, M., Ng, s., de Lasa, H., Cracking catalyst deactivation by nickel and vanadium contaminants, *Indus.& Eng. Chem. Res.*, 1990, 29, 2181-2191.

Lee, L., Chen, Y., Huang, T., Pan, W., 1989. Four lump kinetic model for fluid catalytic cracking process. *Can. J. of Chem. Eng.*, 67, 615-619.

Li, Y. and M. Kwauk, in J.R. Grace and J.M. Matsen (eds.), *Fluidization*, Plenum, New York, 537-544, 1980.

Liguras, D.K., Allen, D.T., 1989a. Structural models for catalytic cracking. 1. Model compound reactions. *Indus. & Eng. Chemistry Research* 28, 665-673.

Liguras, D.K., Allen, D.T., 1989b. Structural models for catalytic cracking. 2. Reactions of simulated oil mixtures. *Indus. & Eng. Chemistry Research,* 28, 674-683.

Louge M. and H. Chang, Pressure and voidage gradients in vertical gas-solid risers, *Powder Technology*, 60, 197-201, 1990.

Louge, M.Y., E. Mastorakos and J.T, Jenkins, The role of particle collisions in pneumatic transport, *J. Fluid Mechanics,* 231, 345-359, 1991.

Mathesian, V., Solberg, T., Hjertager, B.H., 2000. Prediction of gas/particle flow with an Eulerian model including a realistic particle size distribution. *Powder Technology,* 112, 34-35.

Merrow, E.W. 1986 A quantitative assessment of R&D requirements for solids precessing technology, Rand Corporation Note R-3216-DOE/PSSP

Miller, A. and D. Gidaspow, Dense, vertical gas-solid flow in a pipe, *AIChE Journal,* 38, 1801, 1992.

Nakajima, M., M. Harada, M. Asai, R. Yamazaki, and G. Jimbo, "Bubble fraction and voidage in an emulsion phase in the transition to a turbulent fluidized bed," in *Circulating Fluidized Bed III*, Ed., 1991.

Neri, A., Gidaspow, D., 2000. Riser hydrodynamics: Simulation using kinetic theory. *AIChE Journal,* 46 (1), 52-67.

Pugsley, T. S. and F. Berruti, A predictive hydrodynamic model for circulating fluidized bed risers, *Powder Technology*, 89, 57-69, 1996.

Pitault, I., Nevicato, D., Forissier, M., Bernand, J.R., 1994. Kinetic model based on a molecular description for catalytic cracking of vacuum gas oil. *Chem. Eng. Sci.*, 49, 4249-4262.

Pitault, I., Nevicato, D., Blasetti, A.P., Delasa, H.I., Fluid catalytic cracking catalyst for reformulated gasoline-kinetic modeling. *Indus.& Eng. Chem. Res*, 1994, 33, 3053

Rautiainen, A., G. Stewart, V. Poikolainen and P. Sarkomaa, An experimental study of vertical pneumatic conveying, *Powder Technology*, 104, 139-150, 1999.

Rowe, P.N., Experimental properties of bubbles, *Fluidization* (eds. J.F. Davidson and D. Harrison), New York: Academic Press, 121, 1971.

Sabbaghan, H., R.S.Gharebagh and N.Mostoufi, Modeling the acceleration zone in the riser of circulating fluidized beds, *Powder Technology*, 142, 129-135, 2004.

Schlichthaerle, P. and J.Werther, Axial pressure profiles and solids concentration distributions in the CFB bottom zone, *Chem. Eng. Sci.*, 54, 5485-5493, 1999.

Sun, G., Z. Chao, Y. Fan and M. Shi, Hydrodynamic behavior in the bottom region of a cold FCC riser, *Circulating Fluidized Bed Technology VI*, 179-184, 1999.

Yates, J.G. and Simons, S.J.R., Experimental methods in fluidization research, *International Journal of Multiphase Flow*, 20, 297, 1994

Schlichthaerle, P. and J.Werther, Axial pressure profiles and solids concentration distributions in the CFB bottom zone, *Chem. Eng. Sci.,* 54, 5485-5493, 1999.

Subramanya V. Nayak, Saket L. Joshi, Vivek V. Ranade, Modeling of vaporization and cracking of liquid oil injected in a gas-solid riser, *Chem. Eng. Sci.*, 60, (2005), 6049-6066.

Warsito, W., and L.-S. Fan, Measurement of real-time flow structures in gas-liquid and gas-liquid-solid flow systems using electrical capacitance tomography (ECT), *Chem. Eng. Sci.,* 56, 6455 (2001a).

Du, B., W. Warsito and L.-S. Fan, ECT studies of the choking phenomenon in a gas-solid circulating fluidized bed, *AIChE Journal*, 50 (7), 1386 (2004).

Rhodes, M.J. and D. Geldart, A model for the circulating fluidized bed, *Powder Tech.*, 53, 155, 1987.

Ranade, V.V., 2002. Computational flow modeling for chemical reactor engineering. Academic Press, London.

Horio, M., Morishita, K., Tachibana, O. and Murata, N. (1988). Solid distribution and movement in circulating fluidized beds. In *Circulating Fluidized Bed Technology II.* Ed. Basu and Large. Toronto: Pergamon Press

Rhodes, M.J., M. Sollaart and X.S. Wang, Flow structure in a fast fluid bed, *Powder Technology,* 99, 194 (1998).

Richardson, J.F., Zaki, W.N., Sedimentation and fluidization, *Trans. Inst. Chem. Eng.*, 32, 35-53, 1954.

Senior, R.C. and Brereton, C.M.M. (1992). Modeling of circulating fluidized bed solids flow and distribution. *Chem. Eng. Sci.,* 47, 281.

Takatsuka, T., Sato, S., Morimoto, Y., Hashimoto, H., A reaction model for catalytic cracking of residual oil, *Int. Chem. Eng.,* 1987, 27, 107-116.

Theologos, K.N., Markatos, N.C., Lygeros, A.I., 1999. Feedstock atomization effects on FCC riser reactors selectivity. *Chem. Eng. Sci.,* 54, 5617-5625.

Theologos, K.N., Markatos, N.C., 1993. Advance modeling of fluid catalytic cracking riser-type reactors. *AIChE Journal,* 39 (6), 1007-1017.

Van Wachem, B.G.M., Schowten, J.C., Van Den Bleck, C.M., Krishna, R., Sinclair, J.L., 2001. A CFD modeling of gas fluidized beds with a bimodal particle mixture. *AIChE Journal* 1292-1301.

Weekman, V.W., Nace, D.M., 1970. Kinetics of catalytic cracking selectivity in fixed, moving, and fluid bed reactors. *AIChE Journal,* 16 (3), 3397-404.

Weekman, V.W., Nace, D.M., 1970. Kinetics of catalytic cracking selectivity in fixed, moving, and fluid bed reactors. *AIChE Journal*, 16 (3), 3397-3404.

Zhu, C., Yu, Q., and L.S. Fan, Modeling on core-annulus-wall structure in circulating fluidized bed riser, *Circulating Fluidized Bed Technology VIII,* 354, 2005.

Zhu, C. and You, J. An energy-based model of gas-solids transport in a riser, *Powder Tech.*, 175 (2007) 33-42.

You J., Wang D.W., Zhu C., Entrance Effects on Gas-Solid Riser Flow Structure, *Industrial & Engineering Chemistry Research*, 2009, 48, 310-319.

You J., Zhu C., Bing Du, L.S.Fan, Heterogeneous Structure in Gas-Solid Riser Flows, *AIChE Journal*, Vol. 54, No. 6, 1459-1469, 2008.

Zhu C., S.-C. Liang and L.-S. Fan, Particle wake effects on the drag force of an interactive particle. *Int. J. Multiphase Flow*, 20 (1994), 117.